SIG GALILEO FINAL CONVERTER TECHNICAL SUMMARY REPORT

MMM–2864–0055

MAY 1979

by

J. D. HINDERMAN
PROGRAM MANAGER
3M COMPANY

PREPARED FOR POWER SYSTEMS BRANCH
ADVANCED SYSTEMS AND MATERIALS
PRODUCTION DIVISION, DEPARTMENT OF ENERGY
UNDER DoE CONTRACT DE–AC01–78ET–33008

MINNESOTA MINING AND MANUFACTURING COMPANY
ELECTRICAL PRODUCTS GROUP
INDUSTRIAL ELECTRICAL PRODUCTS DIVISION
ST. PAUL, MINNESOTA 55101

DISCLAIMER

LEGAL NOTICE

This report was prepared as an account of Government sponsored work. Neither the United States, nor DoE, nor any person acting on behalf of DoE:

a. Makes any warranty or representation, expressed or implied, with respect to the accuracy, completeness, or usefulness of the information contained in this report, or that the use of any information, apparatus, method, or process disclosed in this report may not infringe privately owned rights; or

b. Assumes any liabilities with respect to the use of, or for damages resulting from the use of, any information, apparatus, method, or process disclosed in this report.

As used in the above, "person acting on behalf of DoE" includes any employee or contractor of DoE, or employee of such contractor, to the extent that such employee or contractor of DoE, or employee of such contractor prepares, disseminates, or provides access to, any information pursuant to his employment or contract with DoE, or his employment with such contractor.

TABLE OF CONTENTS

TABLE OF CONTENTS (Continued)

INTRODUCTION

This report summarizes significant events, activities and achievements on the SIG/Galileo Converter Program at 3M Company during the period June 1, 1978 through May 15, 1979 under Department of Energy Contract DE-AC01-78EG-33008. A stop work order was received from DoE on January 29, 1979 and all subsequent work and close out activities targeted for completion by May 15, 1979.

The report is primarily concerned with the work performed for DoE on converter development and fabrication for the NASA Galileo Jupiter mission as a DoE prime contractor with interface primarily with Teledyne Energy Systems. The activities reported on were directed toward design, analysis and testing of modules and converters SN-1 thru SN-7 and attendant Quality Control and Reliability effort. Although assembly and testing of SN-1 was not accomplished due to the stop work order, the design was virtually completed and a significant amount of subcontracting and manufacturing of both module and converter components was underway. These subcontracting and manufacturing activities were selectively closed down depending upon degree of completion and material or hardware potential usage in the Technology Program (Contract EY-76-C-02-2331).

The primary interface during the program was with Teledyne Energy Systems (TES) for design and assembly of the thermoelectric converter into the generator housing provided by the government as GFE (from TES). Other efforts dealt with test module design and fabrication, quality control and reliability.

The stop work order was received before a detailed program plan was completed. After the receipt of the stop work order a proposal was prepared to reflect the modified statement-of-work associated with the close-out-effort (Ref. "Proposal to Close-Out the Contract DE-AC01-78-ET-33008 (Formerly No. ET-78-C-01-7864)", No. 2864-0049, March 8, 1979). This report therefore serves as both the Final Technical Report and the Program Plan for the SIG/Galileo Converter Program (Contract No. DE-AC01-78ET-33008).

I. ENGINEERING DESIGN

As described in the SIG/Galileo Statement of Work (Section 3.1), the Design Group is responsible for module, converter, and test equipment design. The majority of the work is centered around the design of the modules and converter, and the interface developments with Teledyne Energy Systems (TES).

Section A describes, in detail, the component configurations developed and proposed for the SN-1 converter.[1] This converter was the "Flight Design" with the possible exception of N-leg improvements and a 'cold frame - housing interface' processing change. Included at the end of the converter description is the status of the design at the time of the 'stop work order'.

In Section B, the activities performed to accomplish the design goals are described as they occurred.

Section C lists all pertinent documentation which was developed and issued relating to the design of the converter. This includes drawings, specifications, procedures and analysis.

Operating requirements for the SN-1 converter are given in Table I-1.

TABLE I-1

OBJECTIVES AND REQUIREMENTS FOR SN-1 CONVERTER

- T_H/T_C = 860/160°C
- Voltage = 30 volts
- N-Leg Material Resistance - 22.9 mΩ
- 22 mΩ Contact Resistance on N- and P-Legs
- Nominal Power Output (BOL) = 193 W(e)
- Designed to Withstand and Launch Loads Although Vibration Test Not Planned
- Converter Weight = 16.0 lbs.
- Extraneous Resistance = 12-1/2%
- Cold End Thermal Resistance = 7°C/watt

---

1) The design requirements are listed in Table I-1.

A. CONVERTER CONFIGURATION

3M/TES Interface

Figures I-1 and I-2 show the proposed SIG/Galileo RTG package that was to be supplied by Teledyne Energy Systems (TES). 3M's interface with TES lies in the power section of the generator, shown in Figure I-3. 3M was responsible for supplying the two converter ring assemblies. In addition, 3M would handle the installation of the two converter ring assemblies, the center multi-foil sleeve assembly (TES), center section insulation, and the initial instrumentation wiring into the housing supplied by TES.

A brief version of 3M's installation procedure follows (see Figure I-3):

1. 3M receives aluminum housing from TES
2. Position converter ring No. 2 into housing. Remove assembly tooling.
3. Slide center multi-foil sleeve assembly (see Figure I-4) (Supplied by TES) into position next to converter ring No. 2.
4. Insert converter ring No. 1 into position. Remove assembly tooling.

   Assure that locating pins between multi-foil sleeve and converter rings are in position (see Figure I-5)
5. Make all required power and instrumentation connections and route wires.
6. Stuff fiberfrax insulation between converter ring No. 1 and center multi-foil sleeve assembly as shown in Figure I-5. Slide retainer tab into position.
7. Transfer secured unit back to TES following 3M testing.

Activities involving interface between 3M and TES are covered in Section B.

The 3M thermoelectric converter ring assembly is shown in Figure I-6. It consists of a POCO support ring with 28 segment assemblies located around its periphery. Two converter rings are wired in series within the TES housing (see Figure I-7.) The internal circuit connection of the converter ring is a series parallel with two parallel strings.

Detailed Description of Segment

The segment assembly is shown in Figure I-8. As previously mentioned, each converter ring contains twenty-eight (28) of these segments. Following is a brief description of the individual components within the segment.

Hot Frame: A cylindrical ring containing 28 flats around its circumference serves as the hot end frame for the segment assemblies. The material is POCO AXF-Q1 graphite, selected because of its high temperature strength and purity. The cylinder is 3.0 inches long, 7.66 inches inside diameter, and .23 inches minimum thickness.

PT Foil: Between the hot current strap and the hot frame is placed a .0005 inch thick foil of Platinum to reduce the thermal resistance between the two. Two foils are used in each segment, one for each row of six legs.

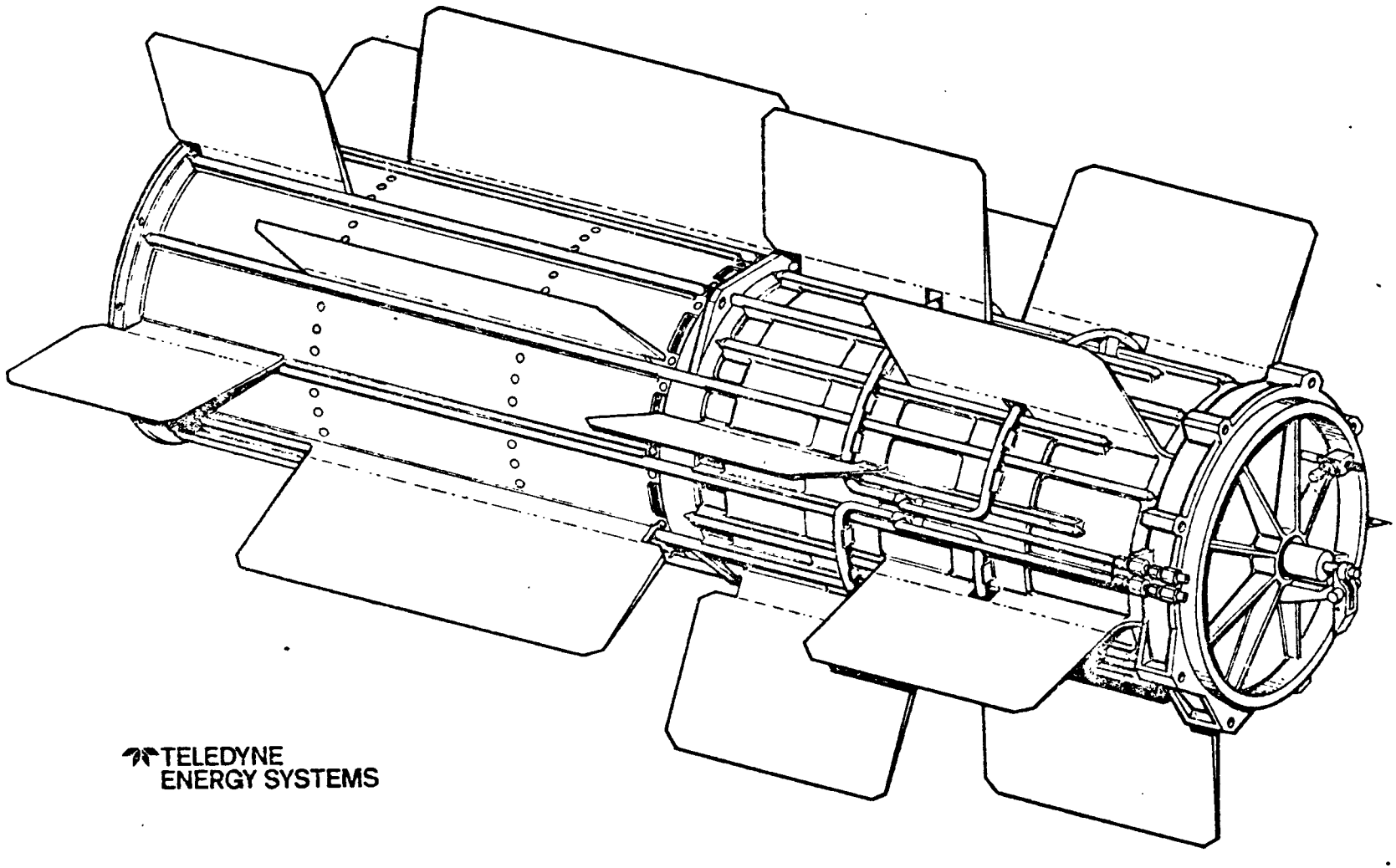

FIGURE I-1: SIG/GALILEO FLIGHT DESIGN

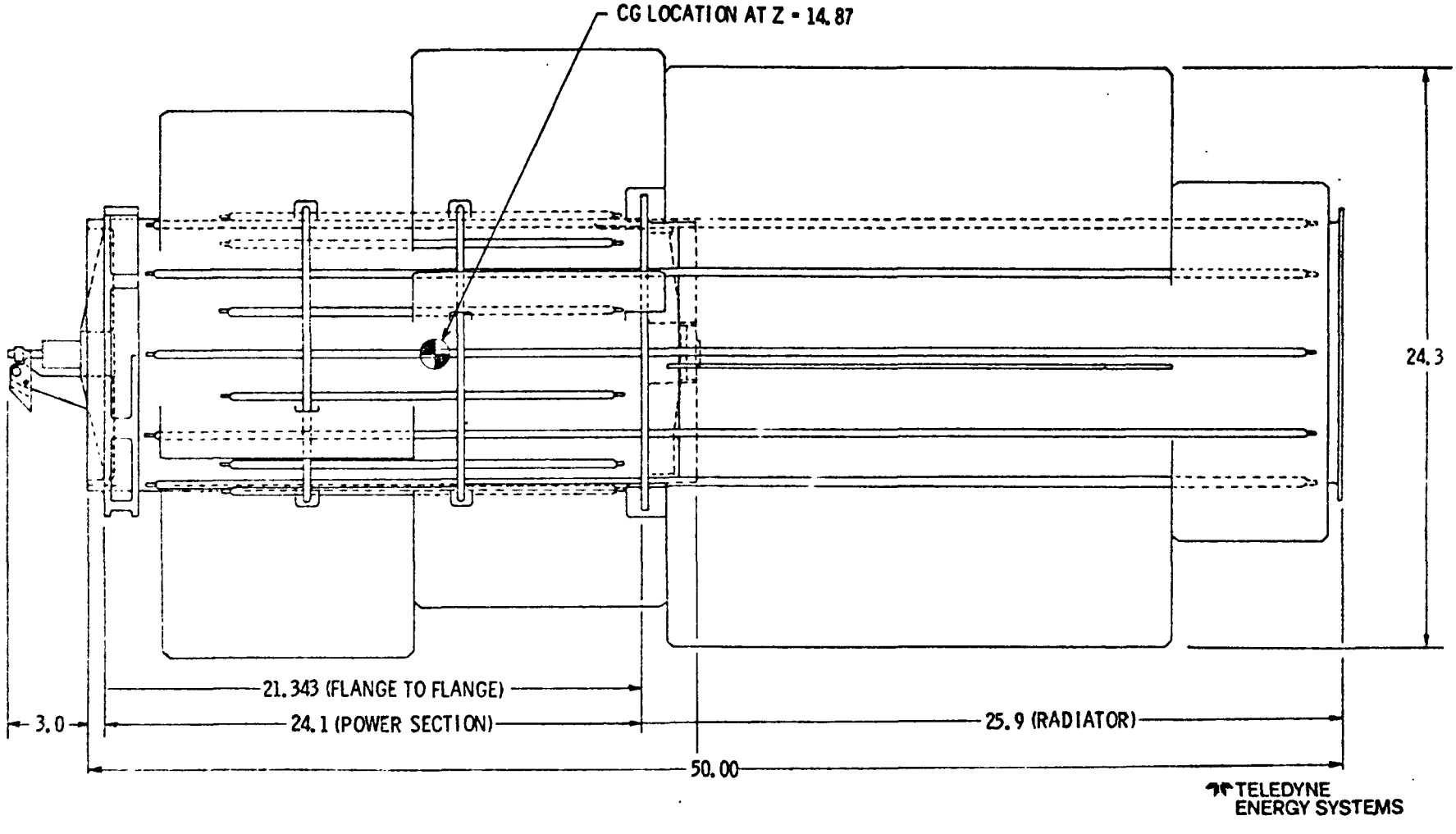

FIGURE I-2: SIG/GALILEO RTG ENVELOPE DIMENSIONS

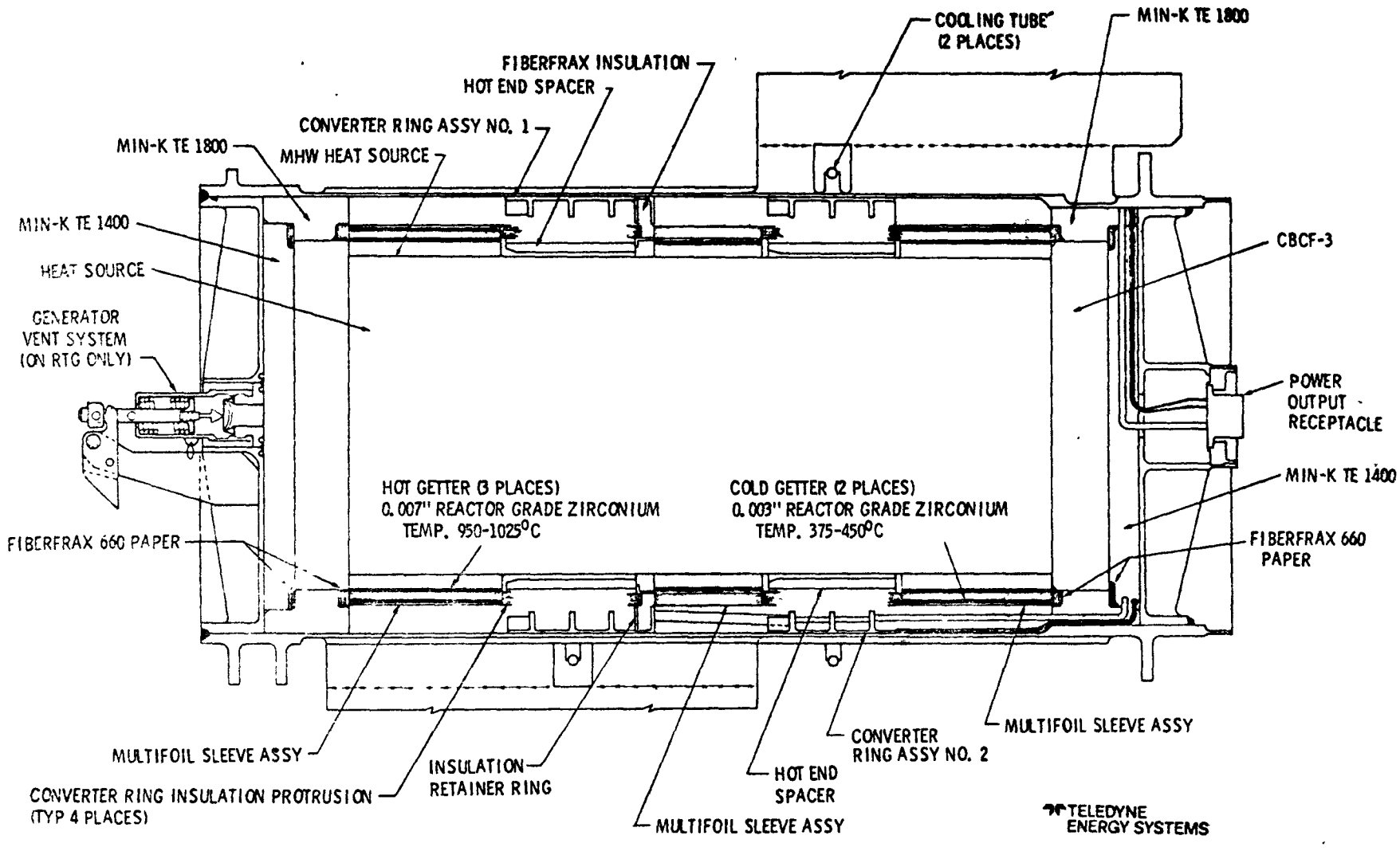

FIGURE I-3: SIG/GALILEO RTG CROSS SECTION

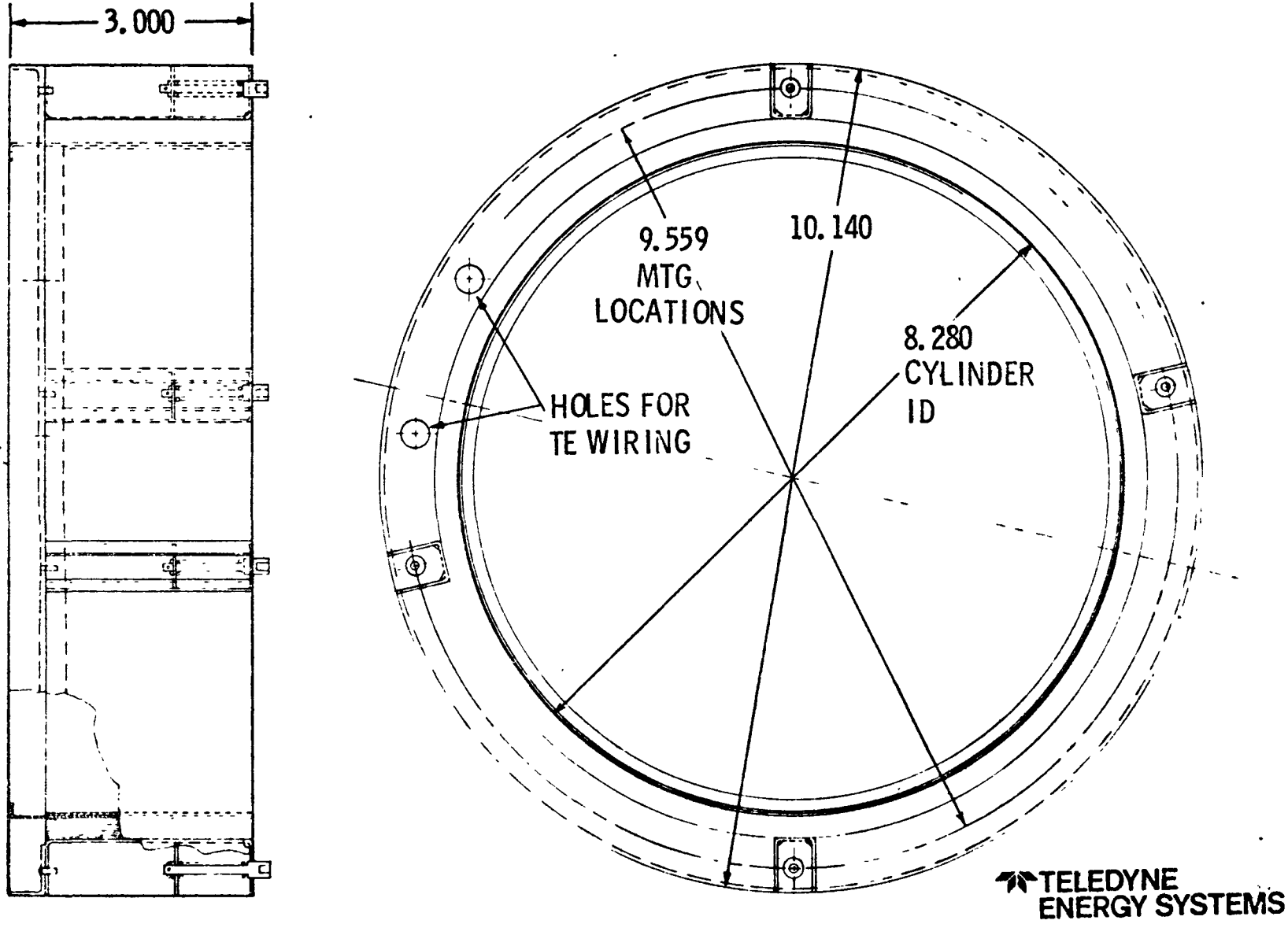

FIGURE I-4: MULTIFOIL INSULATION ASSEMBLY (CENTER SECTION-END SECTIONS SIMILAR)

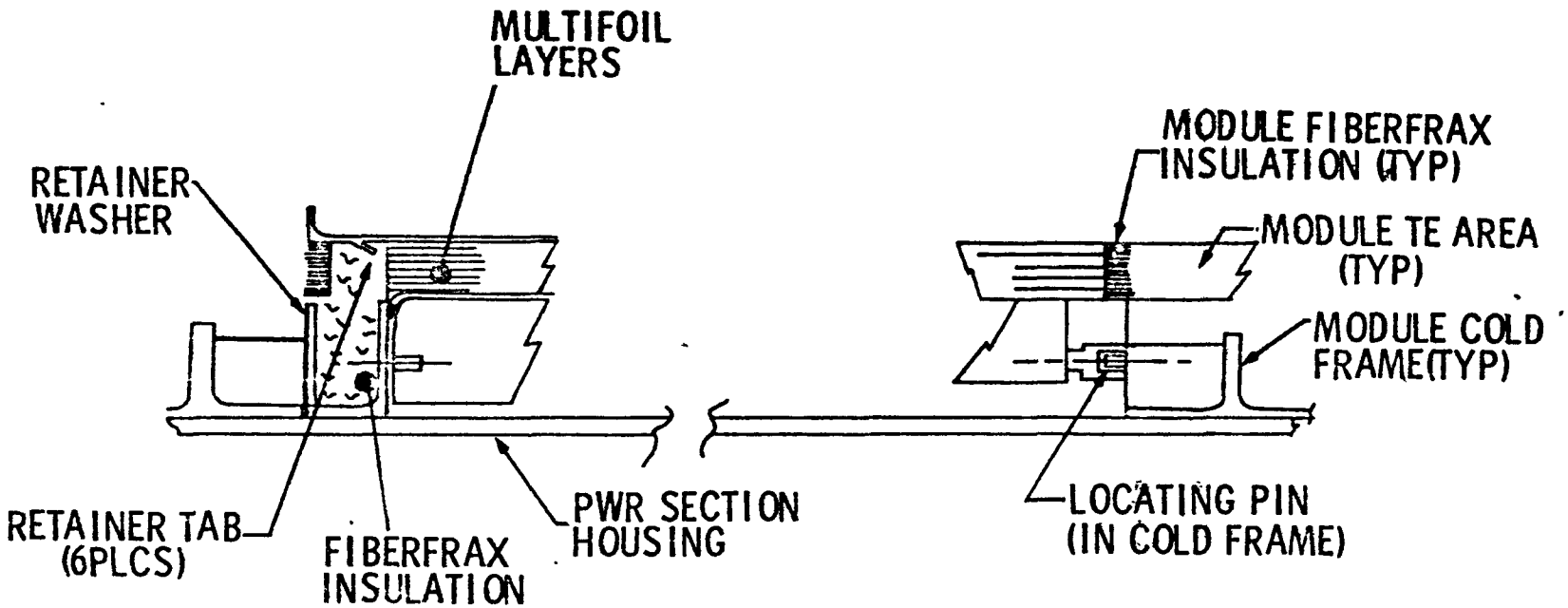

TELEDYNE
ENERGY SYSTEMS

FIGURE I-5: MULTIFOIL/3M MODULE INTERFACE DETAILS

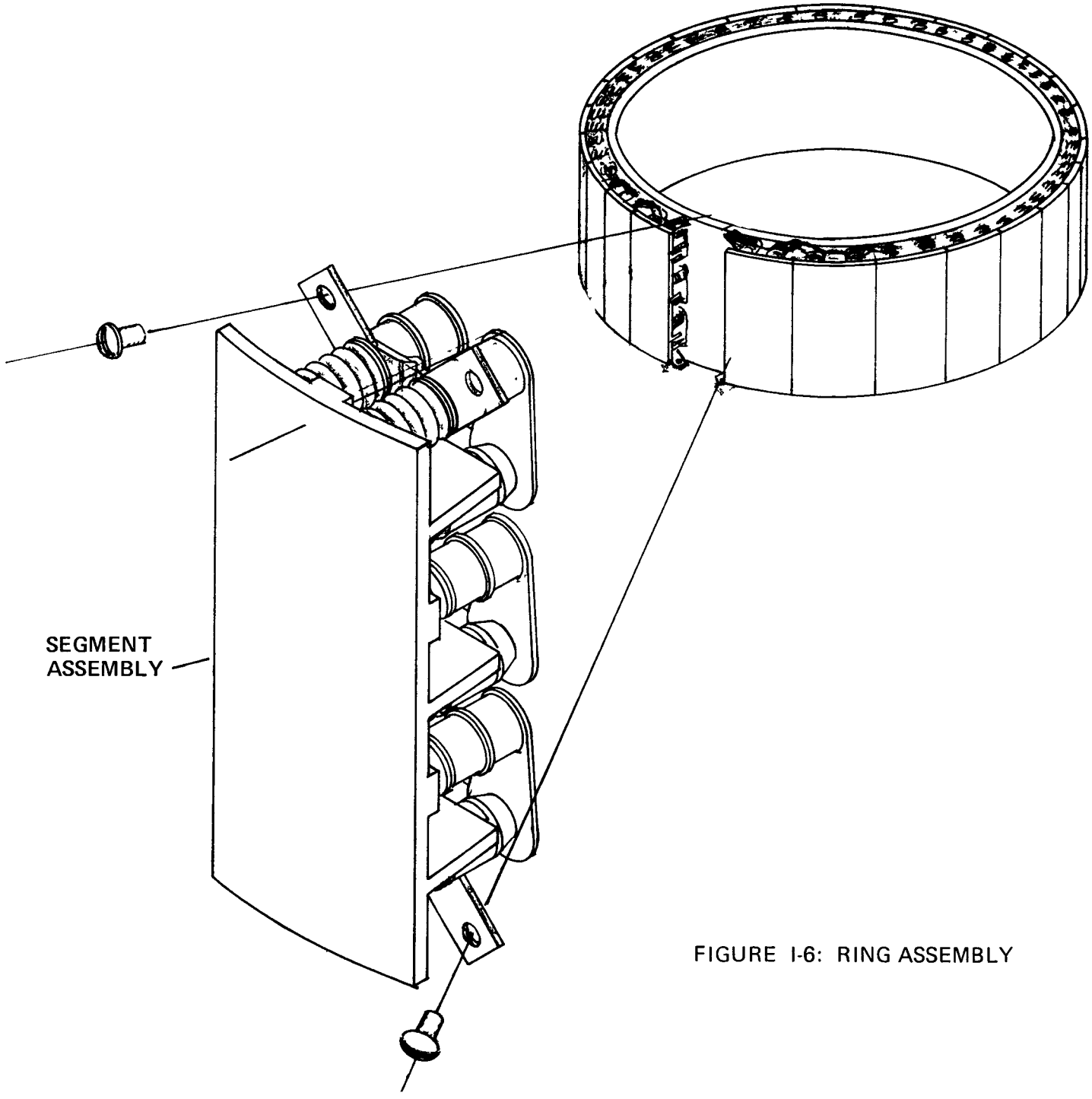

FIGURE I-6: RING ASSEMBLY

Detailed Description of Segment (Continued)

Hot Current Strap: The hot current strap is a sculptered "H" configuration made of Molybdenum, .068 inches thick. The hot side of the strap is sprayed with an .015 inch thick coating of Al_2O_3 to act as the hot side dielectric. Al_2O_3 is known for its long term high electrical resistance.

Al_2O_3 Pin: An alumina pin (Al_2O_3) is used to position the hot strap on the hot frame. The pin is .062 inches in diameter and .206 inches long. It extends from a blind hole in the hot frame, through the Platinum foil and hot current strap, and into a blind hole in the cap of the P-leg.

Gimbal: A conical shaped Molybdenum gimbal is seated into a mating socket of the hot current strap. The purpose of the gimbal is to provide mobility to the N-leg, thereby minimizing high local stresses while maintaining good thermal and electrical contact.

Conducting Disc: A .005 inch thick nickel foil is positioned between the gimbal and the N-leg to minimize thermal and electrical contact resistances while maintaining compatibility with the $GdSe_x$ N-leg material.

N-Leg Assembly: The N-leg itself is made of conventional $GdSe_x$ (.315 inch diameter x .300 inches long). The hot end of the leg is sputtered with a thin nickel coating for contact to the nickel foil. The cold end of the leg is sputtered with silver. A layer of Lead-Silver-solder (95-5) is then pretinned over the silver sputter. This leg assembly along with the Ni conducting disk is seated into a recess in the gimbal.

P-Leg Assembly: The P-leg material is Copper Silver Selenide. The outside dimensions of the P-leg are .260 inch diameter x .300 inches long. A .020 thick WRe cap is bonded to the hot end of the leg, while the cold end of the leg has a copper foil bonded to it. The leg is contained within an Astroquartz/Min-K H_2O slurry wrap to minimize sublimation.

Cold Frame Sub-Assembly: The cold frame sub-assembly consists of two smaller sub-assemblies, solder bonded together with a Lead-Tin-Silver (88-10-2) solder preform. (see Figure I-9)

1. Current Strap Sub-Assembly (Figure I-10)

A soldered assembly using the same Pb-Sn-Ag solder as mentioned above. The components are listed and described below:

Cold End Current Strap – These cold current straps are made of .0015 inch thick copper. There are seven layers diffusion bonded at the ends and corners. This maintains the flexibility requirements while offering an excellent conduction path for both electrical and thermal flow.

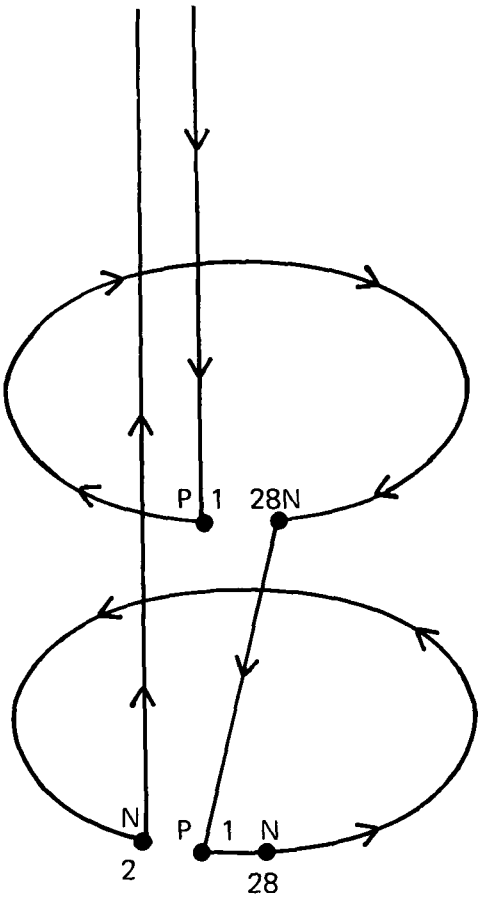

T/C RINGS ALIGNED

NOTES:

1. ARROWS SHOW DIRECTION OF CURRENT FLOW.
2. DIPOLE FIELDS OF TWO RINGS IN EACH RTE ARE OPPOSED.

FIGURE I-7 POWER CIRCUIT

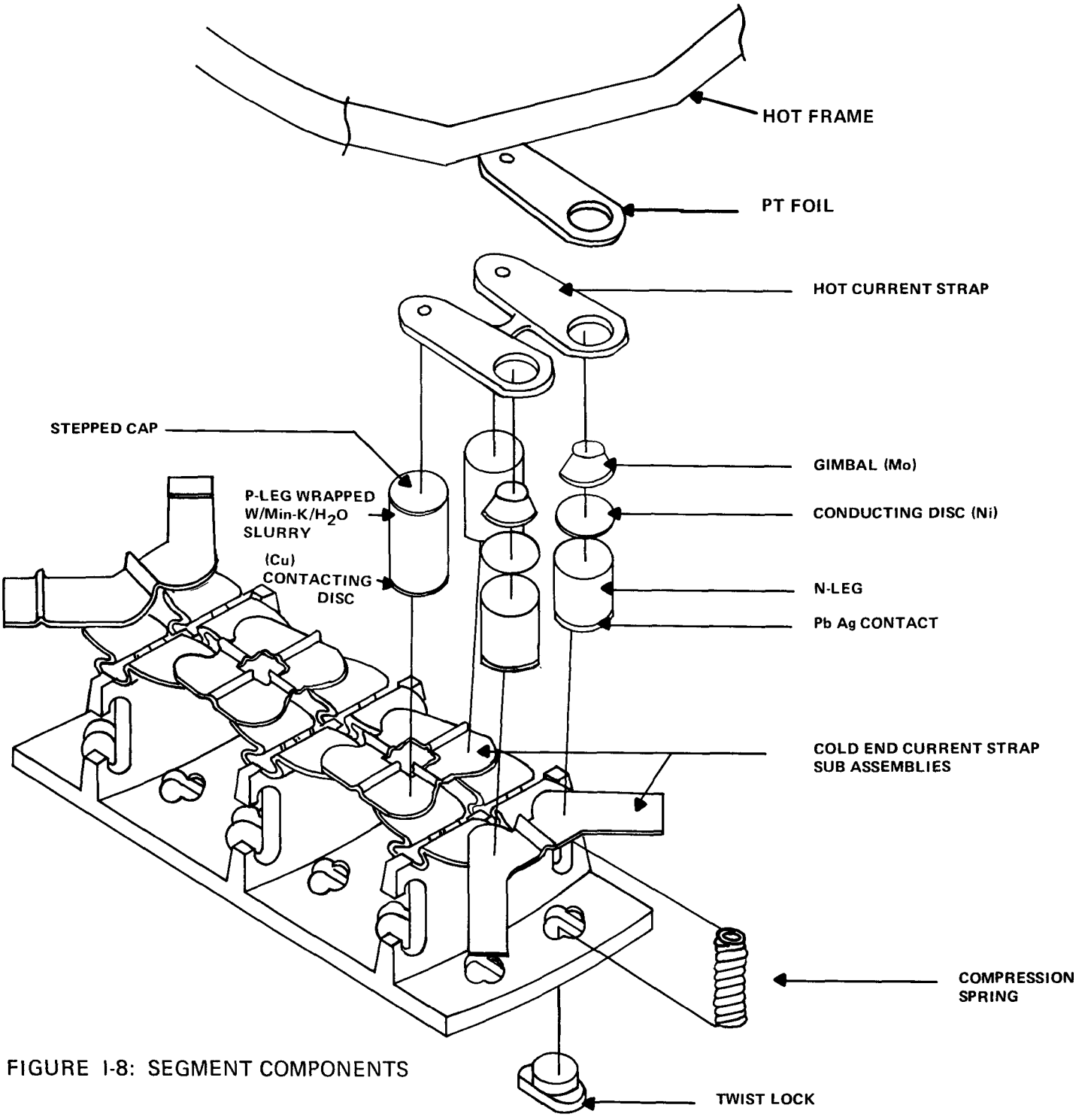

FIGURE I-8: SEGMENT COMPONENTS

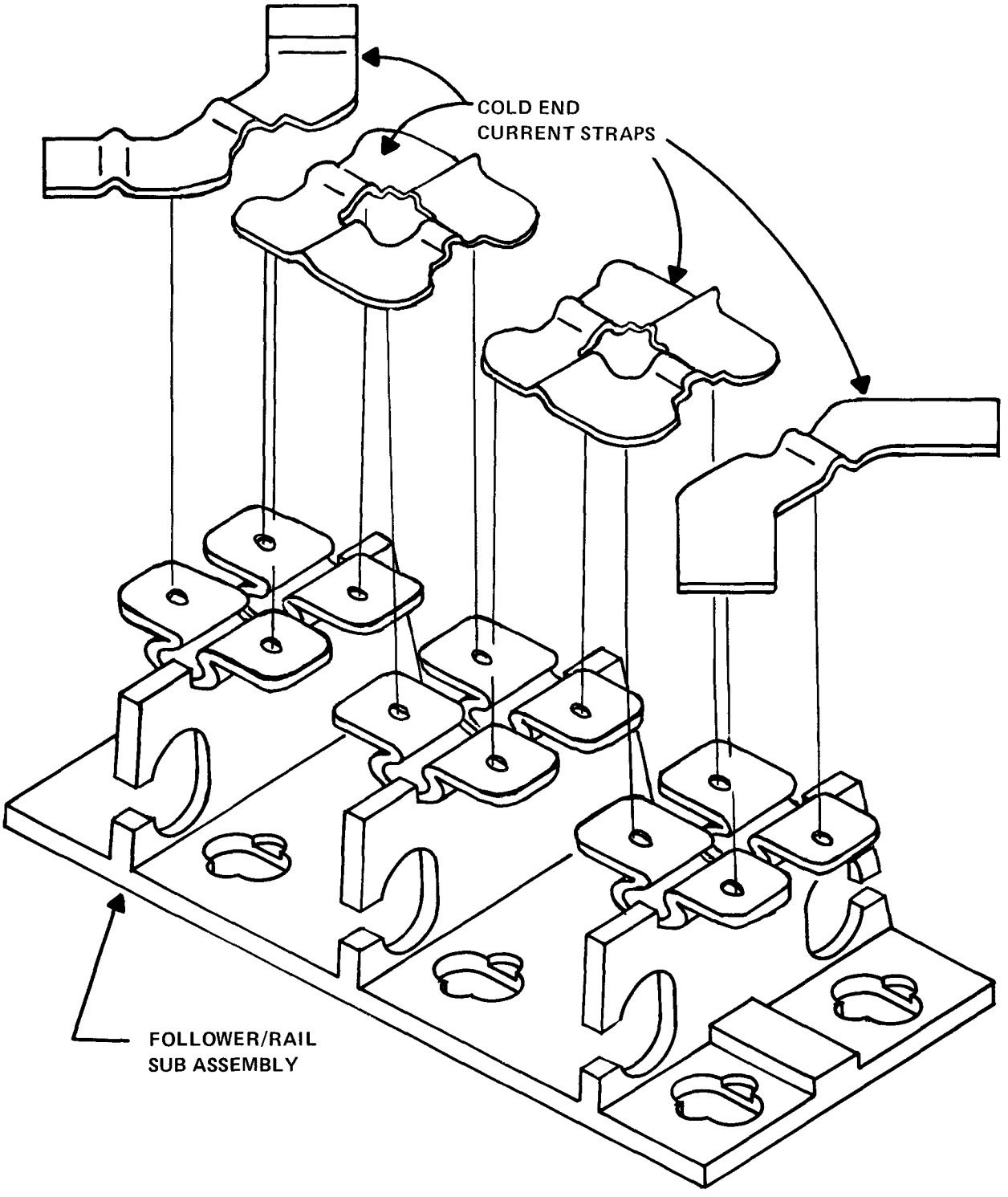

FIGURE I-9: COLD SEGMENT SUB-ASSEMBLY

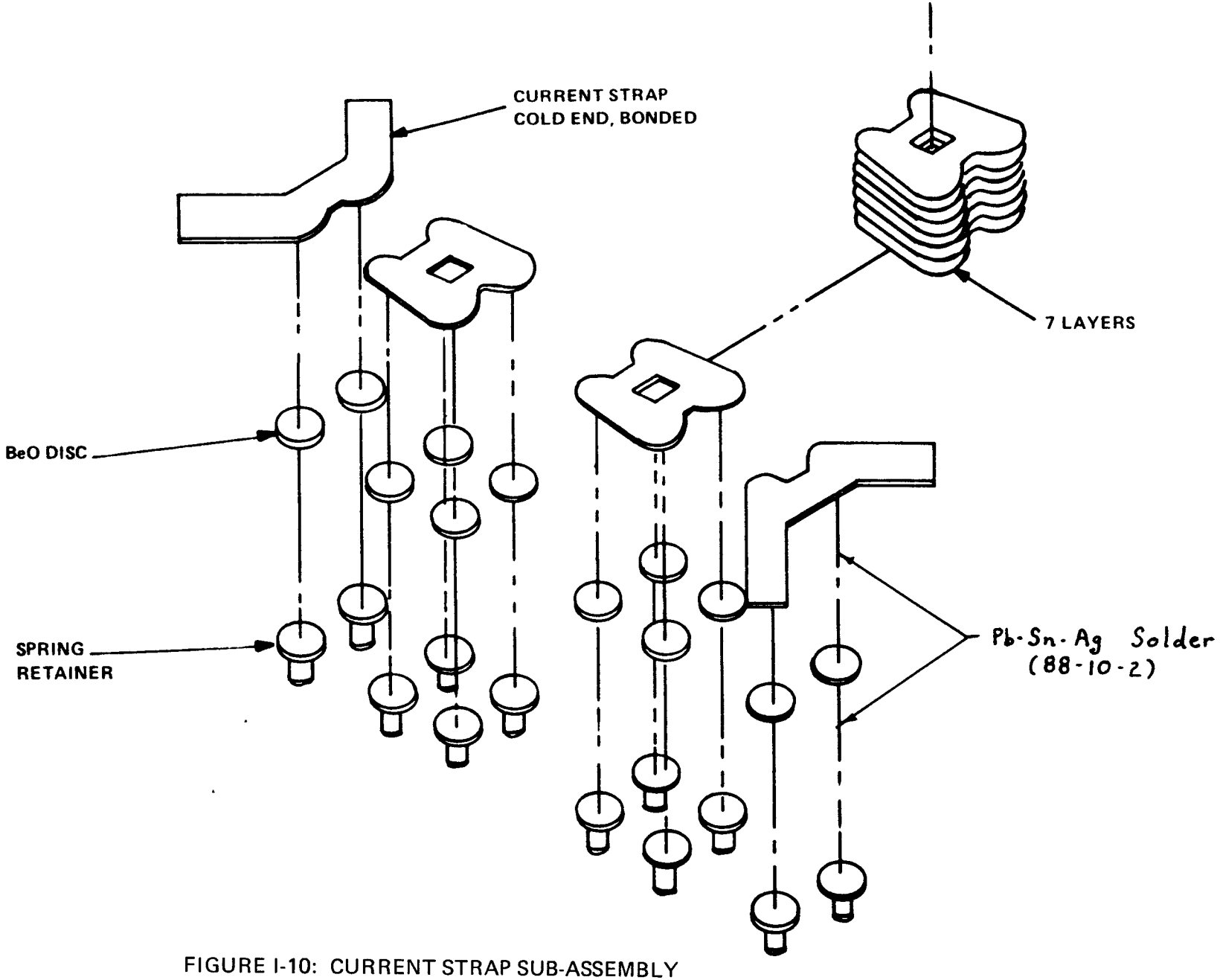

FIGURE I-10: CURRENT STRAP SUB-ASSEMBLY

BeO Disk – This disk of Beryllium Oxide serves as the cold end dielectric. The faces of the disk are metallized with MoMn and Ni plated. This provides for a soldering surface to decrease thermal resistance while maintaining the electrical insulation characteristics of the BeO.

Spring Retainer – A circular copper button which is soldered to the bottom of the BeO disk. This piece serves to locate and retain the top of the compression spring shown in Figure I-8.

2. Follower Rail Sub-Assembly (Figure I-11)

Consists of a soldered and riveted assembly with the following components:

Follower – 14 layers of .0015 inch thick copper, diffussion bonded in three places as shown in Figure I-11. This configuration is bent as shown to allow for flexibility while maintaining a low resistance heat path to the cold frame segment. The follower is soldered to the cold frame segment with Pb-Sn-Ag (88-10-2) solder.

Cold Frame Segment – This segment serves as the thermal path from the followers to the housing, as well as a locator and mount for the compression spring. It is fabricated of 6061 Aluminum. The top of the three ribs are nickel plated to provide a surface to solder the followers.

Copper Rivet – A copper rivet is installed through each follower and rail as a mechanical backup to the solder bond.

Compression Spring – This spring (17-7 PH Stainless Steel) is inserted between the cold frame housing and the spring retainer, under the legs. It supplies the radial force between the inner hot frame and the outer housing which holds the leg stacks in place. When the converter ring is assembled into the TES housing, these springs are over-compressed to allow for easy insertion. After the ring is in position, the springs are released. They force the cold frame segments radially outward until contact is made with the I.D. of the housing. At this time the pressure on the N-leg stack is 300 psi and the pressure on the P-leg stack is 150 psi.

Twist Lock – The twist lock is secured through holes in the cold frame segment. A button protrudes through the cold frame segment and into the bottom of the compression springs, locating and retaining their position. They are made of 6061 Aluminum and are nickel plated to prevent chip particle formation during installation.

Tin Foil – A .001 inch thick foil of tin is placed between the cold frame segments and the I.D. of the housing to minimize thermal contact resistance.

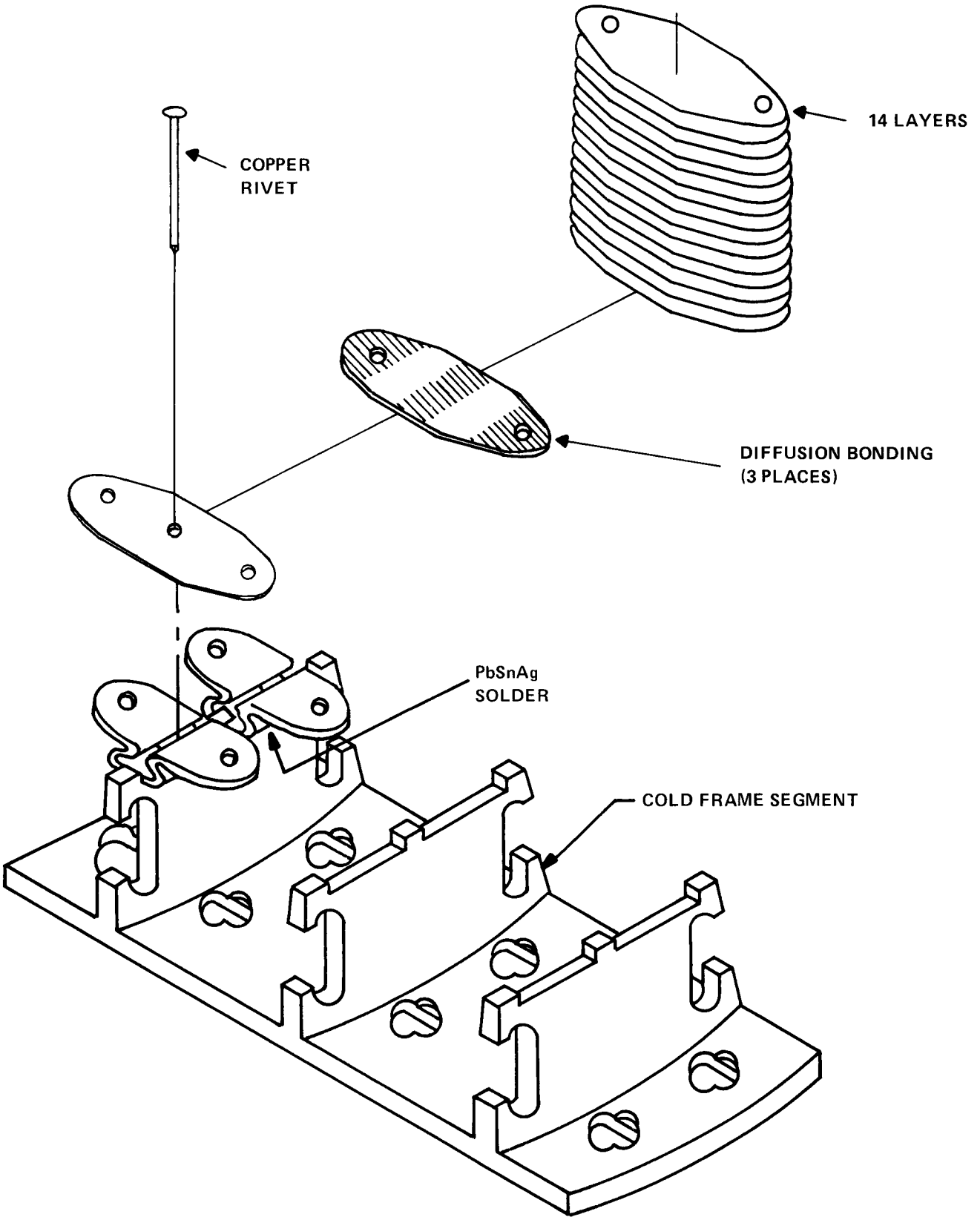

FIGURE I-11: FOLLOWER RAIL SUB-ASSEMBLY

ASSEMBLY TOOLING

The converter ring segments are assembled to the hot frame and secured by means of axial beam tooling. Figure I-12 depicts the means by which each segment is held in place on the POCO hot frame.

1. Components of a segment assembly are built up from the hot frame to the cold frame segments.

2. Pile compression bars are slid through the segments.

3. A cylindrical, aluminum, hot frame support is positioned inside the POCO hot frame.

4. Single rod bar clamps are positioned between the ends of the pile compression bars and the hot frame support.

5. By turning the nut on the ends of the bar clamps, each segment can be compressed in turn until the proper O.D. is obtained to allow for a slip fit into the TES housing.

After the entire converter ring is assembled (28 segments) in this manner, and positioned in the housing, the bar clamps are released and removed, along with the pile compression bars and hot frame support.

STATUS OF DESIGN AT TIME OF STOP WORK ORDER

As of February, 1979, all components of the thermoelectric converter were complete and signed-off. Table 2 lists the drawings that were completed, but not yet reviewed and signed-off.

The interface drawing prepared by TES has been reviewed and signed by 3M and TES.

Design of in-house equipment for manufacturing cold end hardware was completed and installed at ARO Industries. Fabrication had commenced in January.

Processing equipment was on order. Simulated housing, multi-foil insulation, and converter ring components had been fabricated. Assembly techniques were under investigation with a major practice assembly scheduled for early 1979.

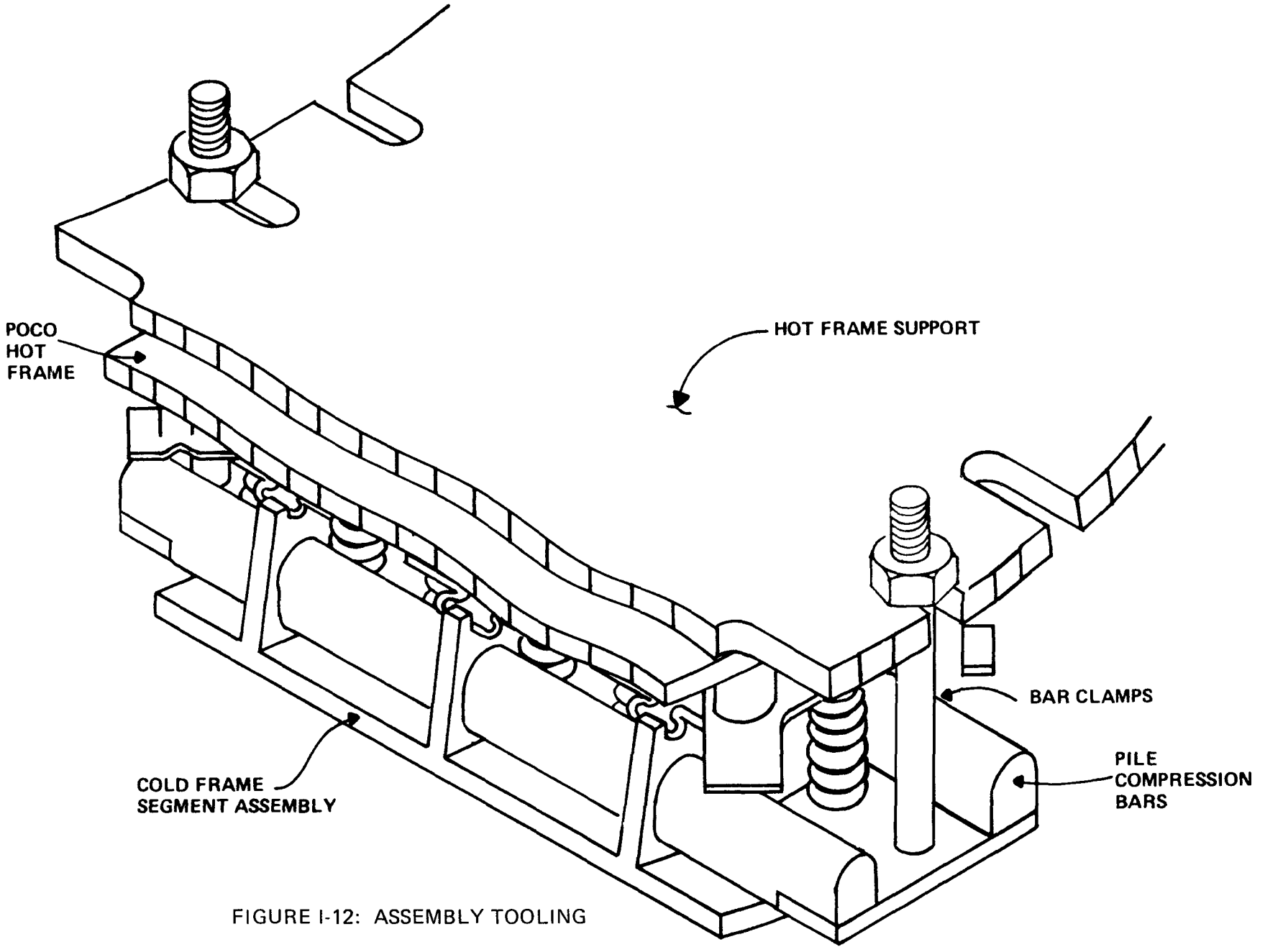

FIGURE I-12: ASSEMBLY TOOLING

TABLE I-2

SN-1 DRAWING LIST

Complete and Signed Off

Hot Frame	SG17-10161
Hot End Current Strap	SG17-10195
and Pt Foil	SG17-10218
N-Leg Mobility Gimbal	SG17-10179-P2
P-Leg Mobility	SG17-10171
N-Leg Assembly	SG17-10317
P-Leg Assembly	SG17-10316
Converter Ring Assembly	SG17-11152
Cold End Hardware	
Cold Frame Assembly	SG17-11178-P1
BeO Disk	SG17-10015-P1
Springs	SG17-11158
Twist Locks	SG17-10131
Converter Thermal Insulation	C-1032
Cold Frame – Housing Tin Interface	C-1055

Ready for Review

Module and Processing Container Details	Completion Date 12/4/78
Circuit Diagram SG17-11153	
Power Lead and Instrumentation Drawings	Completion Date 12/14/78
Module Assembly	Completion Date 12/8/78
Shipping Container and Shock Instrumentation	Completion Date 1/12/79

TABLE I-3

SN-1 Completed Drawings

Drawing Number	Title	Bill of Materials
SG17-11152	Converter Ring Assembly	X
SG17-10161	Spacer, Hot End	
SG17-10218	Foil, Hot Shoe	
SG17-10171	Pin	
SG17-10195	Strap, Current Hot End	
SG17-10316	P-Leg Assembly Wrapped	X
SG17-10314	Capped P-Leg	
SG17-10089-P1	Contacting Disc	
C-1033	Quartz Yarn	
SG17-10317	N-Leg Assembly	X
SG17-10312	N-Leg	
C-1060	Solder	
SG17-11178-P1	Cold Frame Assembly P1	X
SG17-11172	Follower-Rail, Sub-Assembly	X
SG17-11155	Cold Frame Segment	
SG17-11173	Rivet	
SG17-10156	Follower, Multi-Layer Bonded	
SG17-11177-P1	Foil, Cold Strap, Sub-Assembly P1	X
SG17-11177-P2	Foil, Cold Strap, Sub-Assembly P2	X
SG17-11177-P4	Foil, Cold Strap, Sub-Assembly P4	X
SG17-11175-P1, P2	Strap Current Foil End	
SG17-11176-P1	Strap Current Foil End	
SG17-10015-P1, P2	Disc, Insulating	
SG17-10157-P1, P2	Retainer, Spring	
SG17-11158	Spring Element	
SG17-10131	Twist Lock	
C-1032	Insulation, Sheet	
SG17-10179	Gimbal	

B. CONVERTER DESIGN ACTIVITY

By September, 1978, a majority of the piece part designs for SN-1 had been completed.

Extensive efforts were being directed to finalize the design of the flexible follower. It was felt that the new flexible follower design would provide the solution to the follower hang-ups encountered with the older sliding-follower version. The new design would incorporate 14 layers of .0015 inch thick copper into one flexible strap, bonded at the ends. The process to be used for bonding was not yet resolved. Although efforts to ultrasonically bond the copper looked promising, the developement was slow. Diffusion bonding was an alternative which appeared to not only give a good metallurgical bond, but would be relatively easy for initial manufacturing start-up. A glove box and diffusion bonding fixture were installed in September.

Methods of bonding the various cold end hardware components to each other were also being considered. After testing alternate solders, fluxes, and other bonding techniques, it was felt that the job could best be accomplished with a (88-10-2) Pb-Sn-Ag solder and special high temperature flux developed by Kester. The soldering was performed in special holding fixtures under a helium atmosphere. This soldering operation would follow the following sequence:

1. Solder six followers to cold frame segment

2. Solder BeO disk, cold end current strap, and spring retainer together.

3. Solder the sub-assemblies obtained in items No. 1 and No. 2 above, together.

In addition to the solder joint, it was requested that an additional back-up means of securing the followers to the cold rail segments be incorporated. This was accomplished by means of a copper nail which is pressed through the copper and rail, then formed over into a head in the far side. This then, acts as a rivet, providing the positive mechanical securement requested.

Efforts were also being made at this time to investigate alternative methods of producing a .001 inch layer of tin between the cold frame segment and housing. Tin foil (reference design) would be difficult to assemble without producing tears or wrinkles. While TES was requested to look at the feasibility of applying a 1 mil tin plating to the inside surface of the housing, 3M looked at methods of applying a 1 mil tin plating to the outside surface of the cold frame segments. Tinning the cold frame segments, however, had to be done <u>after</u> all soldering was completed because of the low melting temperature of tin. This procedure proved difficult due to the extensive masking required. Efforts to provide an efficient means of masking by several plating firms were dropped. The decision was made to continue to use the 1 mil tin foil.

On October 16, 1978, a preliminary design review was held. Changes to drawings, resulting from the review, were then performed. By late November, these drawings were complete and signed-off. A data package containing these prints was sent to DoE. Table I-3 provides a list of these drawings.

During October and November of 1978, the plans for a complete, full scale practice assembly were developed. Prototype converter components were designed and a simulated plexiglass housing was

ordered. The practice assembly, scheduled for early 1979, would be a valuable aid in investigating the following areas:

a) Development of manufacturing procedures
b) Particle generation
c) Insulation stuffing techniques
d) Instrumentation and power lead routing
e) Installation tooling
f) Circuit connection (riveting) techniques
g) Tin foil installation
h) Leg misalignment

By February, all components and equipment, required to proceed with the practice assembly, were on hand. However, the practice assembly was not initiated before the stop work order was issued.

On November 27-30, a design review was held at DoE, Washington, DC. Shortly following this meeting, most of the remaining designs concerning the converter assemblies and the processing and handling equipment were completed.

Short run production was set up to manufacture cold end hardware components (diffusion bonding, soldering) at ARO Industries. A number of tooling modifications were introduced to the bonding process at this time. These changes were primarily directed at insuring the reproducibility of quality bonds.

During the early part of 1979, short run production at ARO Industries had begun the initial phases of cold end hardware bonding. As the Galileo Contract close-out became apparent, however, activity at ARO Ind. was reduced. During March, 1979, the equipment at ARO was withdrawn back to Building 260 and reinstalled. The amount of hardware bonding has since been limited to technology efforts only.

3M/TES Interface Activity

Throughout the course of the Galileo Contract, frequent meetings between TES and 3M were held. These meetings served to maintain the necessary coordination between 3M and TES on the interfacing issues. In addition to the interface meetings, frequent telephone consultation took place on topics of mutual concern.

The initial meetings in June and July of 1978 were aimed at confirming dimensional parameters and resolving any interface problems between the converter rings and the multi-foil insulation can to be placed between them.

The following list relates the problem areas that surfaced and were resolved during the program:

1. Hot Frame:
   - Dimension information on hot frame was supplied to TES
2. Cold Frame:
   - Dimensional information supplied
   - TES requires 16 RMS finish on cold frame segment
   - TES supplied coordinate axis system to be used for the generator. 3M will position the converter ring assemblies with the No. 1 segment centered on the x + axis (see Figure I-13)
   - Locating pins between the cold frame segments and the housing will be left out initially. They will be added if required for additional stabilization during vibration.
   - Design for two locating pins between the converter ring and multi-foil gussets was completed. The two pins (.032" dia.) would be located in raised bosses of the cold frame segments, 180° apart on a ring. They would lock into special spring plungers located in the TES multi-foil gussets.
3. Foil interface:
   - TES requires .001 inch thick foil of 100% Sn between the cold frame segments and the housing. Tin plating was investigated but did not prove to be a viable alternative.
4. Instrumentation and Power Leads:
   - Gauge and length of wire supplied to TES
   - Orientation of instrumentation wires within the generator were determined.
   - Insulation over wires determined
   - T/C locations determined
   - Power lead runs were defined as running along the x + axis. TES initially recommends a spiral winding to prevent a dipole formation. This was later determined to be unnecessary. The current path of converter ring No. 1, however, must run opposed to the current path of ring No. 2 for the reason mentioned above.

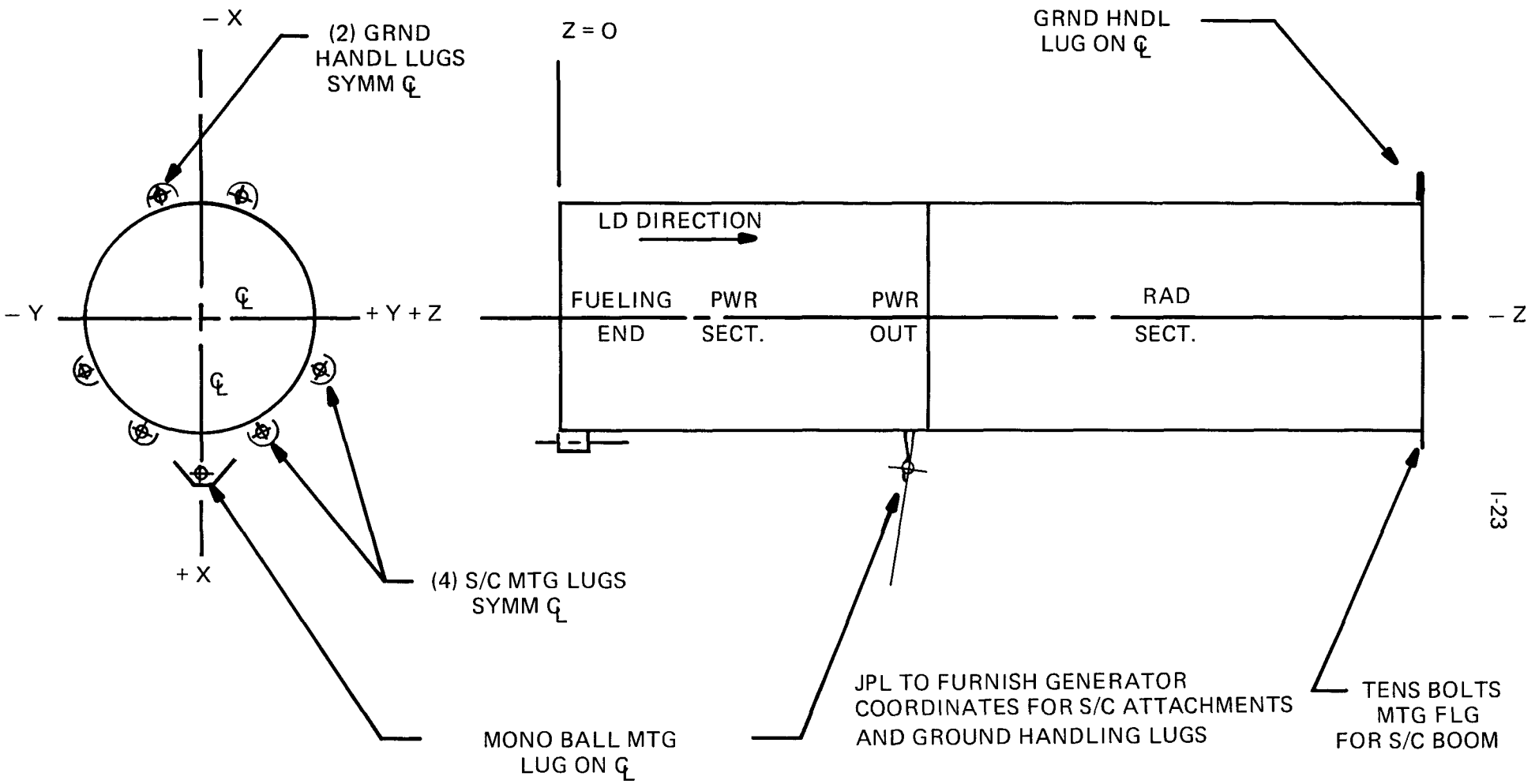

FIGURE I-13: GENERATOR GEOMETRIC DATA SHEET

5. Generator Housing:

   - A step in the I.D. of the housing would prevent the use of the presently designed installation tooling. TES agreed to move the step closer to the power end to allow room for 3M tooling.

6. Auxiliary Cooling Tubes:

   - 3M recommended the location of the auxiliary cooling tube connections.

7. Insulation:

   - The type of insulation between the multi-foil ring and the converter rings, and the assembly procedure related to the insulation were of extreme concern. Table I-4 was presented by TES to relate the various combinations of insulation and tooling gaps to the power output. It is evident from the table that the tooling gaps that must be filled with insulation should be kept to a minimum. 3M redesigned the assembly tooling to provide for 1/8 inch gap in three places, and a 3/8" maximum gap in one place. This was accomplished by going from a double rod clamp (No. 4-40) to a single rod clamp (No. 10-32).

8. Shipping and Processing Container:

   - Dimensional information by TES verified on housing fin O.D.
   - 3M agreed to mount the housing to the processing container from the fuel end rather than the power end.

TABLE I-4

Tooling Gap Effect on Performance

Insulation	Fiberfax (4 Places)				M.F. on Outer Region. CBCF-6/ Min-K Middle 1/8" Fiberfax	CBCF-6/Min-K Throughout (ideal case)
Gap	0	1/16"	1/8"	1/4"		
Power (Watt)	230.5	229.5	228.4	226.3	217.7	216
ΔQ	0	10.5	21	42		

Insulation	Fiberfax – 3 Places / CBCF-6/Min-K – 1 Place		
Gap	1/16"/1/2"	1/8"/1/2"	1/4"/1/2"
Power (Watt)	223.7	222.9	221.4

C. DESIGN DOCUMENTATION

This section lists the various design related documentation that was completed during the contract.

Design Drawing

Table I-5 lists the design drawings which were completed and signed-off for the SN-1 converter, along with the additional designs which were completed but did not reach the final sign-off stage before the stop work order.

Specifications and Procedures

Those engineering specifications and procedures that were completed and issued are shown in Tables I-6 and I-7 as follows:

Table I-6 — Engineering Specifications — Raw Materials

Table I-7 — Manufacturing Standards (those without dates were not completed)

Design Analysis

This section lists some of the significant analysis reports that were used in support of the converter design. These attachments will be found in the back of this section.

Attachment 1	Assembly Tooling Options
Attachment 2	Spring Characteristics of Follower with Increased Thickness
Attachment 3	Assembly of Cold End Hardware
Attachment 4	Compliant Follower Spring Force
Attachment 5	Cold End Hardware Spring Force
Attachment 6	Determination of Stress on N and P Legs
Attachment 7	Load Relaxation in Springs
Attachment 8	Weight and Exposed Surface Area of Cold End Copper Hardware
Attachment 9	SN-1 Weight Analysis
Attachment 10	Initial Phases of Axial Stress on N and P Legs
Attachment 11	Copper Stiffening During Diffusion Bonding
Attachment 12	Reproducibility of Cold End Hardware ΔT

TABLE I-5

SN-1 Completed and Approved

Drawing Number	Title	Bill of Material
SG17-11152	Converter Ring Assembly	X
SG17-10161	Spacer, Hot End	
SG17-10218	Foil, Hot Shoe	
SG17-10171	Pin	
SG17-10195	Strap, Current Hot End	
SG17-10316	P-Leg Assembly Wrapped	X
SG17-10314	Capped P-Leg	
SG17-10089-P1	Contacting Disc	
C-1033	Quartz Yarn	
SG17-10317	N-Leg Assembly	X
SG17-10312	N-Leg	
C-1060	Solder	
SG17-11178-P1	Cold Frame Assembly P1	X
SG17-11172	Follower-Rail, Sub-Assembly	X
SG17-11155	Cold Frame Segment	
SG17-11173	Rivet	
SG17-10156	Follower, Multi-Layer Bonded	
SG17-11177-P1	Foil, Cold Strap, Sub-Assembly P1	X
SG17-11177-P2	Foil, Cold Strap, Sub-Assembly P2	X
SG17-11177-P4	Foil, Cold Strap, Sub-Assembly P4	X
SG17-11175-P1, P2	Strap Current Foil End	
SG17-11176-P1	Strap Current Foil End	
SG17-10015-P1, P2	Disc, Insulating	
SG17-10157-P1, P2	Retainer, Spring	
SG17-11158	Spring Element	
SG17-10131	Twist Lock	
C-1032	Insulation, Sheet	
SG17-10179	Gimbal	

Complete But Not Signed Off

SG17-11151	Module Assembly, SN-1
SG17-11150	Module and Shipping Container Assembly
SG17-11154	Heater Assembly
SG17-11165	Flange, Mounting
SG17-11166	Cover, Shipping Container
SG17-11169-P1, P2	Protector, Mounting Surface
SG17-11180	Heater Block Assembly
SG17-11186	Plate, Clamping
SG17-11185	Heater Support
SG17-11184	Insulator, Support
SG17-11183	Pad, Insulation
SG17-11182	Bracket, Mounting Heater Block
SG17-11181	Heater Block
SG17-11167	Stand-Off, Module
SG17-11168	Eyebolt, Lifting

TABLE I-6

ES's

1000 Series - Raw Materials

1001	POCO Graphite (AXF-Q1) – 12/21/78
1002	Platinum Foil - 99.95% Pure – 12/21/78
1003	Aluminum Oxide – 12/21/78
1004	Molybdenum
1005	Stainless Steel (17-7 PH) – 12/21/78
1006	Aluminum (2024 T351) – 12/21/78
1007	Aluminum (6061 T6)
1008	Beryllium Oxide – 12/21/78
1009	Tungsten - 25 Rhenium - Cold Worked – 12/21/78
1010	Nickel - UNS No. 2201 - Annealed – 12/21/78
1011	Pb-Sn-Ag Solder – 12/21/78
1012	Pb-Ag Solder – 12/21/78
1013	ETP Copper - Alloy No. 110 - Hard – 12/21/78
1015	Astroquartz Fiber – 12/21/78
1016	Min-K 1800 Insulation – 12/21/78
1017	Thermocouple Wire (Pt and Pt/10% Rh) – 12/21/78
1018	Fiberglass Sleeving – 12/21/78
1019	Gadolinium – 12/21/78
1020	Selenium – 12/21/78
1021	Copper – 12/21/78
1022	Silver – 12/21/78
1014	OFE Copper – 12/21/78
1023	Tantalom
1024	Fiberfrax Hi-Fi 660 Paper – 12/21/78
1025	Fiberfrax H-Blanket – 12/21/78
1026	Nickel Foil – 5/9/79
1027	Iron Foil – 5/9/79

TABLE I-7 – Manufacturing Standard Instructions

Assembly Method			Processing			Cleaning Method		
MSI	3001	Thermoelectric Assembly 9/27/77	MSI	2001	Thermoelectric Module Outgassing and Heat-Up Procedure – 8/17/77	MSI	1001	Thermoelectric Module Cleaning Procedure 9/27/77
	3002	Cold Strap Assembly 9/27/77		2003	Outgassing Procedure for Thermal Insulation used in Thermoelectric Modules – 9/27/77		1002	Cleaning Procedure for T/C Wires and Heater Leads – 9/27/77
	3003	Feedthrough Assembly		2004	Outgassing Procedure for POCO Graphite Hot Frame and Heater Block Pieces – 9/27/77		1003	Thermoelectric Module Cold Frame Cleaning Procedure – 9/27/77
	3005	Brazing Procedure – 9/27/77		2005	Processing Fiberglass Sleeving Insulation		1004	Cleaning Method for Metal Parts
	3006	Determining Length of Follower Spring 11028 – 9/27/77		2006	Thermoelectric Module Outgassing Heat-Up and Backfill – 4/13/78			
	3007	Riveting End Current Straps 4/18/78		2012	Outgassing Procedure for POCO Graphite Hot Frame and Heater Block Reworked Pieces – 4/5/78			
	3008	Diffusion Bonding Followers 10/20/78		2008	P-Leg Processing Procedure 10/17/75			
	3009	Folding of Current Straps and Bonding Procedures		2009	N-Leg Processing Procedure 4/28/76			
	3010	Procedure for Soldering Complete Current Straps and Cold End Straps to Follower and Rail Assembly		2013	Outgassing Procedure for Thermal Insulation			
	3011	Soldering of Spring Retainers to Current Straps		2014	Thermoelectric Converter Outgassing and Heat-Up Procedure			
	3012	Procedure for Soldering Follower to Rail		2015	Thermoelectric Module Outgassing and Heat-Up Procedure – 12/12/78			
	3013	Procedure for Solder Spring Retainers, BeO Discs to Cold End Straps						
	3020	Folding of Follower Foils						
	3021	Folding of Current Strap Foils (4-Plex)						

TABLE I-7 – Manufacturing Standard Instructions (Continued)

Assembly Method		Processing	Cleaning Method
3022	Folding of Current Strap Foils (P-End)		
3023	Folding of Current Strap Foils (N-End)		
3024	Rivet Forming		
3025	Procedure for Diffusion Bonding of Follower Foils		
3026	Diffusion Bonding of Current Strap Foils (4-Plex)		
3027	Diffusion Bonding of Current Strap Foils (P-End)		
3028	Diffusion Bonding of Current Strap Foils (N-End)		
3030	Instrumentation of "P" Legs 4/30/79		

D. ATTACHMENTS TO SECTION I

ATTACHMENT 1

Assembly Tooling Options

A number of alternatives for assembly tooling have been investigated. The method which appears to be the optimum design for reducing the tooling gap is the single rod clamp. This method is very similar to the original design. However, instead of two (2) No. 10-32 rods for clamping, only one (1) No. 10-32 rod is used. This allows positioning of the clamps directly adjacent to each other. There is now no need to allow additional clearance for the nuts. The tooling gap which can now be expected has been reduced from .5 inches to .28 inches. The remaining tooling options produce a tooling gap from .38 inches to .45 inches.

In addition to the decrease in tooling gap, the following other advantages have been noted:

1. Reduced labor in assembly:

   The single rod clamps reduce the number of nuts that have to be assembled and disassembled from 112 to 56.

2. Ease in handling:

   Other tooling options that were investigated required the use of No. 4-40 size nuts and rods. This is a very difficult size to work with during assembly with gloves. The No. 10-32 size of the single rod clamp eliminates this problem.

3. Reduced stress on legs:

   When assembling and disassembling the double rod clamp tooling, the four rods and nuts for each segment must be alternately turned. This causes stresses on the legs in four directions. The use of single rod clamps reduce the number of directional stresses to two.

Tooling, which makes use of the single rod clamp, was ordered for SN-1. An additional set of tooling was ordered for practice assembly.

Designs have also been drawn and parts are on order to use the single rod clamp on M21 through M29. These will give sufficient data to determine if there are any problems associated with the use of this tooling method.

ATTACHMENT 2

Spring Characteristics of Follower with Increased Thickness

A test was conducted on the six-couple station with the compliant hardware and it was detected that the heat transfer through the follower was not as good as anticipated. One possible solution to this problem is to increase the layers of foil in the follower from fourteen (14) to sixteen (16) or eighteen (18), but with this increased thickness, the follower will get stiffer. If this stiffness would get too large, the follower would take up too much of the spring force and the stress on the legs would fall below the required value. Therefore, this attachment describes the results from tests to determine the spring characteristics of sixteen (16) and eighteen (18) layer followers.

Results

The results are in the form of two (2) graphs (Figures 2-1 and 2-2) which are a sixteen (16) and eighteen (18) layer follower displaced and returned to original position.

Note: Tension is positive, compression negative, and the directional sign follows Figure 2-3.

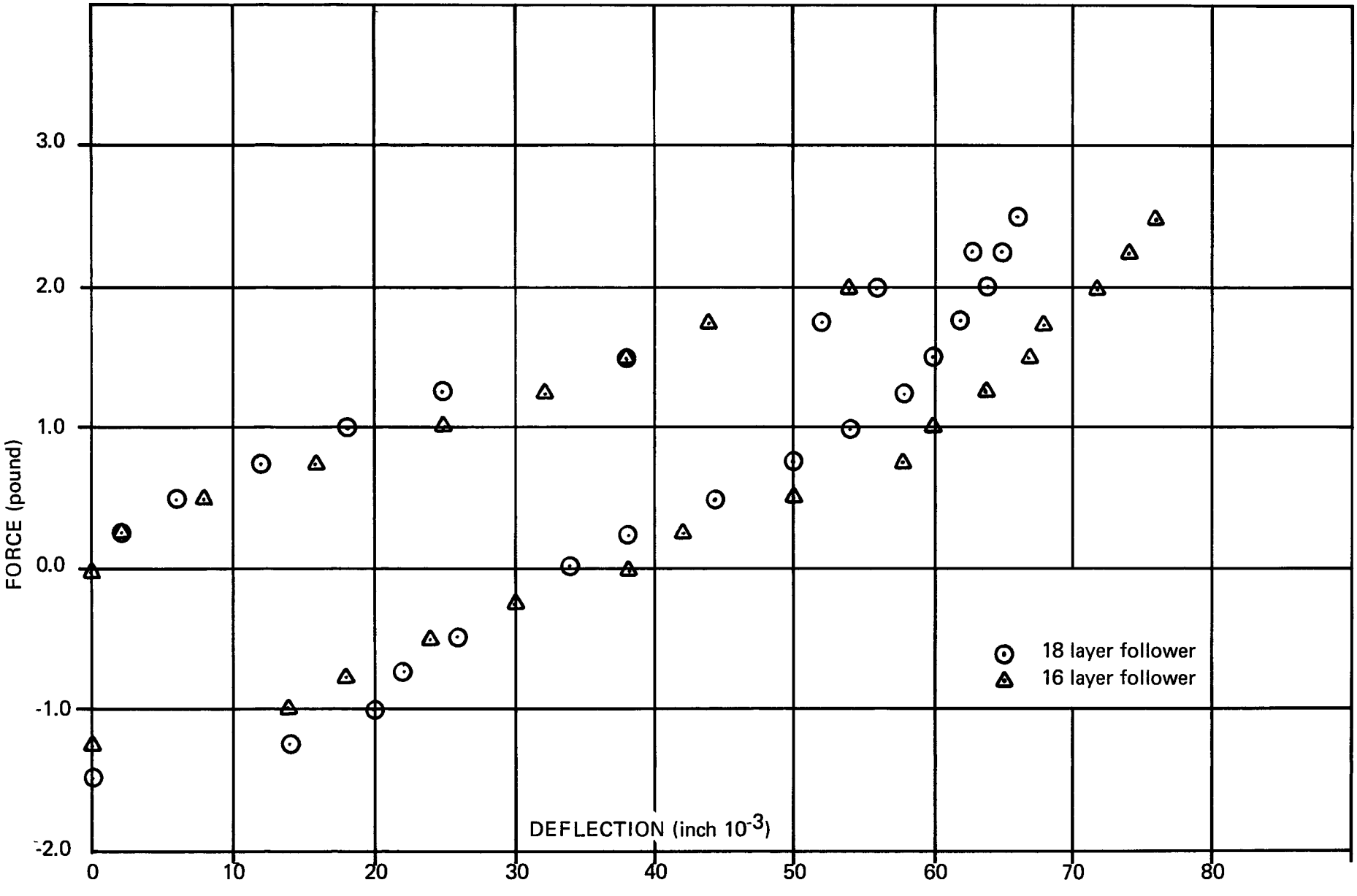

FIGURE 2-1: FORCE 'VS' DEFLECTION

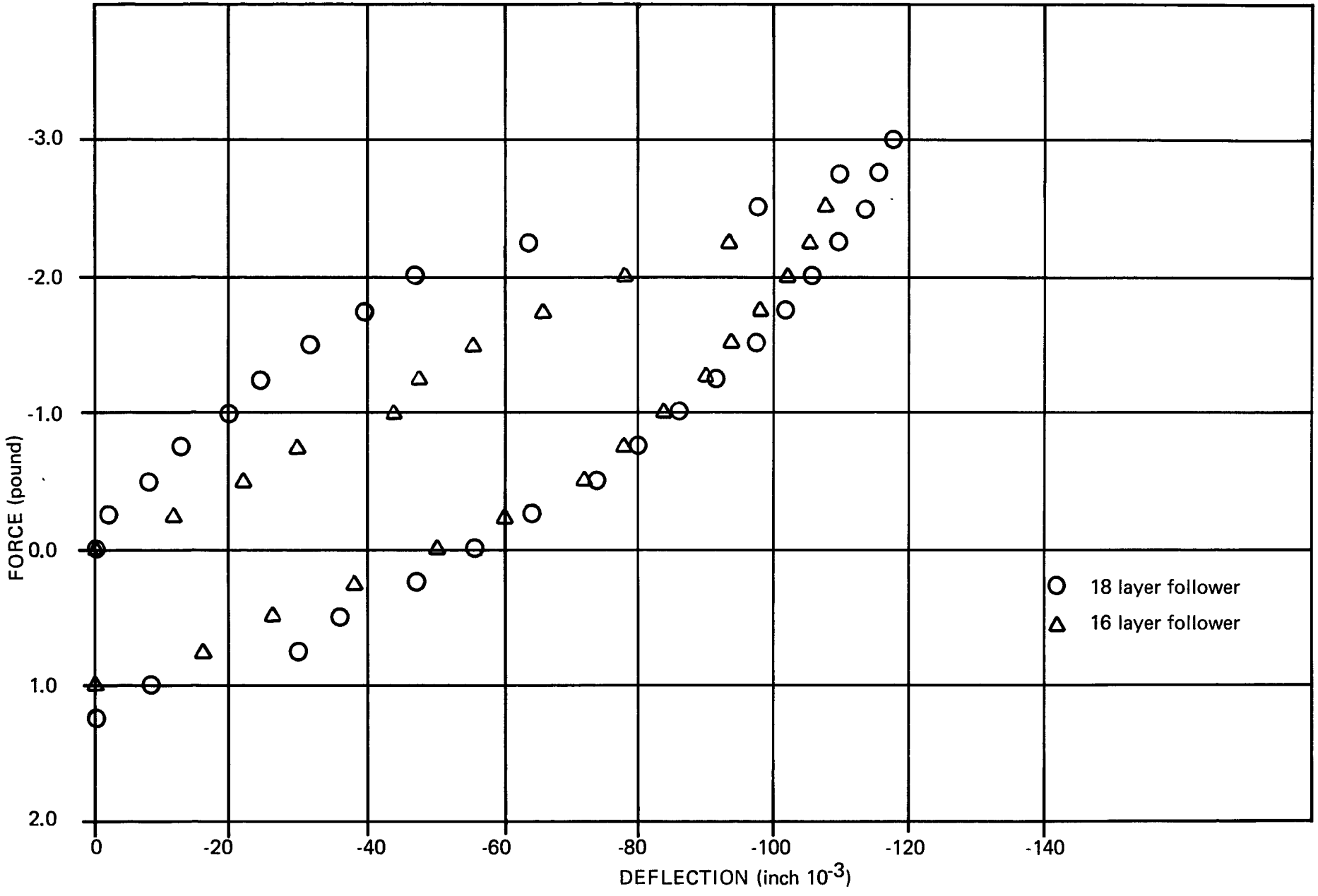

FIGURE 2-2: FORCE 'VS' DEFLECTION

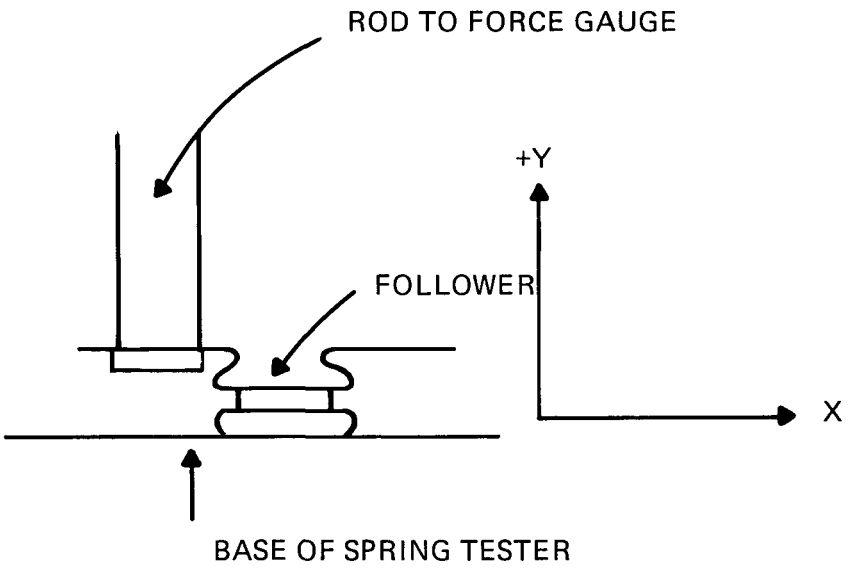

FIGURE 2-3

ATTACHMENT 3

Assembly of Cold End Hardware

The following is a procedure for the assembly of cold end hardware. Due to the complexity of the procedure, it was felt that an outline would tend to clarify any misunderstandings or uncertainties.

The procedure can be treated as a reference towards the final assembly specification. An alternative procedure has been included to delineate some options. Figure 3-1 should supplement the text.

Cold End Fabrication

A. Fabrication Procedure for Sub-Assembly No. 1

1. Reference
   - Diffusion bond cold end current straps consisting of seven (7) 1.5 mil copper foils that have been annealed and pre-stamped.
   - Bond sub-assemblies (each consisting of 2 end straps, 2 flexible straps, 12 metallized BeO discs and 12 copper spring retainers) with a Cu-Ag braze.
   - Sputter a thin coat of Ag onto the exposed surface of the spring retainers, masking off all other surfaces.
2. Alternative
   - Diffusion bond current straps as in reference procedure.
   - Electroplate the spring retainers with Ag.
   - Bond sub-assemblies as in reference procedure.

B. Fabrication Procedure for Sub-Assembly No. 2

1. Reference
   - Diffusion bond flexible followers, consisting of fourteen (14) 1.5 mil copper foils that have been annealed and pre-cut.
   - Drill holes for spring retainers into the followers.
   - Sputter a thin coat of Ag onto predesignated portions of each side of the followers.
   - Drill tapered pin holes into the tips of the rails.
   - Coat the cold frame segments with .5 mils of electroless Ni.
   - Electroplate the segments with 1.0 mil of Sn, then etch it away everywhere except on the undersides and on the tips of the rails.
   - Apply a thin film of Pb-Ag solder to the tips of the rails and to the sputtered portion of the undersides of the followers.

- Bond the followers to the rails, two followers at a time, with a special bonding fixture.
- Drive Cu ring-shank nails through the center of the followers and into the pin holes in the rails, using a special template for alignment.
- Bend the followers into their design configuration.

2. Alternative
   - Ultrasonically bond flexible followers.
   - Ultrasonically bond the followers to the tips of the rails.
   - Drill holes for spring retainers through the followers.
   - Drill tapered pinholes through the center of the followers and into the rails.
   - Drive Cu ring-shank nails into the pinholes.
   - Sputter a thin coat of Ag around the spring retainer holes on the topsides of the followers.
   - Bend the followers into their design configuration.

   Comment: There are two options on the cold end interface configuration for this procedure. A 1.0 mil tin foil at the interface is consistent with the above procedure. Also, by adding a preliminary step, the reference design could be implemented.

C. Joining the Two Sub-Assemblies

1. Reference
   - Using the spring retainers as the alignment tooling, set sub-assembly 1 onto sub-assembly 2, incorporating annular preforms of Pb-Sn-Ag solder between the spring retainers and the followers.
   - Clamp and bond the two sub-assemblies with a special fixture.

2. Alternative
   - Same as reference procedure except pre-apply the Pb-Sn-Ag solder directly to the individual sub-assemblies rather than use preforms.

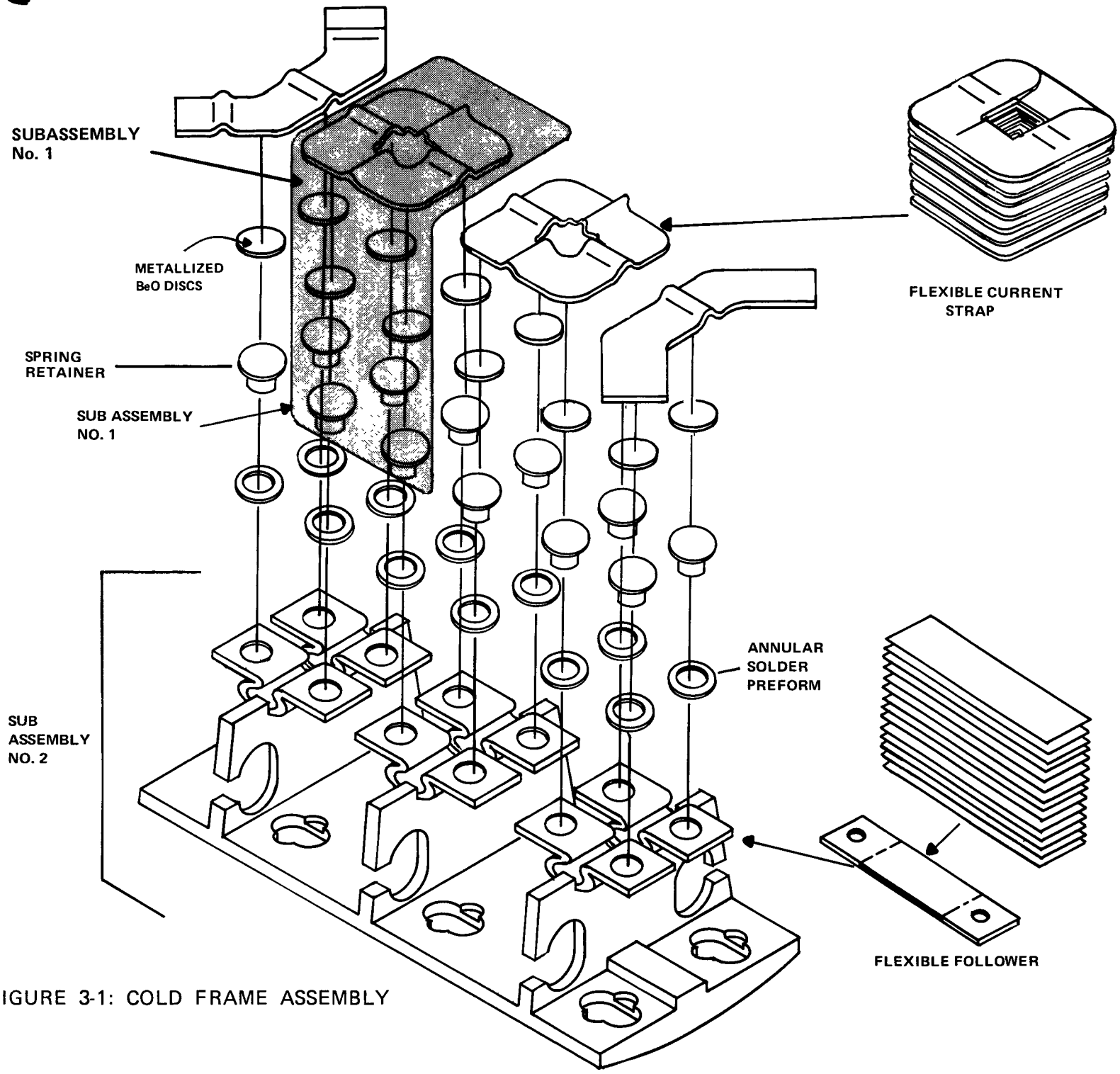

FIGURE 3-1: COLD FRAME ASSEMBLY

ATTACHMENT 4

Compliant Follower Spring Force

Tests were undertaken on the compliant followers to determine the spring force for deflection. The tests were done on a Chatillon Spring Tester and the deflection was measured by an optical comparator.

The results are presented in the form of the following which graphs can be summarized as:

Figure 4-1, 4-2, 4-4 – typical followers displaced and returned to original position to show hysteresis.

Figure 4-3 – typical follower put through a cycle of displacement in the position y (Figure 4-6), negative y, and returned to original position.

Figure 4-5 – oxidized follower displaced and returned to original position.

Figure 4-7, 4-8 – typical followers bonded to rail displaced and returned to original position.

Note: Tension is positive, compression is negative, and the directional sign follows Figure 4-6.

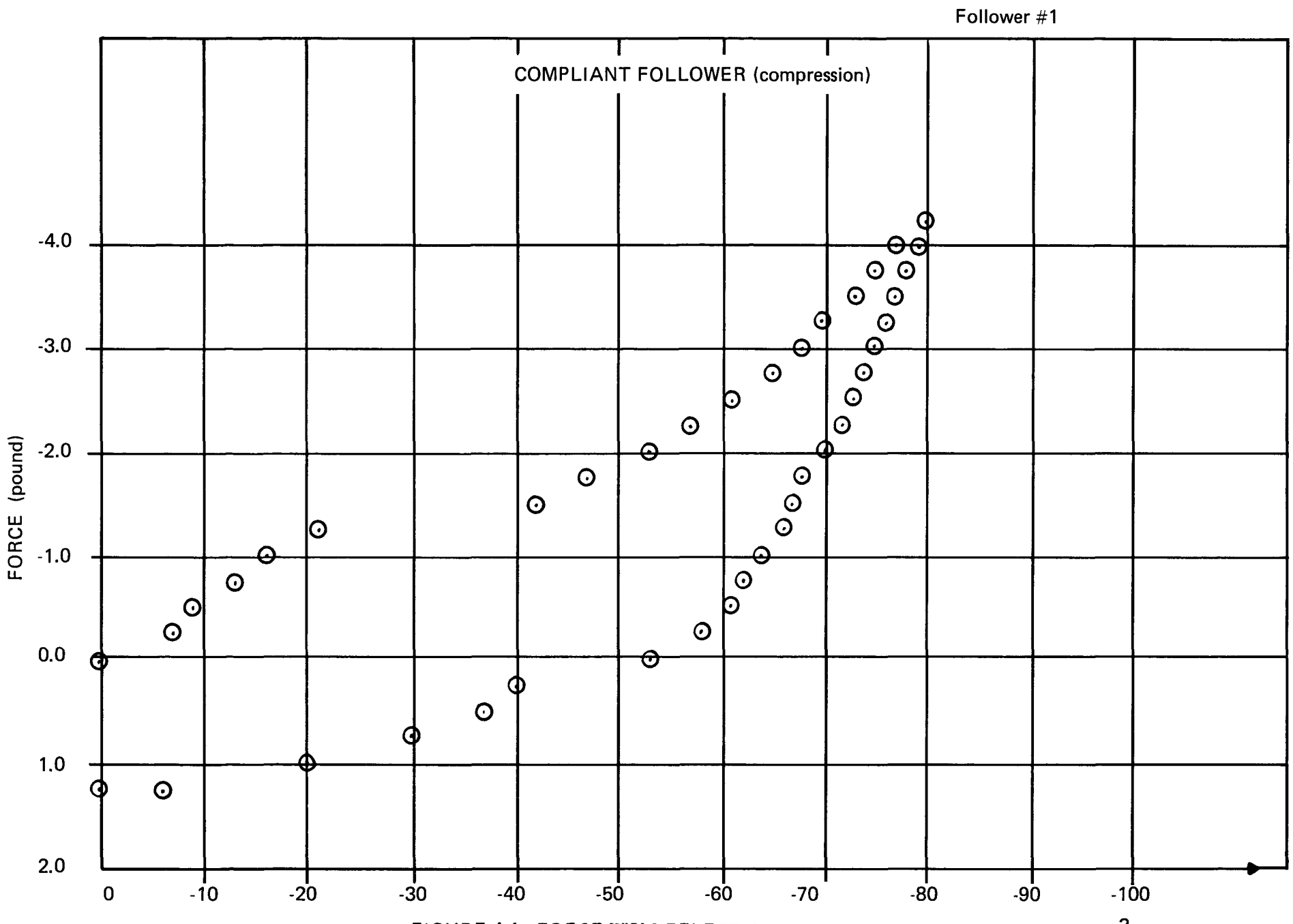

FIGURE 4-1: FORCE 'VS' DEFLECTION

follower #1

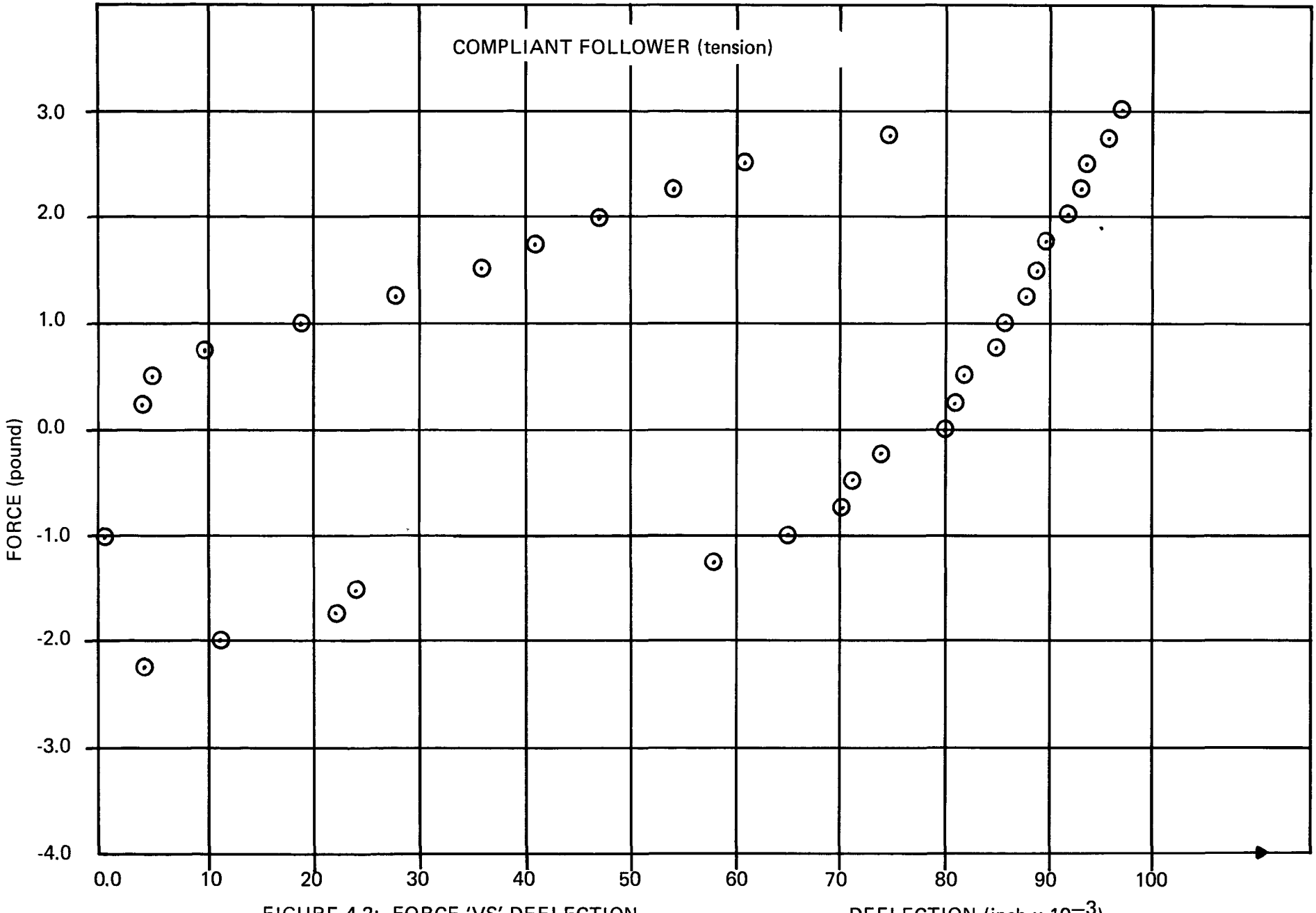

FIGURE 4-2: FORCE 'VS' DEFLECTION

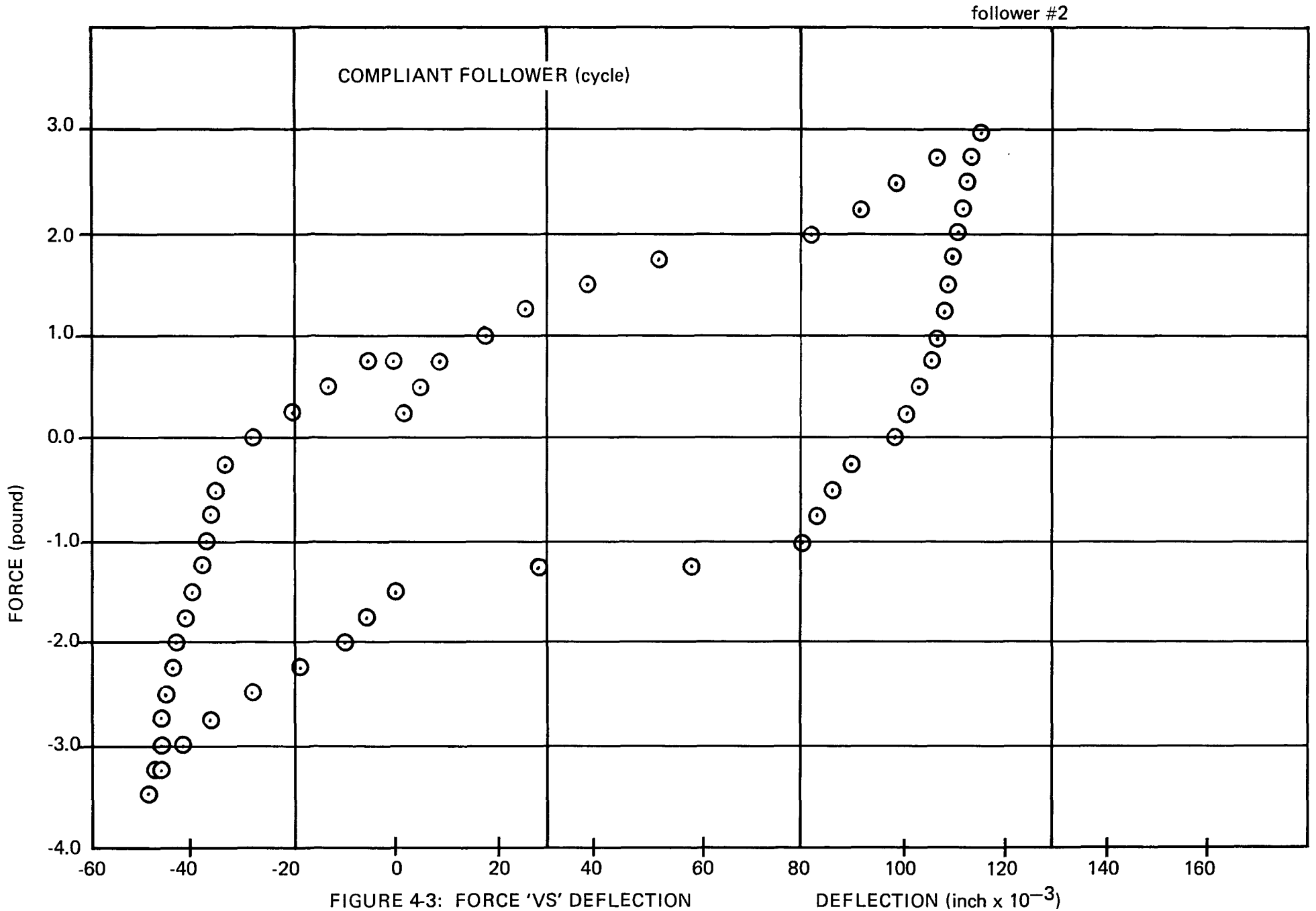

FIGURE 4-3: FORCE 'VS' DEFLECTION

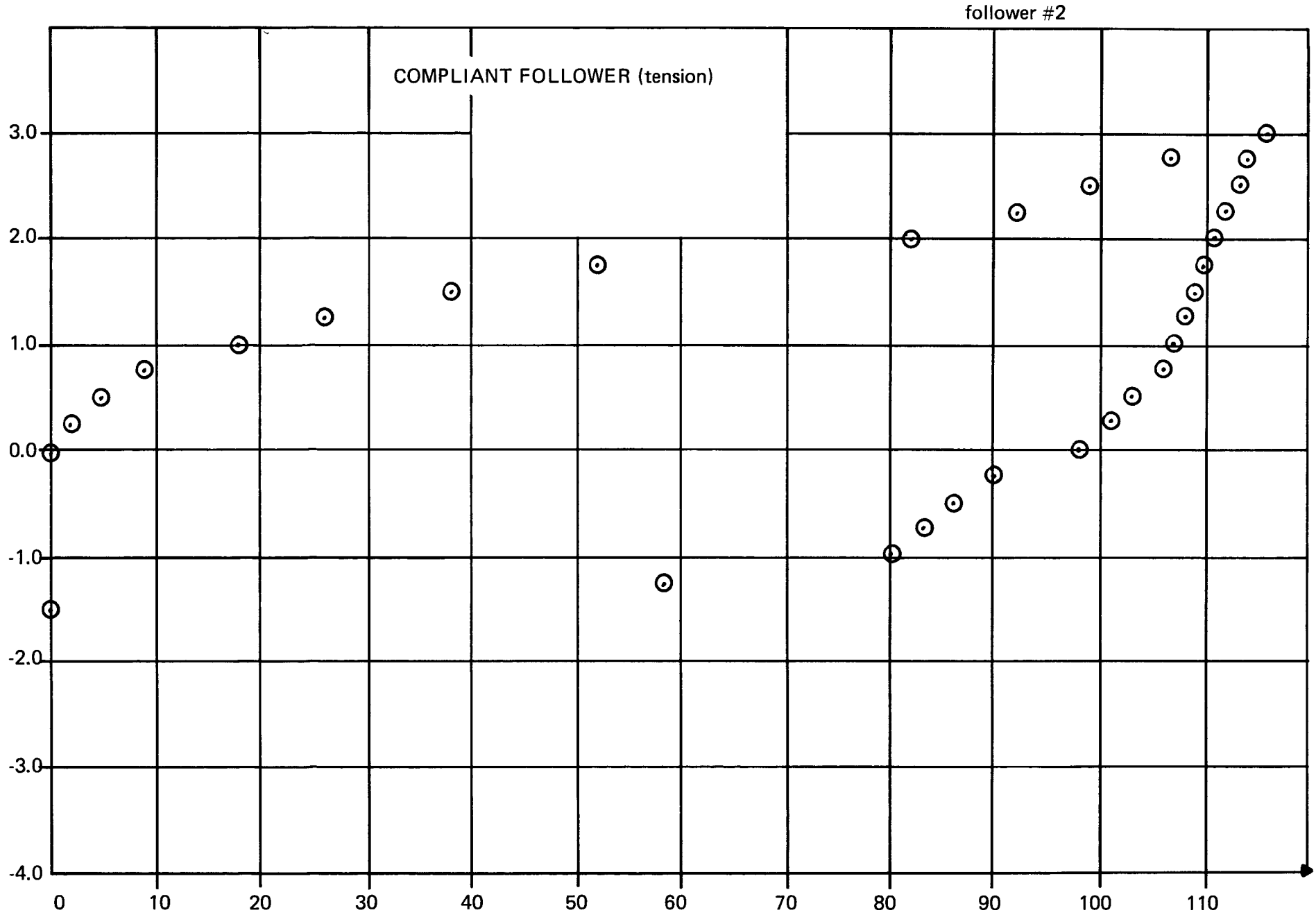

FIGURE 4-4: FORCE 'VS' DEFLECTION

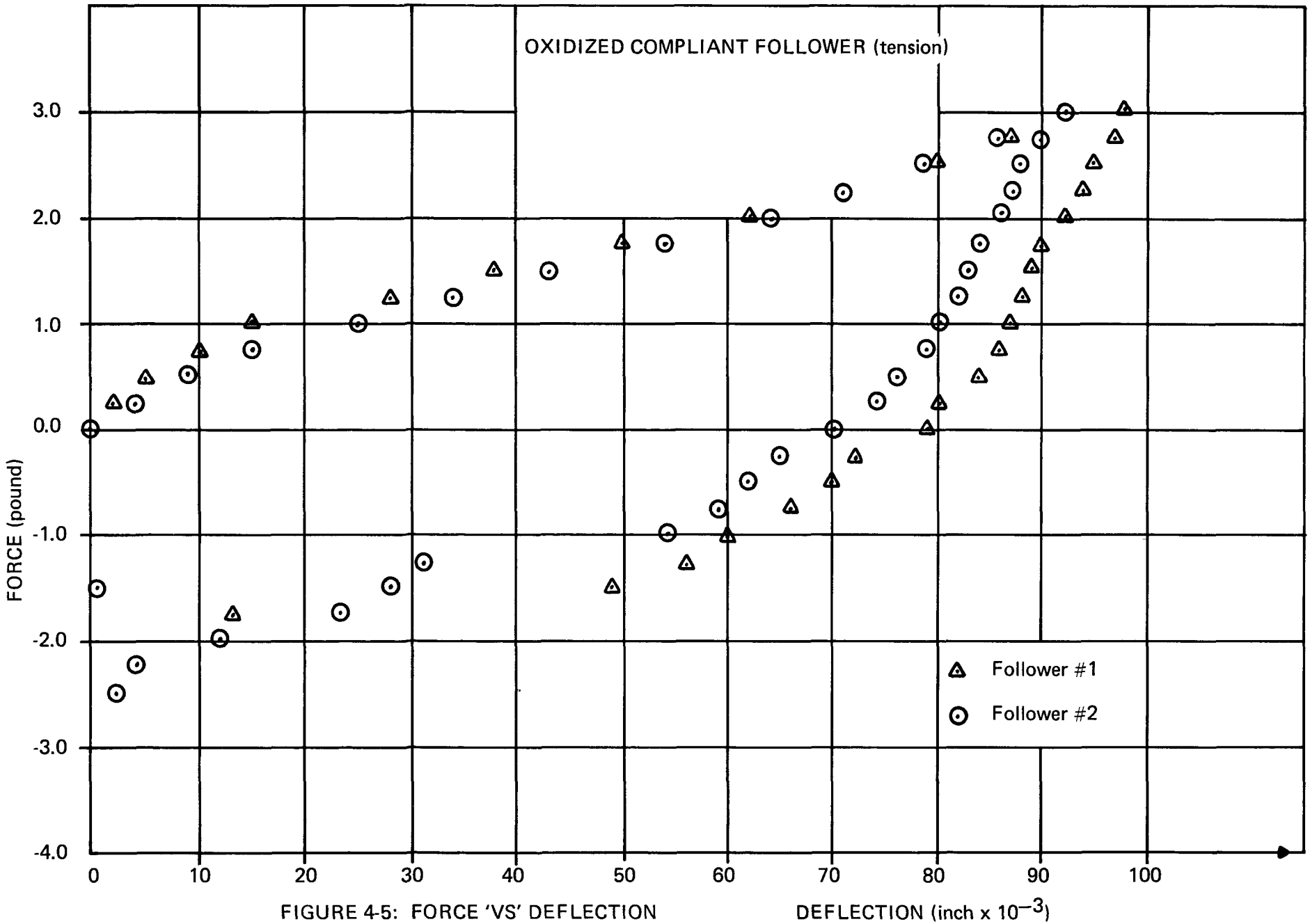

FIGURE 4-5: FORCE 'VS' DEFLECTION

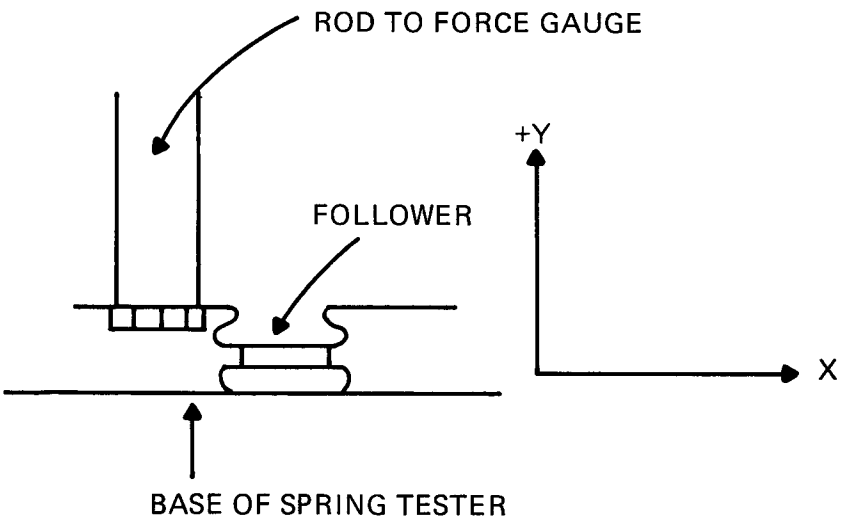

FIGURE 4-6

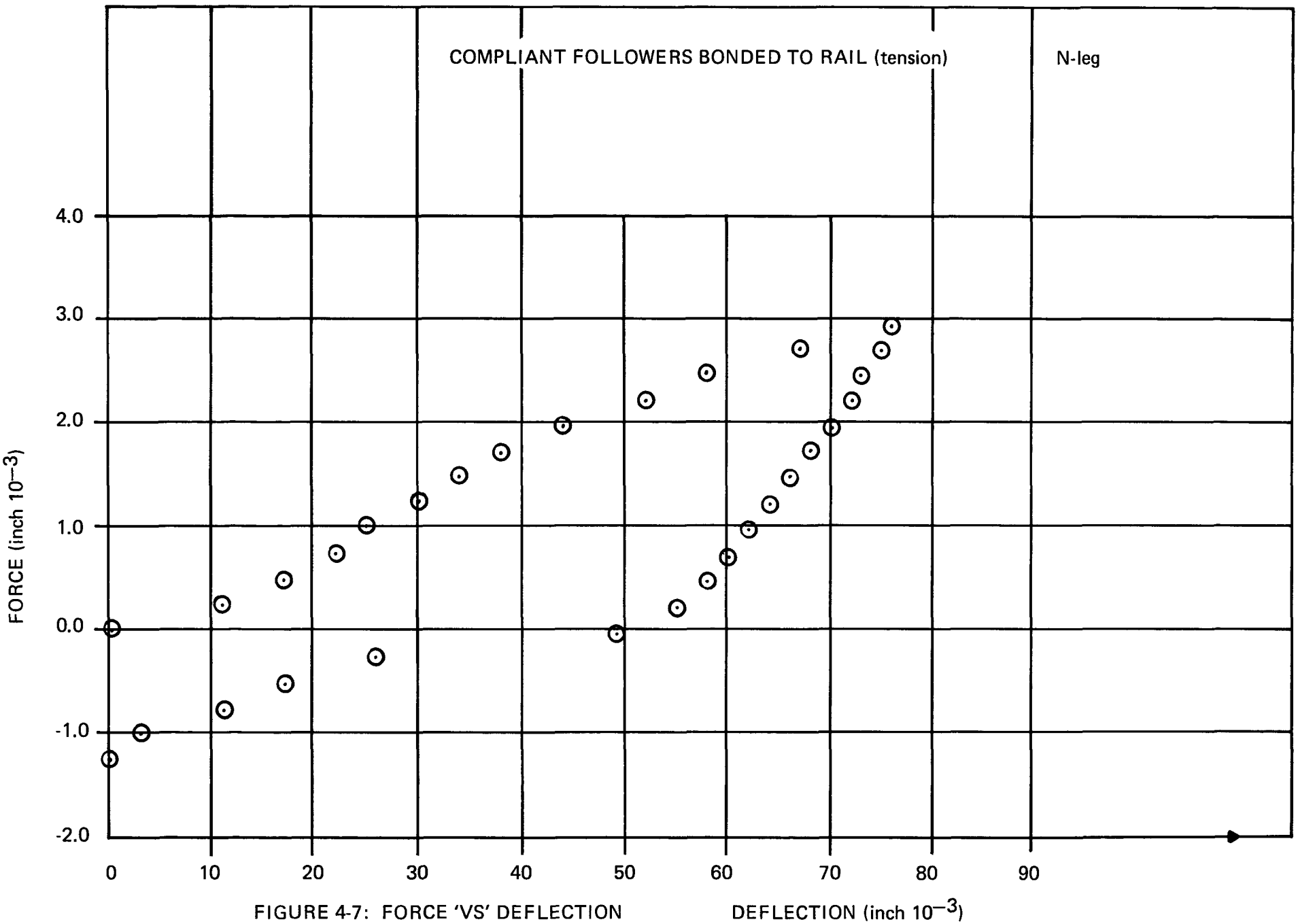

FIGURE 4-7: FORCE 'VS' DEFLECTION

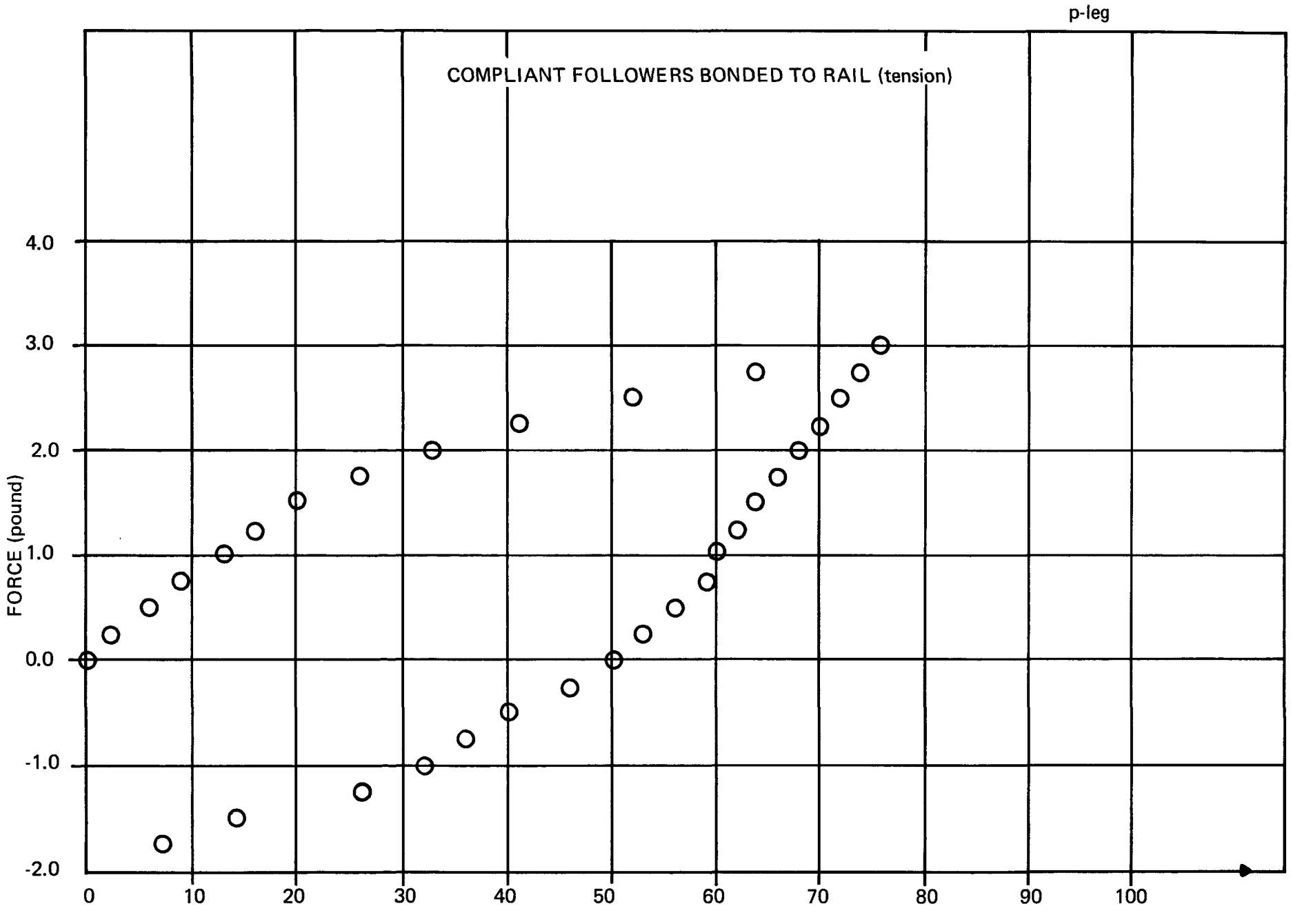

FIGURE 4-8: FORCE 'VS' DEFLECTION

ATTACHMENT 5

Cold End Hardware Spring Force

A 6-couple cold end hardware assembly with bonded compliant followers was fabricated and a spring force test performed. The results are attached in the form of graphs and can be summarized as:

Figure 5-1, 5-2 – Cold straps displaced and returned to original position.

Figure 5-3, 5-4 – Current strap displaced and returned to original position.

Note: Tension is positive and compression is negative.

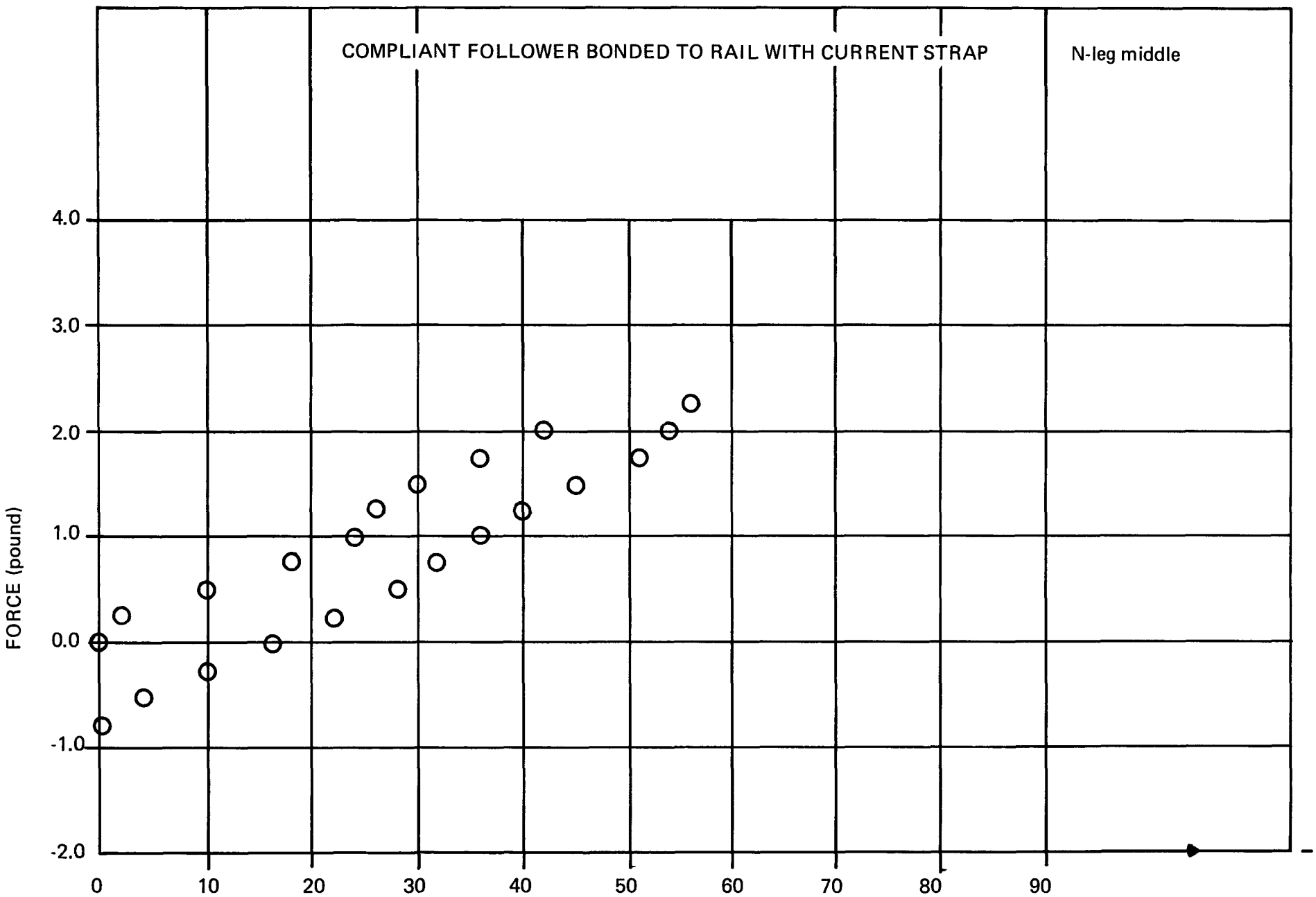

FIGURE 5-1: FORCE 'VS' DEFLECTION

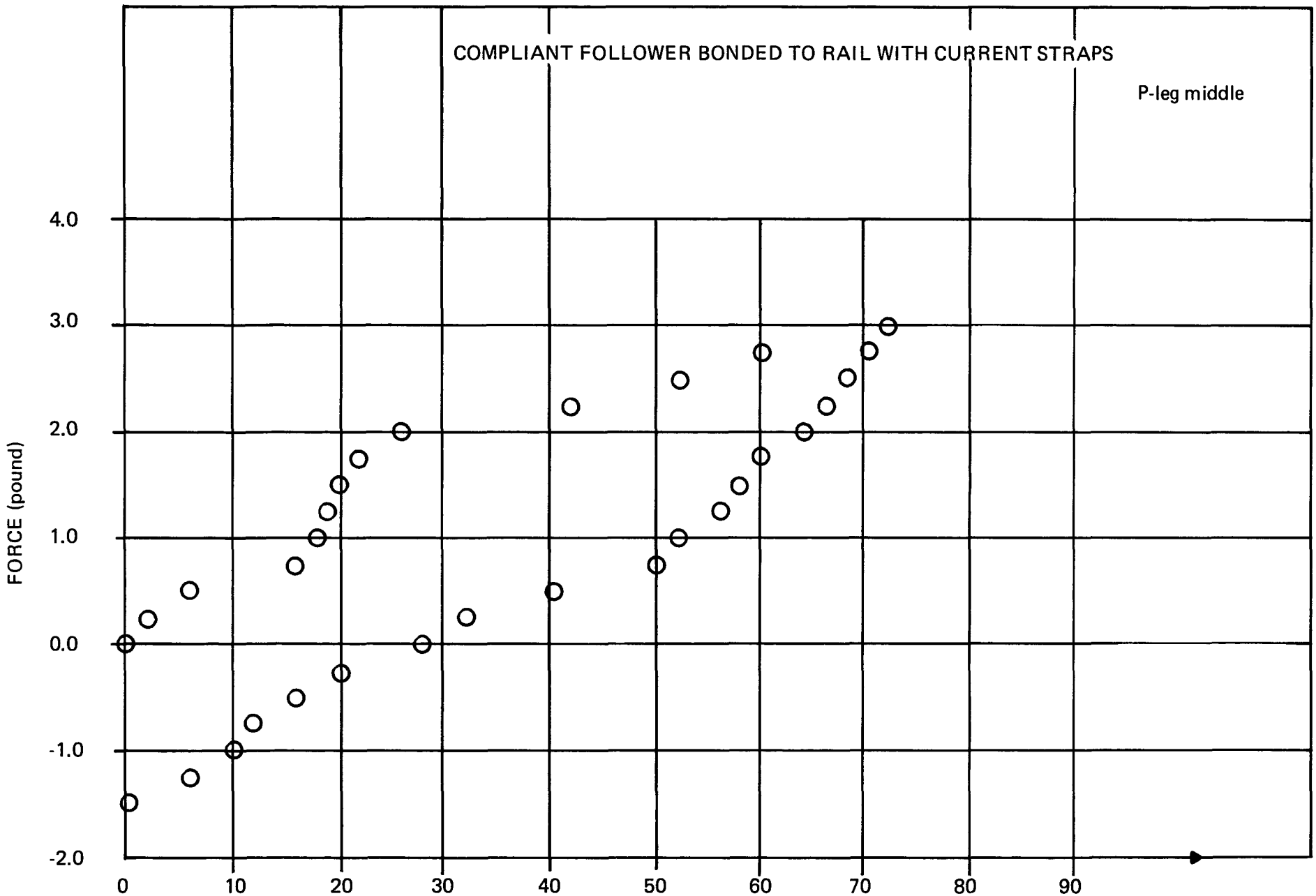

FIGURE 5-2: FORCE 'VS' DEFLECTION

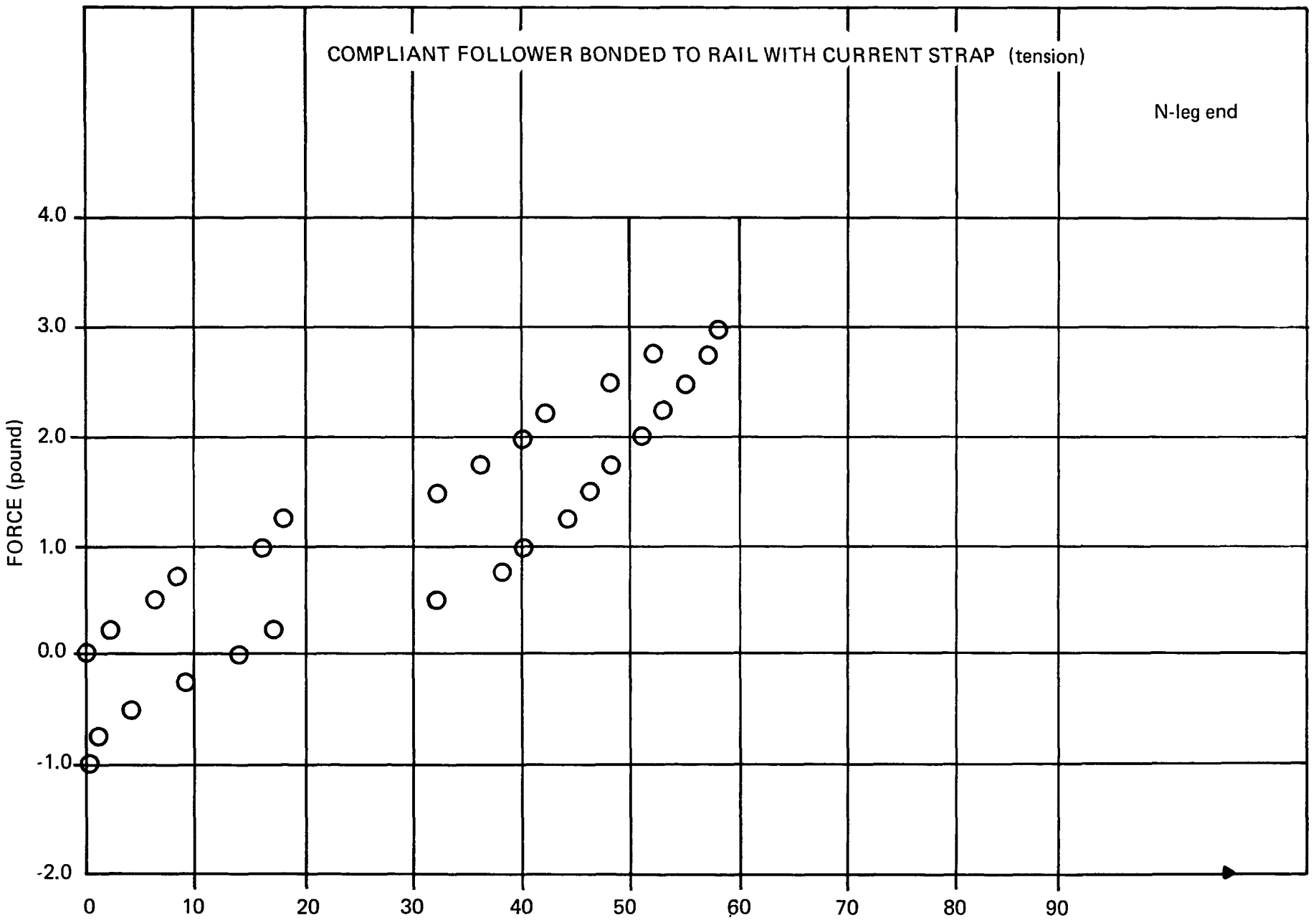

FIGURE 5-3: FORCE 'VS' DEFLECTION

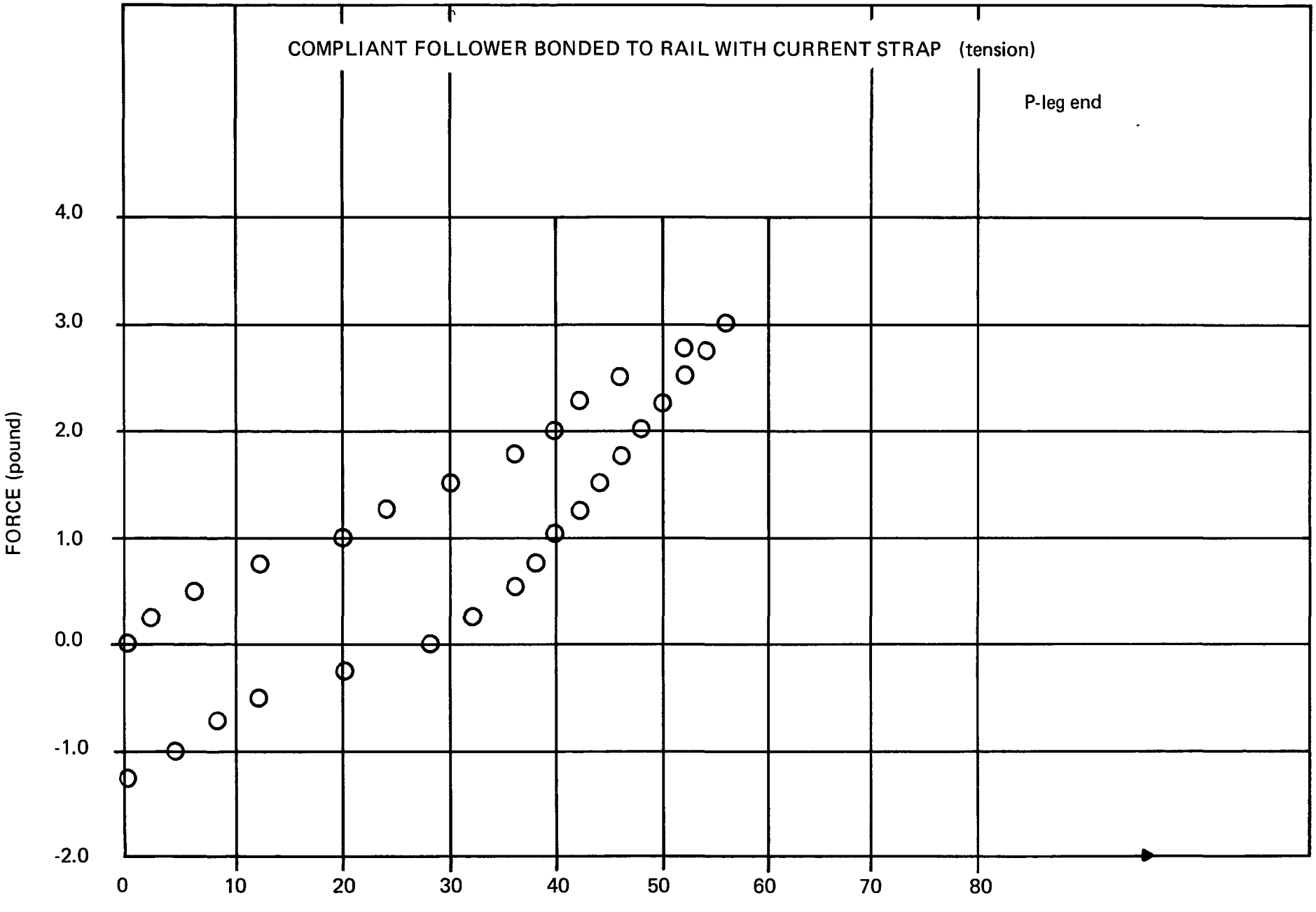

FIGURE 5-4: FORCE 'VS' DEFLECTION

ATTACHMENT 6

Determination of Stress on N and P-legs

Introduction:

With the increased number of modifications being done on the cold frame assembly, there is becoming a need for analysis of the mechanical behavior of these assemblies. The main area that needs to be examined is the change in stress on the legs as sublimation, creep, thermal expansion, etc., take place. This stress should be known because a low stress could cause high resistance or damage to the leg during dynamic loading, and a high stress could cause the leg to crack.

This attachment describes how the stress changes as the follower changes position. The method by which the deflection occurred will not be examined, so these results can be applied to any condition.

Procedure:

The stress on the legs is a combination of spring force, insulation compliance, and restoring force of the hardware. The spring force is the easiest to determine because all that is needed is the spring constant, Figure 6-1, and deflection, while the insulation compliance and hardware force have to be determined experimentally.

The insulation compliance was determined by compressing HiFi paper on the Instron and producing a stress 'vs' strain graph. This was curve fit on a Wang calculator to a 4th order polynominal, Figure 6-2.

Hardware force information was obtained by putting the hardware through a loading cycle on a spring tester, and measuring the force for deflections. This data is presented in the form of a graph on Figure 6-3.

The tolerances for stack height can greatly effect the initial spring force, so each condition was calculated for the maximum, nominal, and minimum initial spring force. In this way, it can safely be said that the stress would lie within the maximum and minimum curves. The equations used for the calculation of stress are shown in Figure 6-4.

Results:

The results are in the form of graphs which can be summarized as:

Figures 6-5, 6-6, 6-7, 6-8 –	Compression stress on the leg as creep or sublimation would take place.
Figures 6-9, 6-10, 6-11, 6-12, 6-13 –	Compression stress as thermal expansion takes place.
Figure 6-14 and 6-15 –	Illustrates how each component (spring, insulation and hardware) contribute to the stress for a nominal initial spring force.

SPRING P1, "P" LEG

TYPE: COMPRESSION

O.D. = 0.211 ± 0.005

WIRE DIA. = 0.041

ENDS: CLOSED, GROUND & SQUARE
WITH O.D. WITHIN 0.004
GROUND AREA AT LEAST 3/4
OF CIRCUMFERENCE

FREE LENGTH (AFTER GRINDING):
0.555 ± .010

SOLID LENGTH: 0.345 ± .005

FORCE AT 0.465 LENGTH = 8.5 LB.
± 0.5 LB.

DIRECTION OF COILS: R.H.

SPRING P2, "N" LEG

TYPE: COMPRESSION

O.D. = 0.282 ± 0.005

WIRE DIA. = 0.056

ENDS: CLOSED, GROUND & SQUARE
WITH O.D. WITHIN 0.004
GROUND AREA AT LEAST 3/4
OF CIRCUMFERENCE

FREE LENGTH (AFTER GRINDING):
0.555 ± .010

SOLID LENGTH: 0.376 ± .005

FORCE AT 0.465 LENGTH = 23.4 LB.
± 1.5 LB.

DIRECTION OF COILS: R.H.

FIGURE 6-1: SPRING DATA

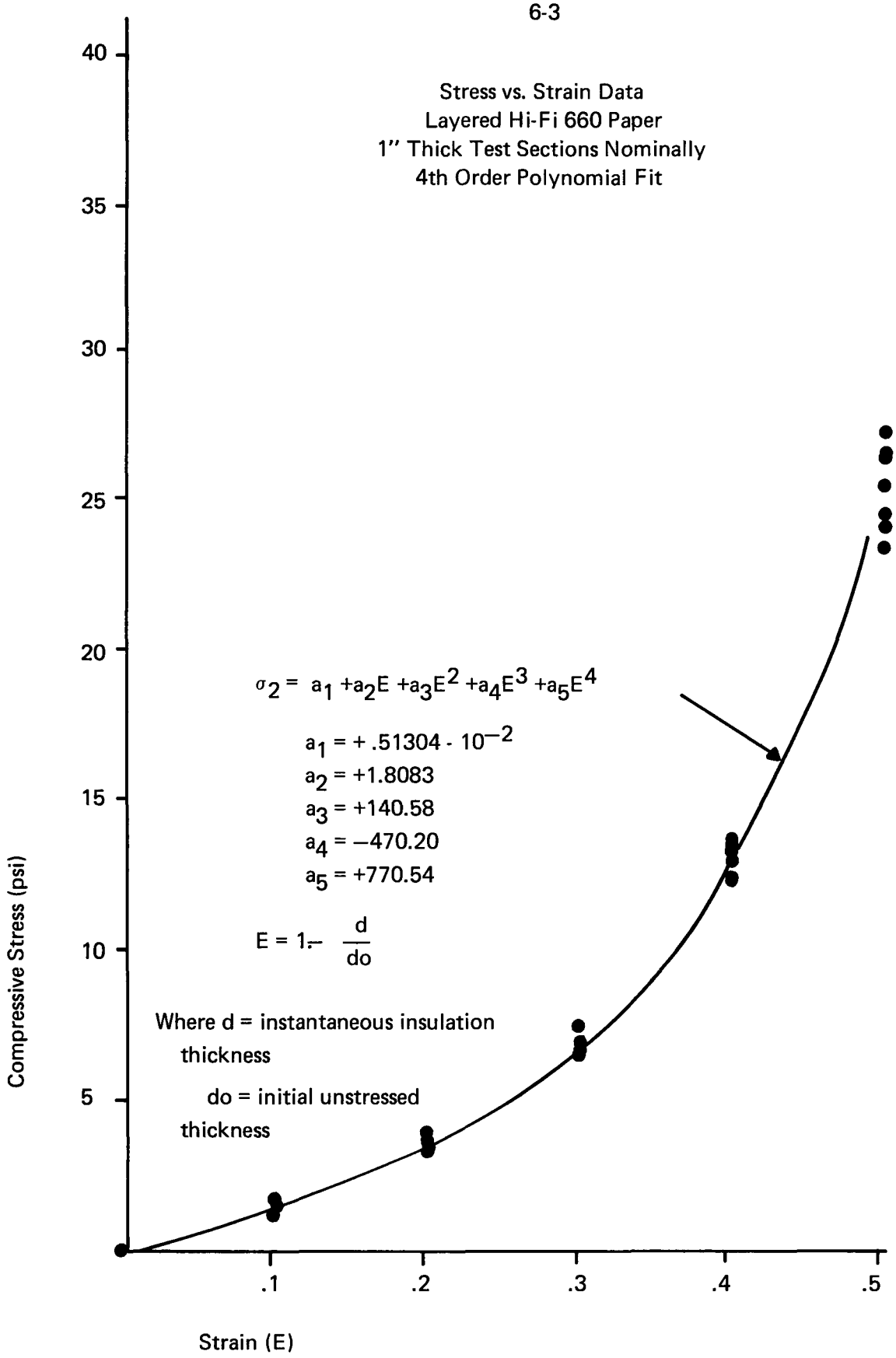

FIGURE 6-2: INSULATION COMPLIANCE

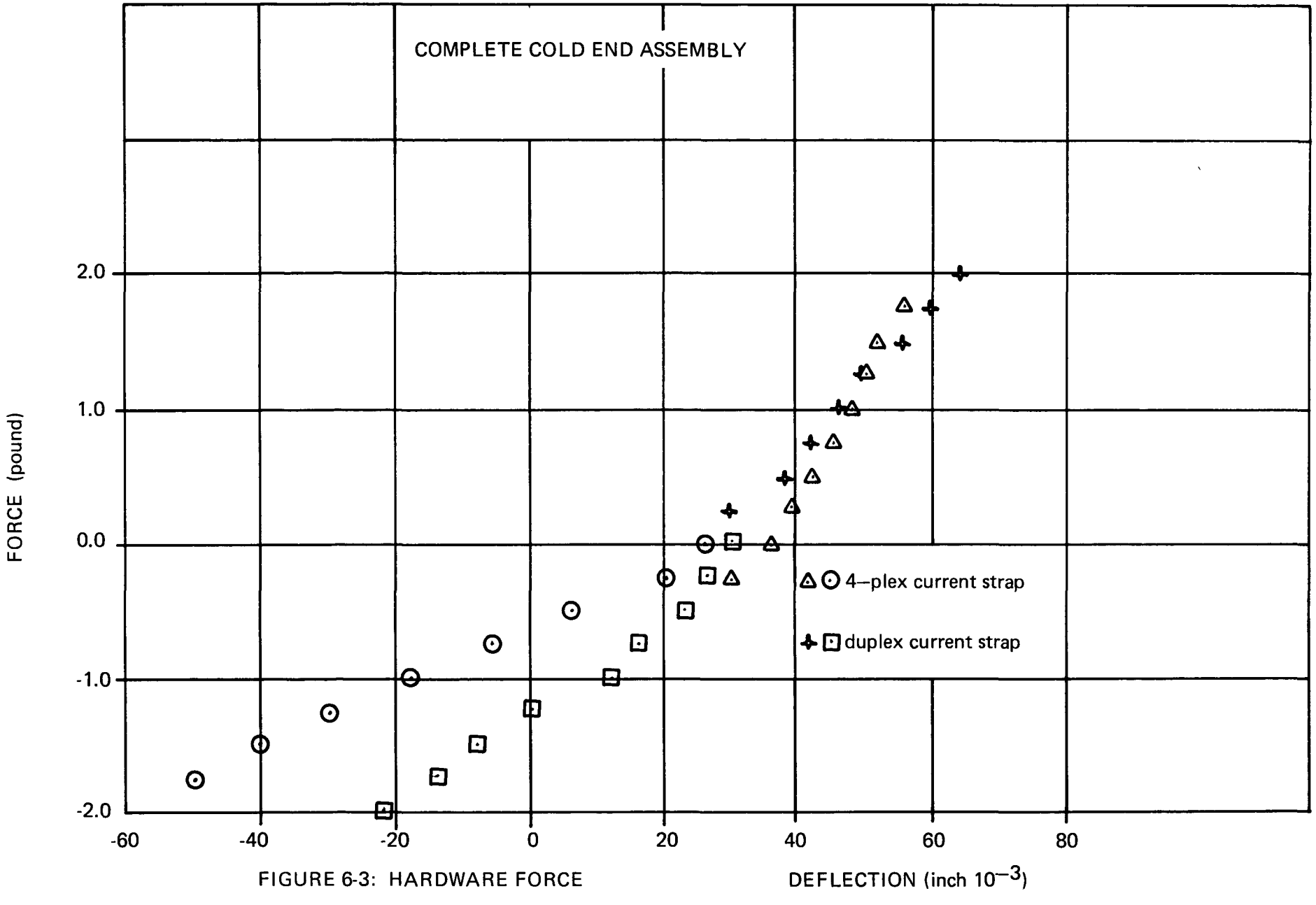

FIGURE 6-3: HARDWARE FORCE

$$F_{ToT} = Fs - Fr = P_1 + P_2 = \sigma_1 A + \sigma_2 A_2$$

$$\therefore \sigma_1 = \frac{1}{A_1} \left[Fs - Fr - \sigma_2 A_2 \right]$$

where $Fs = Fsi - K(L-Li)$

$$\sigma_2 = a_1 + a_2 E_1 + a_3 E^2 + A_4 E_1^3 + a_5 E_1^4$$

where $E = 1 - \frac{L}{Lo}$

$$a_1 = +.51304 \times 10^{-2}$$
$$a_2 = +1.8083$$
$$a_3 = +140.58$$
$$a_4 = 470.20$$
$$a_5 = +770.54$$

Fr is obtained from Figure 3

LIST OF VARIABLES

Fs	Spring Force
Fr	Strap-Followers restoring Force
σ_1, P_1	Stress, Force on Leg
σ_2, P_2	Stress, Force on Insulation
A_1, A_2	Cross-sectional Area of Leg, Insulation
Li	Initial Leg Length
Lo	Unstressed Insulation Layer Thickness
K	Spring Constant
Fsi	Initial Spring Force
L	Instantaneous Leg Length

FIGURE 6-4: STRESS EQUATIONS

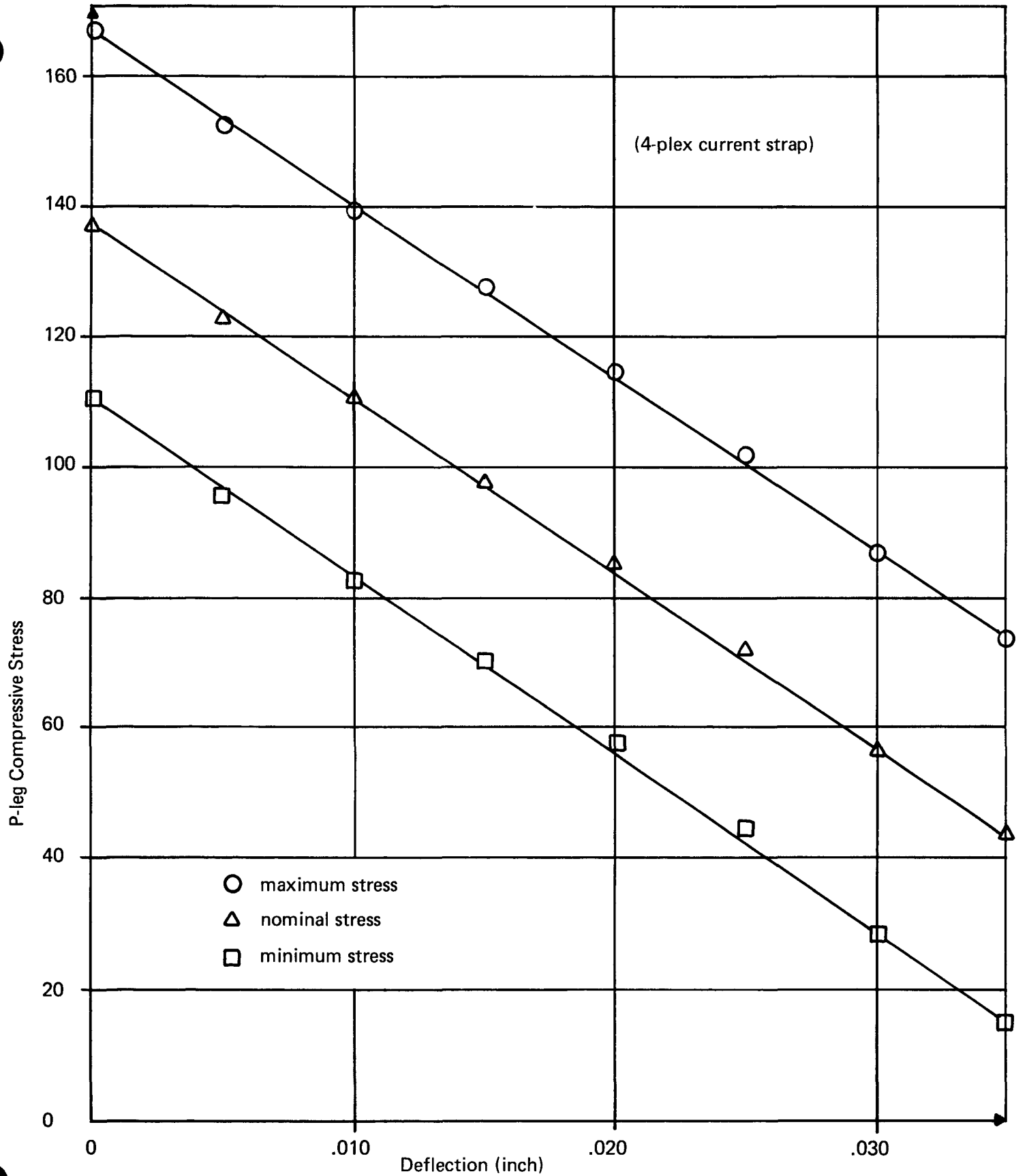

FIGURE 6-5: P-LEG COMPRESSIVE STRESS 'VS' DEFLECTION

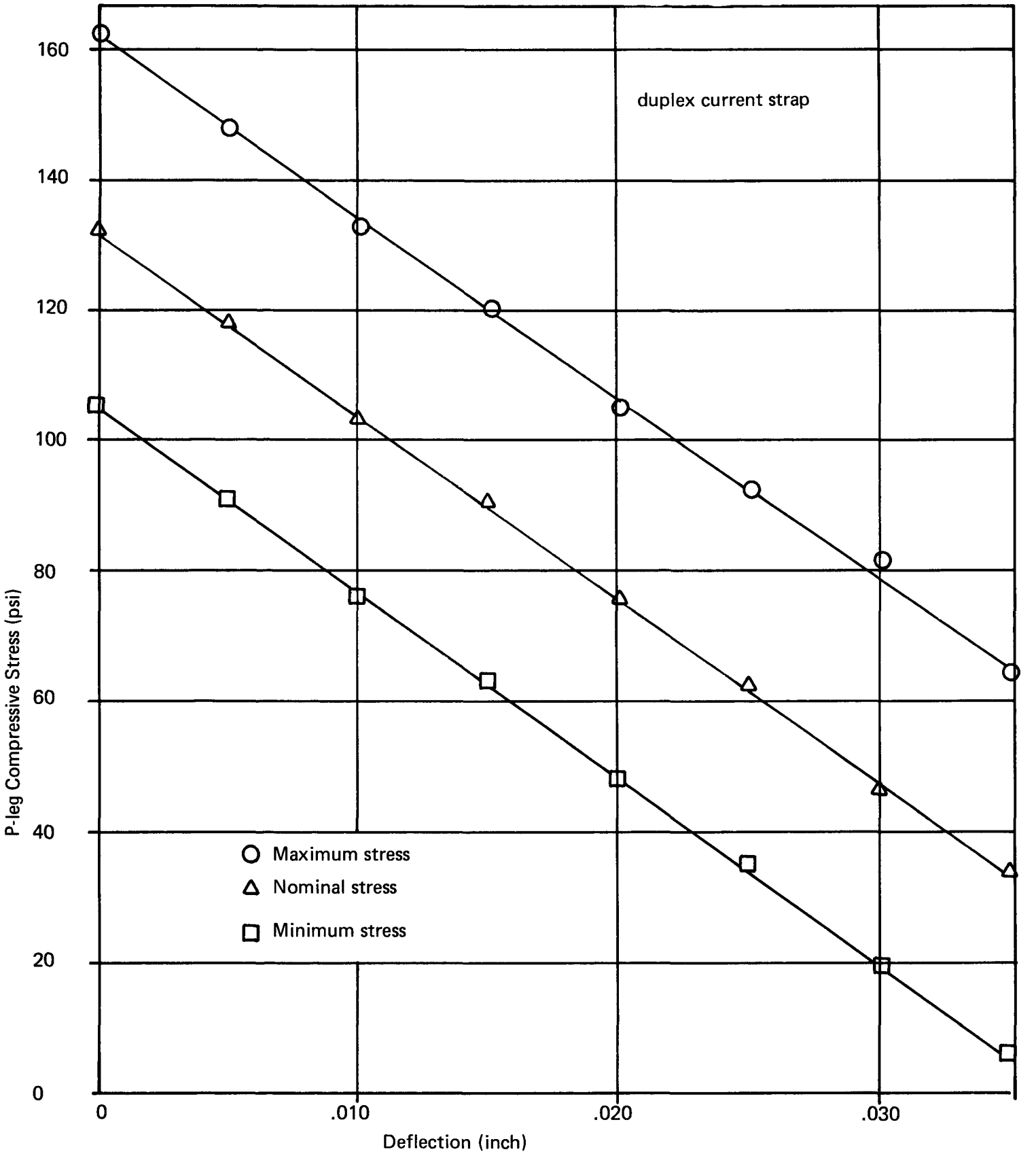

FIGURE 6-6: P-LEG COMPRESSIVE STRESS 'VS' DEFLECTION

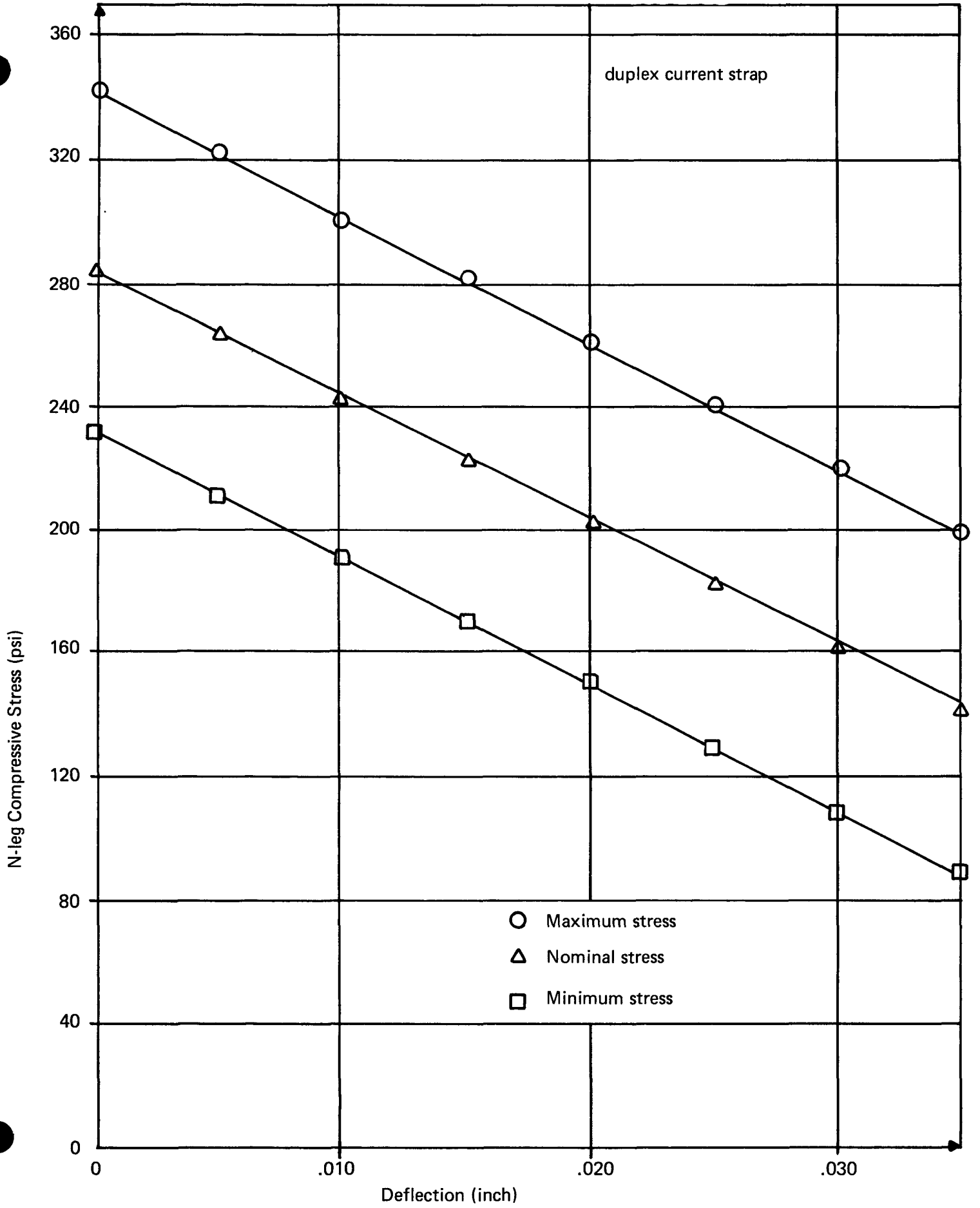

FIGURE 6-7: N-LEG COMPRESSIVE STRESS 'VS' DEFLECTION

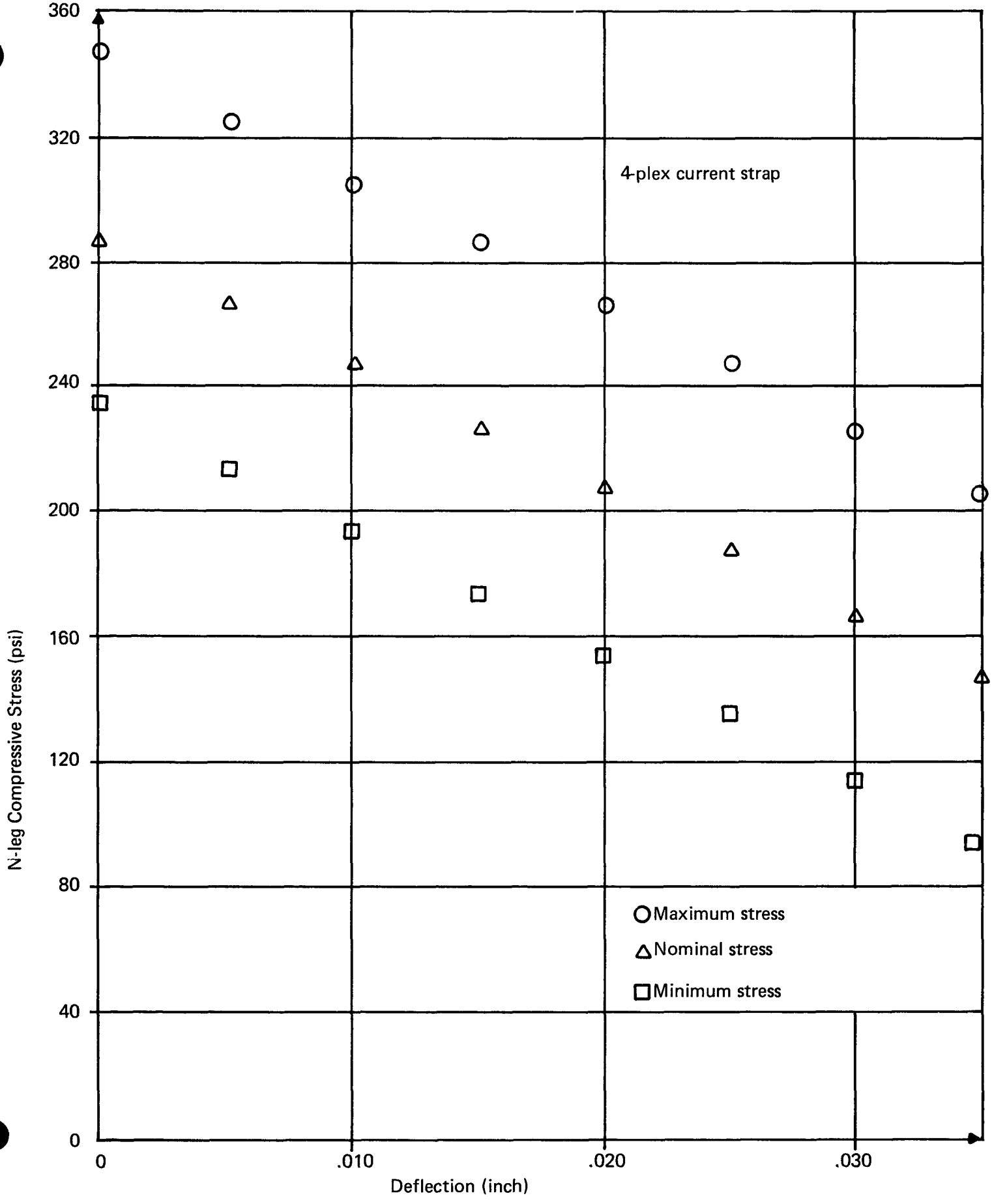

FIGURE 6-8: N-LEG COMPRESSIVE STRESS 'VS' DEFLECTION

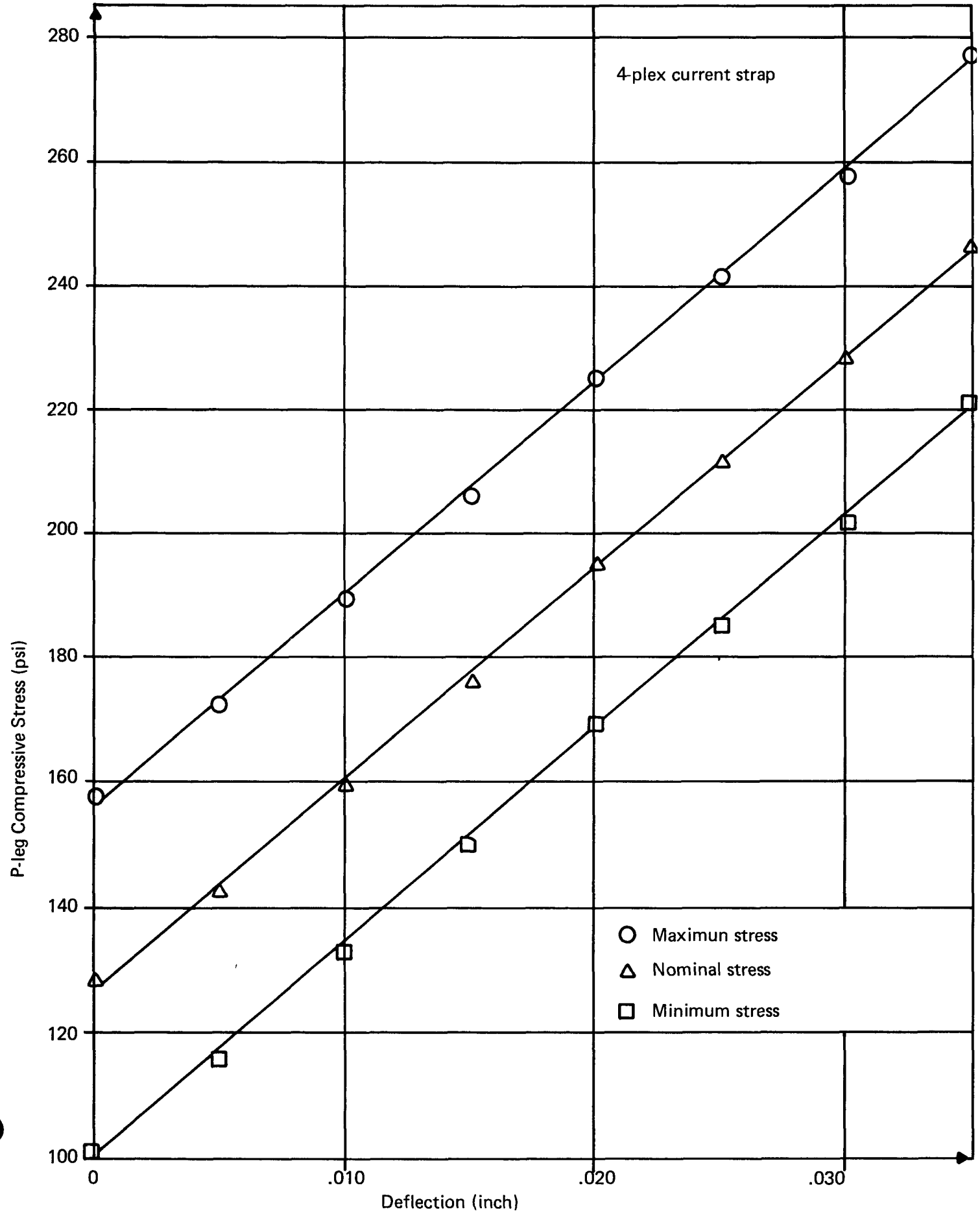

FIGURE 6-9: P-LEG COMPRESSIVE STRESS 'VS' DEFLECTION

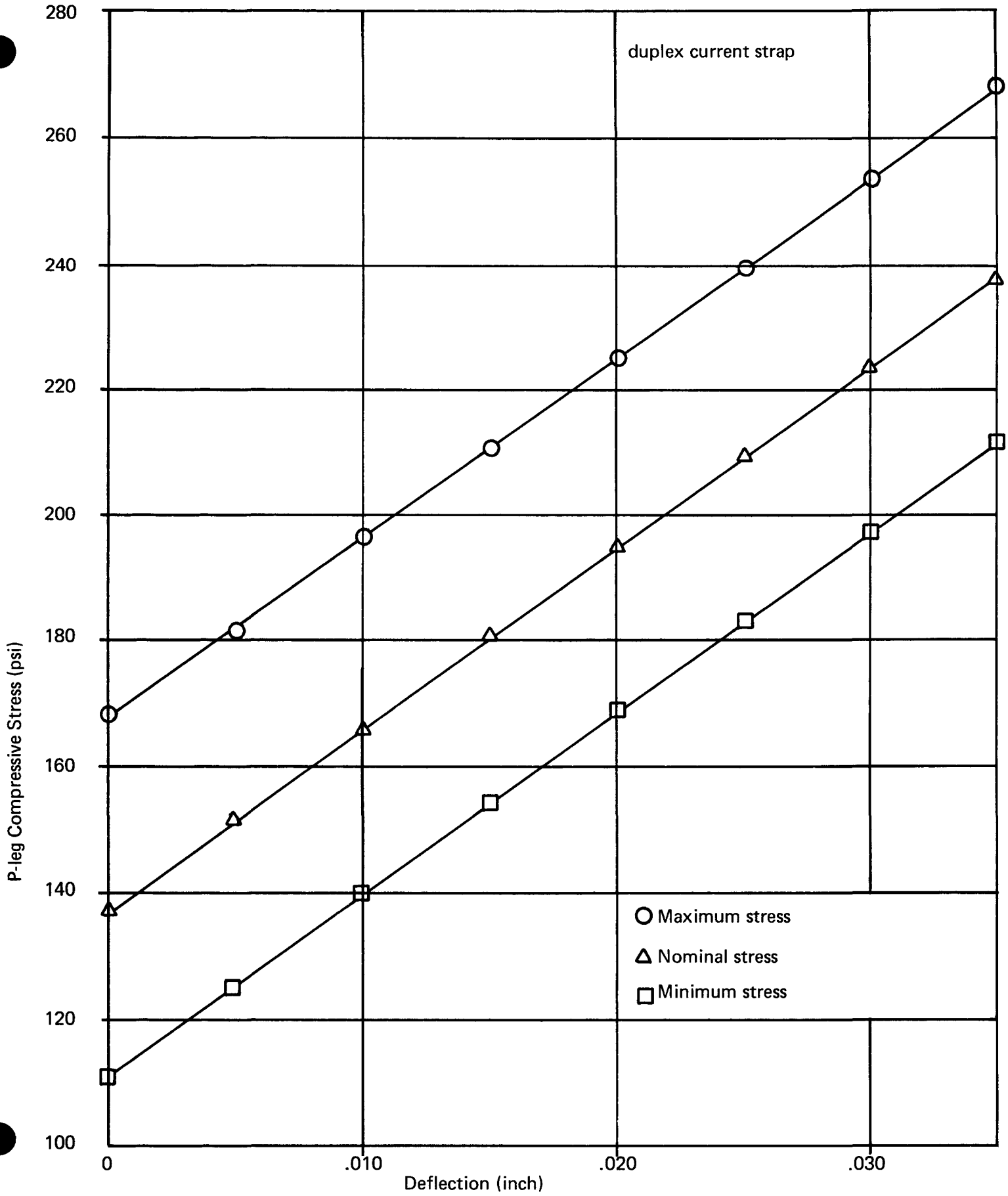

FIGURE 6-10: P-LEG COMPRESSIVE STRESS 'VS' DEFLECTION

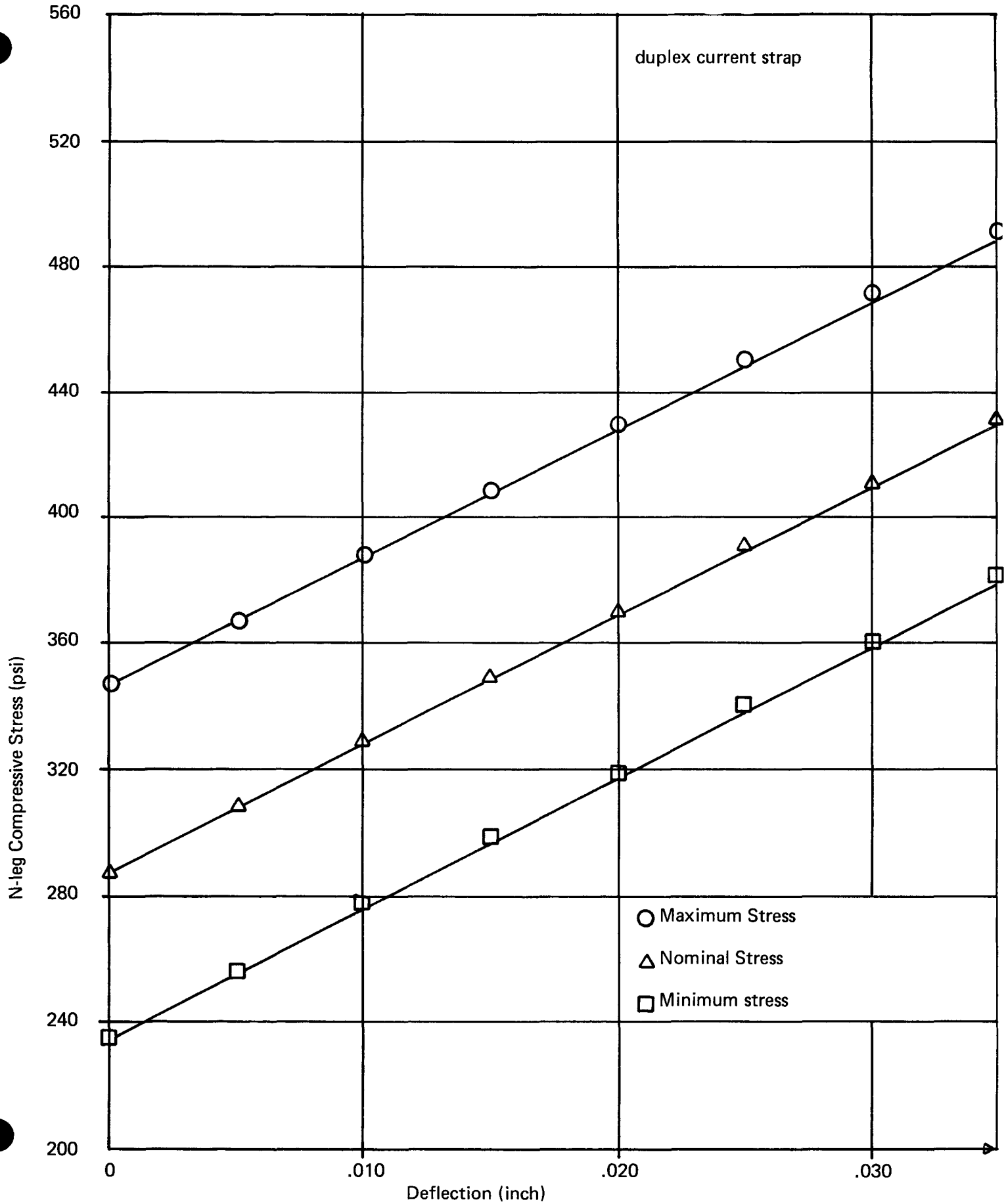

FIGURE 6-11: N-LEG COMPRESSIVE STRESS 'VS' DEFLECTION

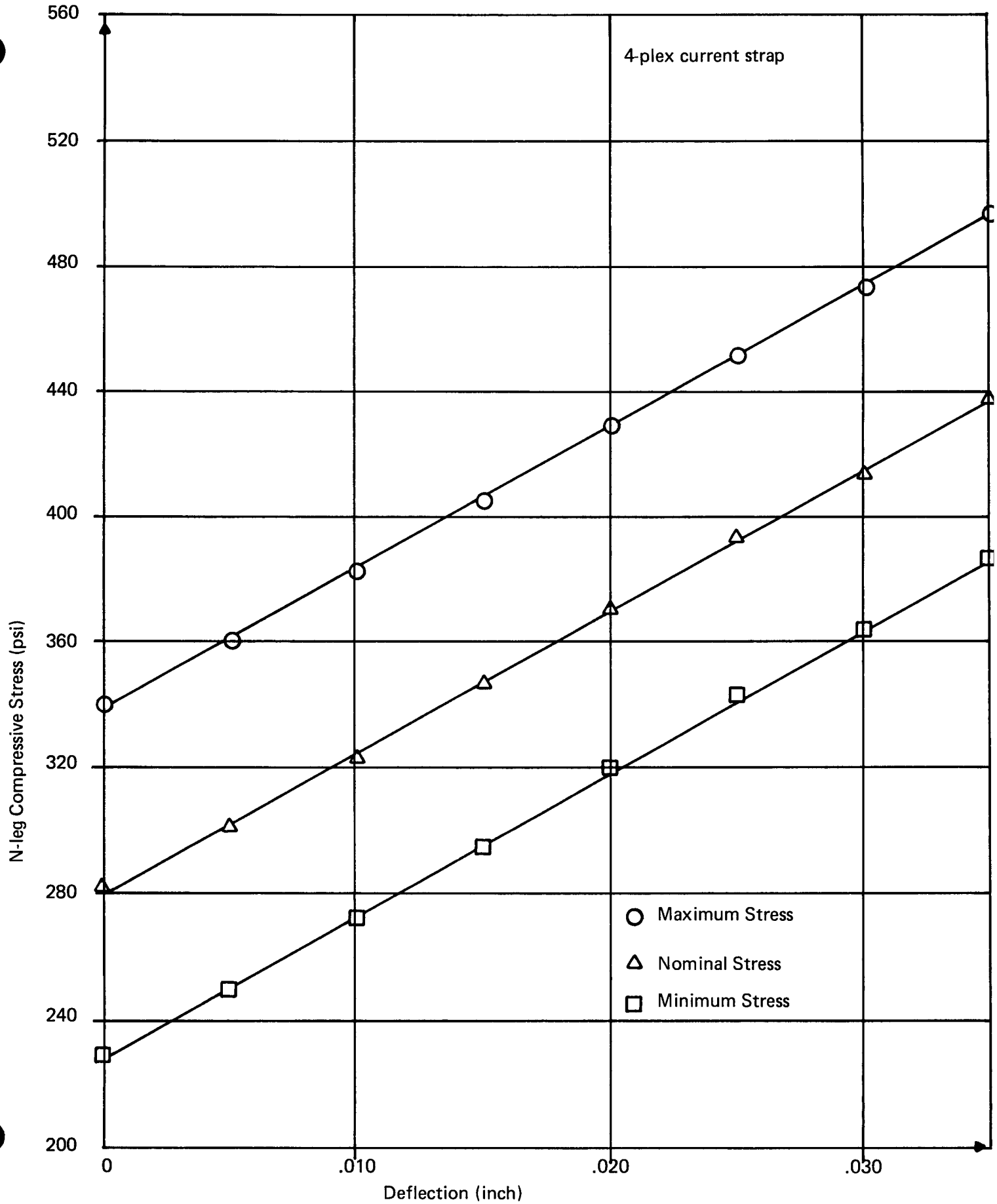

FIGURE 6-12: N-LEG COMPRESSIVE STRESS 'VS' DEFLECTION

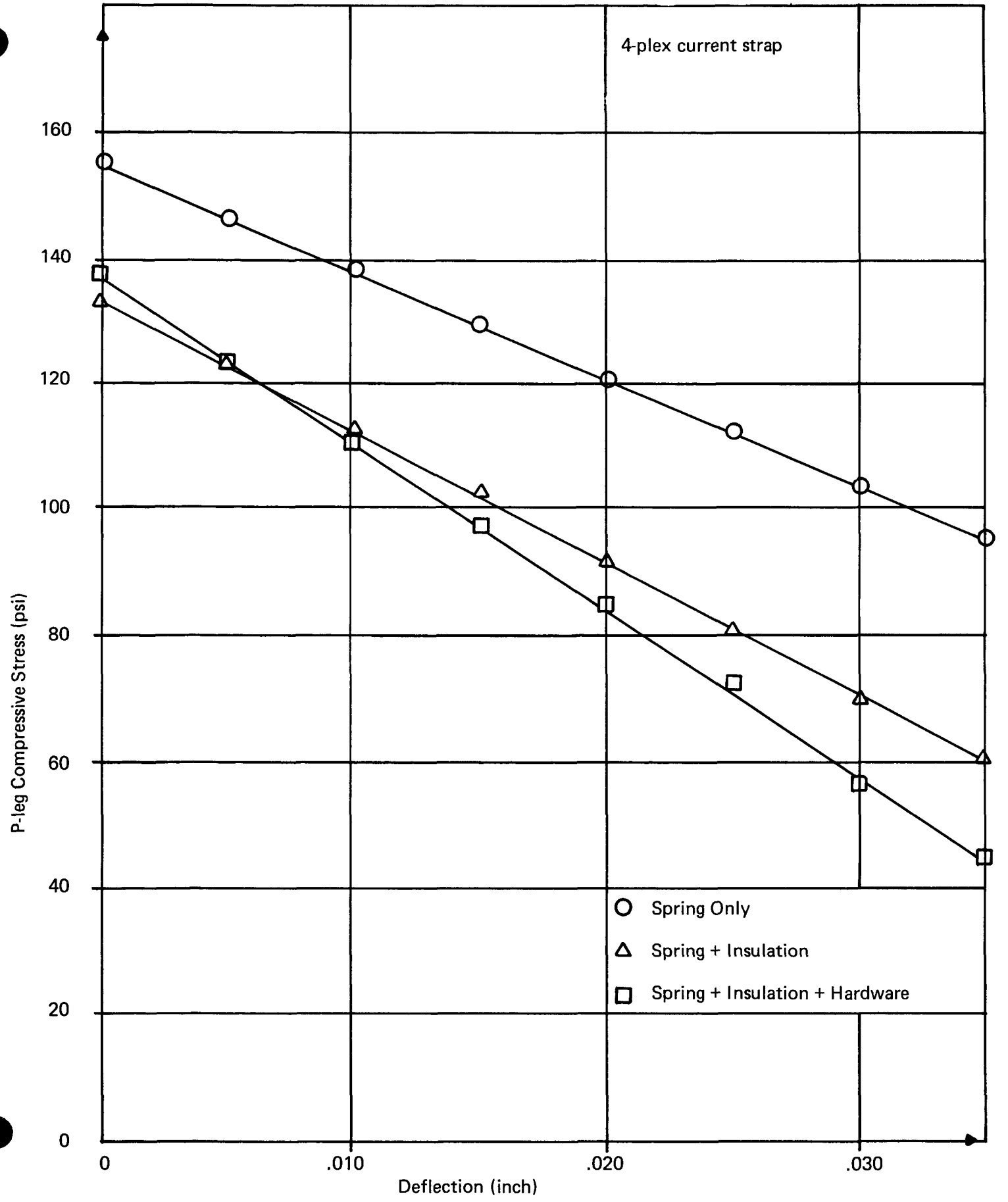
4-plex current strap
160
140
120
100
80
60
40
20
0
P-leg Compressive Stress (psi)
0
.010
.020
.030
Deflection (inch)
Spring Only
Spring + Insulation
Spring + Insulation + Hardware

FIGURE 6-13

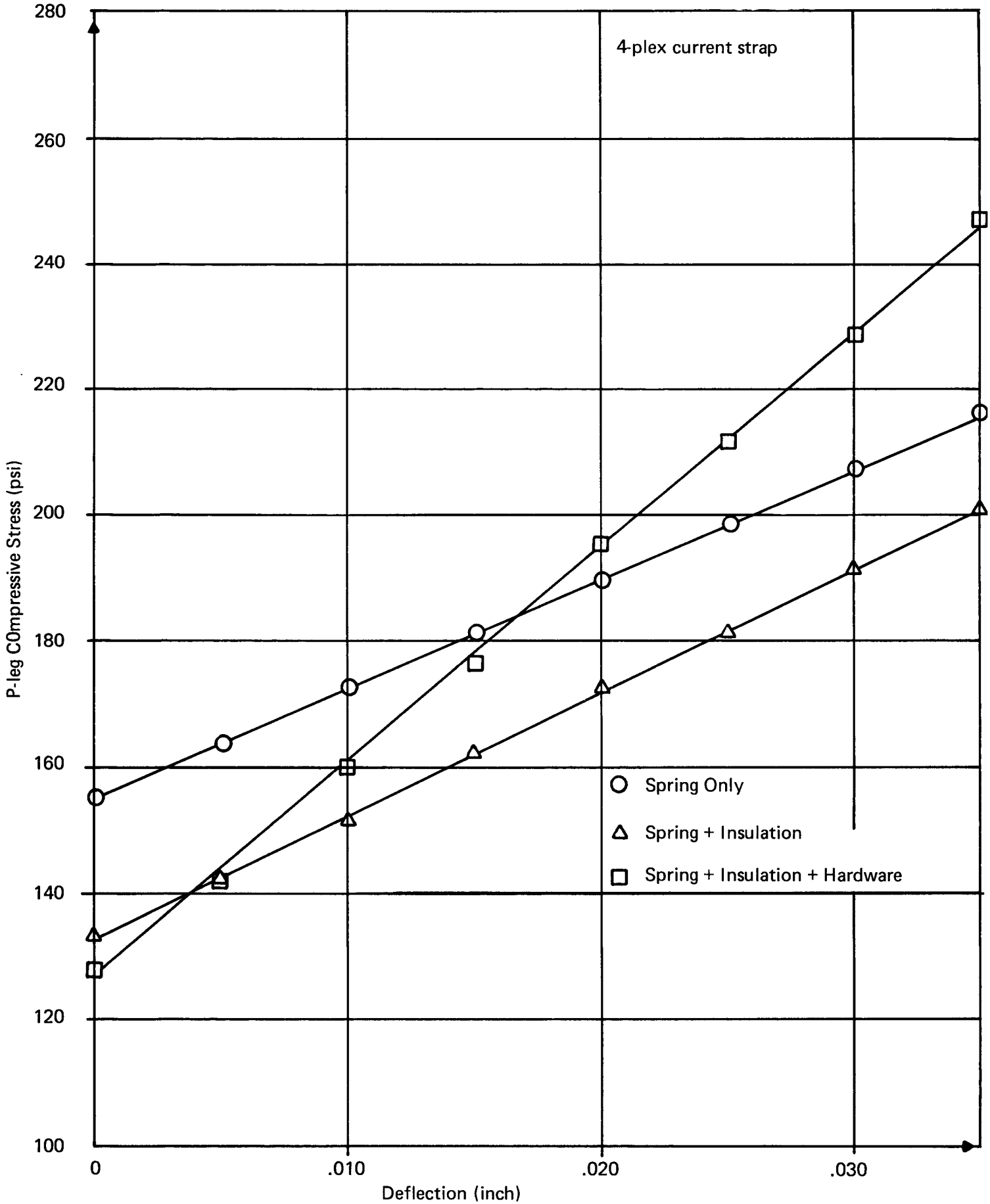

FIGURE 6-14: P-LEG COMPRESSIVE STRESS 'VS' DEFLECTION

ATTACHMENT 7

Load Relaxation in Springs

1. Description

N and P-leg springs in M7 experienced severe load relaxation problems. Post test analyses showed that at operating spring height, P-leg compressive loads ran between 1 and 4 pounds, less than 50% of specification. Spring designs have been changed since then, and the latest design should do much to eliminate this problem.

The old springs were made from AISI A401 tempered Chrome-Silicon spring wire. The wire was coiled, ground and then stress relieved at 650-700° F for 45 minutes.

The new springs are being made from 17-7 PH 900C stainless steel, a material specially developed for high temperature use and having load relaxation characteristics superior to AISI A401. The fabricating procedure is also different. The wire is coiled for a free length longer than the design specification. The springs are then set (compressed to solid height) at room temperature in order to induce some inelastic deformation in the spring. This process will decrease the rate at which the load relaxes. Following the set, the springs are heat treated at 900° F to increase the hardness of the material, and afterwards are ground to the specified free length.

There are two (2) questions that need to be answered in order to evaluate the security of the current design:

1) Is the relaxation problem directly related to design?

2) Is it related to the operating environment?

The design stress levels in the springs are moderately high, ranging between 70 ksi for the P-leg spring, and 100 ksi for the N-leg spring (although the stress levels may have been as high as 130 ksi in the M-7 springs for some conditions). These nominal stress levels are reasonable. Also, for an operating temperature of 150°C, A401 Chrome-Silicon steel should be adequate. However, literature that has been found indicates that 17-7 PH should be a superior material. Additional spring material will be evulated as this effort continues under the ongoing Technology Program.

It is quite likely that the excessive load relaxation encountered in module M7 is attributable to the absence of a set procedure. It is generally accepted by the spring industry that a set spring will relax at a much lower rate than an unset spring. Some springs are set at elevated temperature. It is not clear whether a high temperature set provides additional protection against relaxation, but some quick tests performed for us by Lee Spring indicate that it might. Other than this slight modification, there are no others that we know of that might provide us with a better spring.

It is possible that the springs could be reacting with vapors present in the environment. Possible contaminants include Se and O.

2. Efforts which will continue under the Technology Program

1) M7 springs are being analyzed to confirm that the material is indeed A401. They will also be analyzed for Se and O content, and in the event that either is found in significant concentrations, cross-sectional concentration profiles will be measured.

2) A test fixture for aging springs at operating temperature was fabricated. Tests are isothermal rather than ingradient. Free length and spring constant are monitored vs log time. Tests will be terminated after 200 hours. Figure 7-1 describes briefly the first six tests. These tests were run at 150°C. A more complete description of this test effort is contained in the System Testing Section (Section III-A).

Run No.	Material	Type of Spring	No. of Springs	No Set	Room Temperature Set	High Temperature Set	Air Environment	Vacuum* Environment	Se Vapor Present
1	A-401	N-Leg	6	√			√		
2	302 Stainless	N-Leg	6	√			√		
3	17-7 PH	N-Leg	6		√		√		
4	17-7 PH	N-Leg	6			√	√		
5	17-7 PH	N-Leg	6		√			√	√
6	A-401	P-Leg	6	√				√	√

* Any test performed in vacuum will be monitored only before and after the run.

FIGURE 7-1: TEST MATRIX

ATTACHMENT 8

Weight and Exposed Surface Area of Cold End Copper Hardware

The following is the weight and surface area of the copper cold end hardware in the SN-1 generator.

Weight of Copper in Generator

Component	Unit Wt.	No./ Segment	Segment Wt.
N Spring retainer	.566 gm	6	3.396
P Spring retainer	.264 gm	6	1.584
N Current Strap	1.129 gm	1	1.129
P Current strap	.871 gm	1	.871
4-Plex strap	.652 gm	2	1.304
Follower	1.192 gm	6	7.152
		Total =	15.436 gm/segment

(15.436 gm) x (56 segments/generator) = 864.4 gms of copper/generator

Exposed Surface Area (in^2)

Component	Unit Area	No./ Segment	Segment Area
P Spring retainer	.00048	6	.00288
N Spring retainer	.00155	6	.0093
P 2-Plex Current Strap	1.0898	1	1.4814
N 2-Plex Current Strap	1.4814	1	1.0898
4-Plex strap	.6420	2	1.284
Follower	.6998	6	4.1988
		Total =	8.066 in^2/segment

(8.066 in^2) x (56 segments/generator) = 451.7 in^2 exposed surface area of copper in generator

ATTACHMENT 9

SN-1 Weight Analysis

Objective:

- To analyze the component weights of the SN-1 thermoelectric rings.
- Use these weights to obtain a composite weight picture of the thermoelectric ring assembly.

Conclusions:

Based on the information shown in Table 9-1, it can be seen that the actual weight of the thermoelectric ring assemblies for SN-1 will be 13.8/14.5 lbs. The design target was 16.0 lbs.

Weight Analysis:

Two (2) methods were used to derive the weights of the components listed in Table 9-1. In all cases where SN-1 component parts were available, samples from bonded stock were randomly selected and weighed. Whenever bonded stock components were not available, weight calculations were performed based on the material and dimensional properties shown in the appropriate SN-1 drawing. The method used for each component is noted in the table.

TABLE 9-1

SN-1 WEIGHT SUMMARY (LBS.)

Part	Nom. Unit Wt.	Quantity/Gen.	Nom. Total Wt/Gen.	Weight Tolerance
Hot Frame	.8883*	2	1.780	1.560/1.850
Foil, Hot Shoe	.0000357*	112	.004	.004/ .007
Ceramic Pin	.000089	336	.030	.028/1.031
Strap, Current, H.E.	.0100	168	1.680	1.613/1.747
Gimbal	.00192	336	.644	.632/ .659
Ni Foil Disk	.000132	336	.044	.044/ .045
P-Leg Assembly	.00583	336	1.960	1.940/1.990
N-Leg Assembly	.0062	336	2.090	2.070/2.120
Cold Frame Assembly	.06805	56	3.811	3.783/3.822
P-Spring	.0015	336	.504	.484/ .518
N-Spring	.0029	336	.974	.967/ .988
P-Twist Lock	.00036	336	.122	.121/ .123
N-Twist Lock	.00068	336	.228	.227/ .229
Tin Foil	.025*	2	.050	.040/ .060
HiFi Insulation	.006*	56	.316	.302/ .330
Multifoil Pins	.000045*	13	.0006	.0005/.0006
		Generator Total:	14.238	13.816/14.520

*Based on calculations.

ATTACHMENT 10

Initial Phases of Axial Stress on N and P Legs

Objectives:

The purpose of this attachment is to analyze the various modes of axial stress on the thermoelectric legs in the SN-1 generator. Analysis will cover:

1. Range of stress at initial room temperature:
   a) in the overcompressed assembly stage
   b) in the fully assembled stage
2. Range of stress at initial heat-up

Conclusion:

Table 10-3 summarizes the range of stress on the legs for the various modes mentioned. The values given for stresses after heat-up may now be used as initial starting conditions.

Analysis of Static Stresses:

The initial stress on the legs is a factor of spring force and insulation compliance.

Spring Force:

To determine the force applied to each leg by the spring, the following calculations were performed for each mode, using nominal, maximum, and minimum values.

a) Determine stack heights using the known values of the housing and POCO hot frame, the approximate conditions. (Shown in Table 10-1)
b) Add the individual components in the stack (shown in Table 10-2).
c) Subtract this value from the appropriate stack height value in Table 10-1 to obtain the compressed spring length.
d) Subtract this compressed length from the free length of the spring to obtain the amount of spring compression.
e) Multiply this compression by the appropriate spring rate to obtain the spring force.

Insulation Compliance:

The initial spring force is reduced by the insulation compaction. With the use of an Instron Machine, this reduction of force has been determined to be 1.25 lbs.

The net stress applied to the legs is then determined by:

Stress = (Spring Force - Insulation Compliance)/Area of Leg

The following pages describe these calculations in detail. A summary of the room temperature and heat-up stresses are summarized in Table 10-3.

SN-1 Stack Height Calculations

Three (3) stages of stack height will be encountered by the thermoelectric ring:

1. Overcompressed Stack Height:

   This describes the condition of the ring immediately prior to insertion into the housing. The amount of overcompression is .030" radially.

2. Fully Assembled Stack Height:

   This condition occurs after rings have been completely assembled and released in the housing. The stress applied by the ring will cause the housing to deflect .0025 inches radially. This deflection is taken into account in the stack height calculations.

3. Heat-Up Stack Height:

   This condition occurs after SN-1 has been brought up to temperature and accounts for .020 radial expansion (thermal) of the POCO hot frame.

Table 10-1 lists the various stages of stack height along with the tolerance range associated with each respective stage. The tolerance ranges are based on component tolerances taken from the design drawings.

Below is a sample calculation of the nominal overcompressed stack height:

Housing I.D. = $10.159 \pm .008$ inches

POCO across flats = $8.117 \pm .08$ inches

Stack Height = (Housing I.D. – POCO O.D. (Across flat))/2 – radial overcompression

= (10.159 – 8.117)/2 – .030

= .991 inches

Initial Stress Calculations

Nominal: $\sigma_i = \frac{1}{A_{nom}} [F_{si\ nom} - F_{i\ nom}]$

where $F_{si\ nom} = K_{nom} [L_{FL\ nom} - L_{C\ nom}]$

Maximum: $\sigma_i = \frac{1}{A_{min}} [F_{si\ max} - F_i]$

where $F_{si\ max} = K_{max} [L_{FL\ min} - L_{C\ min}]$

Minimum: $\sigma_i = \frac{1}{A_{max}} [F_{si\ min} - F_i]$

where $F_{si\ min} = K_{min} [L_{FL\ max} - L_{C\ max}]$

Variables

σ_i = Stress on leg

A = Cross-sectional area of leg (from leg spec.'s)

F_{si} = Initial spring force

F_i = Insulation compliance force (initial = 1.25 lbs)

K = Spring constant (calculated from spring specifications)

L_{FL} = Spring free length (from spring spec.'s)

L_C = Spring compressed length (calculated from Tables 1 and 2)

Examples of Stress Calculations for P-leg in Overcompressed Stage:

Nominal

from Tables 10-1 and 10-2

L_C = Stack Height – Component Height Total

L_C = .9910 – .5775

L_C = .4135 inches

$F_{si} = K [L_{FL} - L_C]$

$F_{si} = 94.4 [.545 - .4135]$

F_{si} = 12.41 lbs.

$$\sigma_i = \frac{1}{A} [F_{si} - F_i]$$

$$\sigma_i = \frac{1}{.0547} [12.41 - 1.25]$$

σ_i = 204 lbs/in^2

Maximum

$L_{C\,min}$ = Minimum stack height – maximum component height total

$L_{C\,min}$ = .9865 – .5915

$L_{C\,min}$ = .3950 inches

$F_{si\,max} = K_{max} [L_{FL\,min} - L_{C\,min}]$

= 112.5 [.535 – .395]

= 15.75 lbs.

$$\sigma_{i\,max} = \frac{1}{A_{min}} [F_{si\,max} - F_i]$$

$\sigma_{i\,max}$ = 267 lbs/in^2

Minimum

$L_{C\ max}$ = Maximum stack height – Minimum component height total

= .9955 – .5645

= .431

$F_{si\ min} = K_{min}\ [L_{FL\ max} - L_{C\ max}]$

= 80 [.555 – .431]

= 9.92 lbs.

$$\sigma_{i\ min} = \frac{1}{A_{max}}\ [F_{si\ min} - F_i]$$

$$= \frac{1}{.0551}\ [9.92 - 1.25]$$

$\sigma_{i\ min}$ = 157.4 lbs/in^2

The remainder of the initial stress calculations will not be shown. The results are summarized in Table 10-3.

TABLE 10-1

STACK HEIGHTS (INCHES)

	Nominal	Maximum	Minimum
Overcompressed Stack Heights (.030 overcompression)	.9910	.9955	.9865
Fully Assembled Stack Heights (with .0025 housing deflection)	1.0235	1.0280	1.0190
Heat-Up Stack Height (with .020 POCO expansion)	1.0035	1.0080	.9990

TABLE 10-2

Summation of Components in Stack

N-Leg Stack Dimensions (inches)

Component	Nominal	Maximum	Minimum
Pt. Hot End Foil	.0005	.0005	.0005
Hot Strap and Gimbal	.100	.101	.099
Ni Foil	.005	.006	.004
N-Leg Assembly	.305	.308	.302
Cold End Strap Assembly	.075	.081	.069
Twist Lock	.039	.041	.037
Cold Frame Assembly	.040	.042	.038
Tin Foil	.001	.001	.001
Total:	.5655	.5805	.5505

P-Leg Stack Dimensions (inches)

Component	Nominal	Maximum	Minimum
Pt. Hot End Foil	.0005	.0005	.0005
Hot Strap	.068	.069	.068
P-Leg Assembly	.354	.357	.351
Cold End Strap Assembly	.075	.081	.069
Twist Lock	.039	.041	.037
Cold Frame Segment	.040	.042	.038
Tin Foil	.001	.001	.001
Total:	.5775	.5915	.5645

TABLE 10-3

Initial Leg Stress Summary (PSI)

	P-LEG			N-LEG		
	Nominal	Minimum	Maximum	Nominal	Minimum	Maximum
Overcompressed State	204	157	267	384	284	515
Fully Assembled State	148	110	200	276	196	381
Heat-Up State	182	139	241	341	250	464

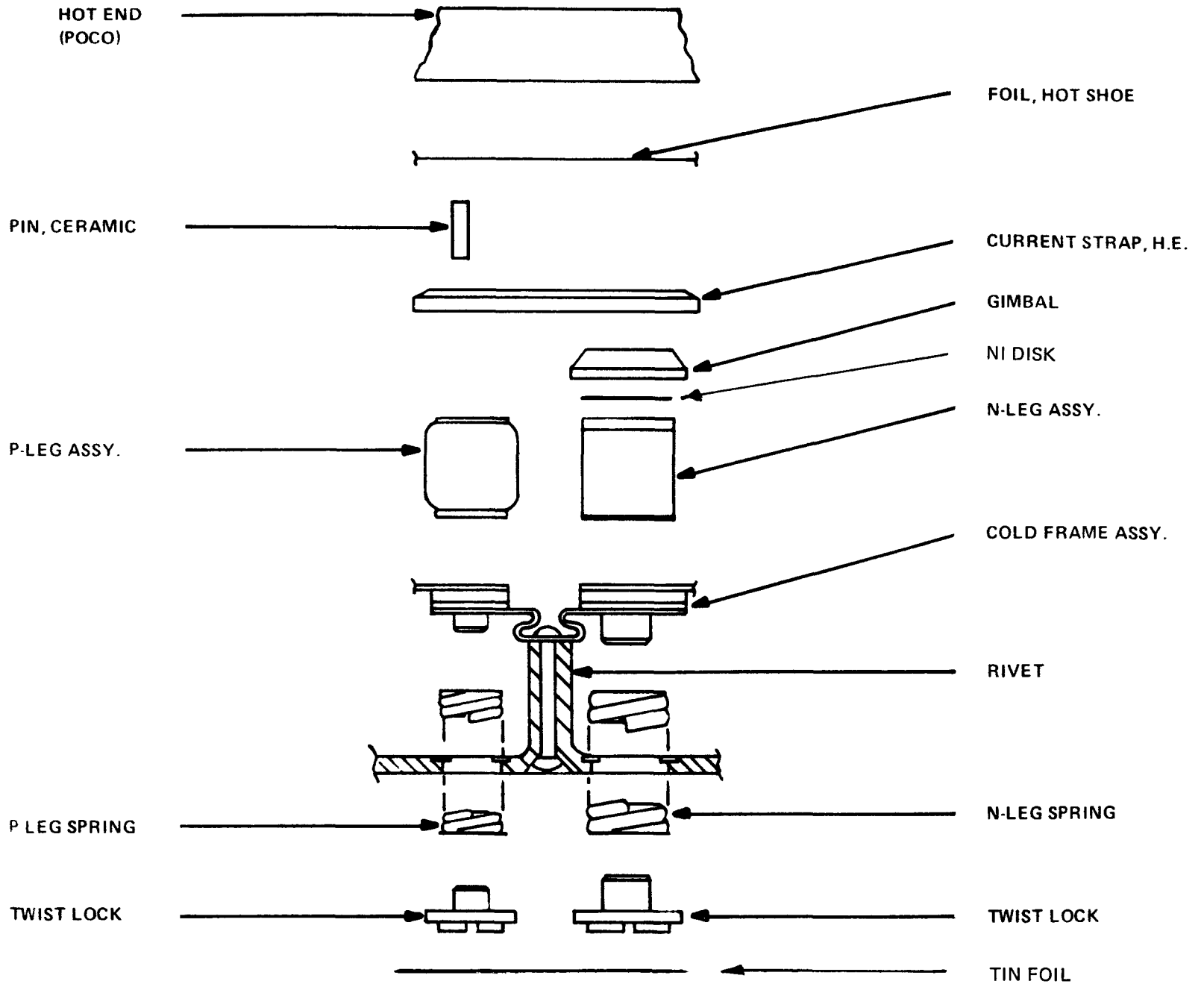

FIGURE 10-1: TYPICAL COUPLE HARDWARE

ATTACHMENT 11

Copper Stiffening During Diffusion Bonding

During the early part of January, the T/E cold end diffusion bonding process was transferred to ARO Industries. During the initial installation of the glove box, a few alterations were introduced as follows:

1. A new pressure scale was altered to allow for operation in a high temperature environment.
2. The press was secured to the scale to prevent slipping during bonding.
3. The Pyrometer used to sense the heater temperature was calibrated.
4. A new heater block and firebrick retainer were installed.
5. New POCO pressure pads and retainers were fabricated to comply with the revised shape of the straps and followers.

After the installation was complete and the first followers were diffusion bonded, a drastic decrease in flexibility in the unbonded region was noted. A strong effort was immediately initiated to find the reason for this problem.

The new scale, secured press, and calibrated pyrometer seemed the least likely candidates for the problem.

The new POCO was analyzed by Central Research. Although some surface impurities were found (small amounts of sulpher and chlorine), the operating temperature of the POCO (1020°C) will act as a natural processing step to eliminate them during bonding. No vanadium or other metallic contamination was detected.

Varying the operating temperature, pressure, and bonding time was attempted with little change in the excessive stiffness of the products.

The new design of the pressure pads and retainers was then investigated. It was found that by bonding the followers with no retainer produced a good flexible follower comparable to the old style that was bonded at 3M. The new retainers were found to have a tighter fit to the followers. While bonding, the retainer is at or near the temperature of the heater block. With the tight fit between the edges of the follower, pressure pad, and retainer, a bond at the edges of the follower was being produced.

By recessing the inside surface of the retainer in the flexible region of the followers, the problem was eliminated.

In an effort to further increase the flexibility and assure that bonding does not occur in the flex area, a new procedure as shown below was initiated.

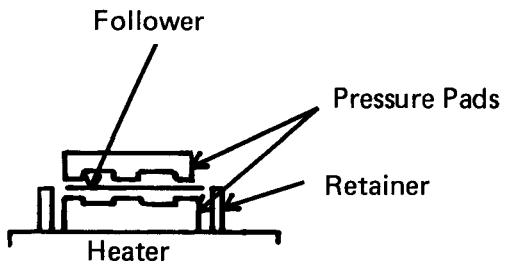

NEW

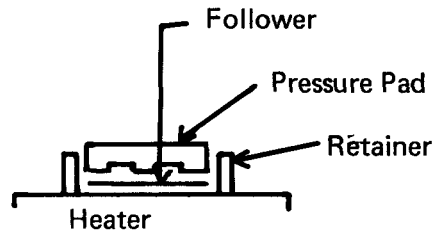

OLD

By inverting a thin pressure pad on top of the heater, the extreme, direct heat being applied to the bottom of the follower in the flexible regions is eliminated. This procedure will also be used for bonding the cold straps.

ATTACHMENT 12

Reproduceability of Cold-End Hardware ΔT

Introduction

The sliding hardware has a high thermal resistance at the interface of the follower and rail. This resistance inhibited the flow of heat out of the element, and the proper temperature gradient was not obtainable. One of the reasons the compliant hardware was designed was to alleviate this problem. The heat pathway for the compliant hardware is illustrated on Figure 12-1. An important link in the pathway is the solder bond, and it can vary with each cold end assembly. The effect the quality of this bond has on the thermal resistance should be determined in order to insure the elements can obtain design operating conditions. This document will describe an effort that was made to determine the thermal resistance of six cold end assemblies, and the correlation to the bond qualities.

Procedure

The thermal resistance of the hardware was determined by exposing the follower assembly to a known heat flux, measuring the temperature difference between the base of the rail and follower, and then calculating the thermal resistance:

$$\overline{R} = \frac{(\overline{T_f - T_r})}{\overline{Q}}$$

when: $\overline{Q}$ = average heat flux through one leg

T_f = temperature of follower

T_r = temperature at the base of rail

$\overline{R}$ = average thermal resistance of the thru rail pathway

X-rays were taken of the hardware, and inspected to differentiate between the quality of the bonds. The criteria used to decide on the grade of a bond was the melt of the solder.

Results

TABLE #1

Assembly #	Thermal Resistance (°C/W)	Bond Quality
1	5.04	Good
2	7.08	Poor
3	7.92	Fair
4	6.40	Poor
5	6.42	Good
6	6.22	Poor

Note: Quality control specifications 7 $\pm$ 3 °C/W

Conclusion

The thermal resistance of each specimen was compared to the X-ray, and it is concluded that there is no correlation between the thermal resistance and the quality of the bond as indicated by the X-ray. The variation that did occur in the values can be explained by the different contact resistances experienced by the cold end assemblies in the test fixture.

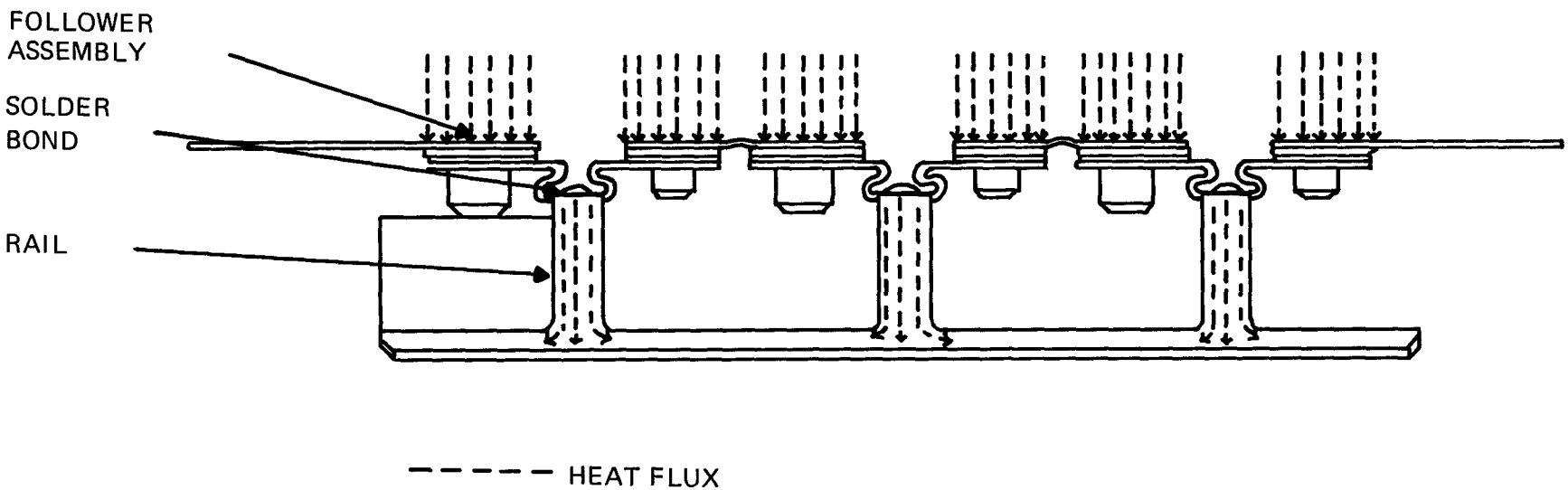

FIGURE 12-1: COLD END ASSEMBLY

II. DESIGN ANALYSIS

A. COUPLE PERFORMANCE PROGRAM

1. Description of the Program

Through a cooperative effort between the Pioneering Lab and an independent support group within 3M, a program for evaluating couple performance was developed. The approach used was to write an algorithm that solves the conservation of energy equation for the case of temperature dependent thermophysical properties. With the temperature profile and property profiles in hand it is a simple matter to compute the relevant performance indicators, e.g. heat flux input, power output and load voltage. The program was written to handle only one-dimensional configurations (perfectly insulated), and currently accepts only specified temperature boundary conditions. Also both N- and P-leg models may be segmented. The program is sufficiently general as to allow it to be used not only for evaluation of existing designs, but also as a design tool. Property data for several state-of-the-art materials was incorporated in order to permit meaningful studies of relative potentials. The material library is listed in Figure II-1.

For the one-dimensional case, the equation describing the temperature distribution in a thermoelectric element is:

$$-\frac{d}{dx}\left(k(T)\frac{dT}{dx}\right)+T\frac{d\alpha(T)}{dx}-\rho(T)J^2=0 \qquad (1)$$

where k(T) is thermal conductivity, $\alpha(T)$ is the Seebeck coefficient, $\rho(T)$ is the electrical resistivity, J is the current density, T is temperature and x is the spatial coordinate. This equation, when integrated over a finite control volume, yields the finite difference equation:

$$\dot{Q}_{x+dx}=\dot{Q}_x+\dot{Q}_{gx}\ ,\ \dot{Q}_{gx}=-I\overline{T}_x(\alpha_{x+dx}-\alpha_x)+I^2R_x \qquad (2)$$

where $\dot{Q}$ represents heat flux, the subscript g means internally generated, $\overline{T}_x$ is a locally averaged temperature, I is the current flow, and R_x is a local electrical resistance. Figures II-2 and II-3 illustrate how the difference equation is utilized. Note that this is a forward integration algorithm.

As Figure II-3 shows, it is necessary to iterate for property values simultaneously with temperature since the properties are temperature dependent. With the exception of P-leg carrier concentration, all property data is stored in subroutines. The carrier concentration is calculated within the program itself. The equation describing the distribution of extrinsic carriers is:

$$\vec{\nabla} n_o = B\frac{I}{A}\left(\frac{T}{773}\right)^{2/3} \qquad (3)$$

The solution to this equation can be suitably approximated by:

$$n_o\,(x + dx) = n_o\,(x) + B\,\frac{I}{A}\left(\frac{T(x) + T(x + dx)}{(2)\ (773)}\right)^{2/3} dx \qquad (4)$$

where B is a constant of known value, A is cross-sectional area, and (x) means at location x. Note that n_o at x = 0 ties down the carrier concentration throughout the leg. (Recall that the carrier concentration at x = 0 (the cold end of the P-leg) is tied down by bonding a copper disc onto the leg there.)

It is known that at very high temperatures, the excitation of intrinsic carriers becomes important. Since the equations describing P-leg property values in the program are expressed in terms of total carrier concentration n_+:

$$n_+(x) = n_o\,(x) + g \qquad (5)$$

where

$$g = aT^4 \exp\ [-6605/T]\ n_+^{-.92} \qquad (6)$$

and a is a known constant. Notice that equation (5) requires an iterative solution. Figure II-4, essentially a modification of Figure II-3, illustrates how this computation fits into the algorithm.

Figure II-5 shows a flow chart for the entire program. It shows how the forward integration algorithm fits in.

2. Accomplishments

1. The algorithm's accuracy has been verified by comparison with an exact solution available in the literature[1]. The problem treated was sample 2 from the source cited. The problem was chosen because the thermoelectric properties are temperature dependent. The numerical solution appears in Figure II-6 and the exact solution is given in Figure II-7. The problem was solved for maximum thermoelectric efficiency.

The excellent agreement between the two (2) solutions permits the following conclusion to be made: Discrepancies between experimental data and numerical data are attributable either to deviation from one-dimensional flow of heat and/or current, or to inaccuracy in property data equations.

---

1) Sherman et al, J. Appl. Phys., 31 - 1, Jan., 1960

Library of Materials and Sources of Property Data

	Material	Type	Source
1.	$NdSe_x$	N	Largely from cubic $GdSe_x$ data (should be similar); Partial confirmation on S and ρ from single element tests P/S 75 (Ref. Top Summary Report 107, Table 4)
2.	Orthorhombic $GdSe_x$	N	S and ρ data from N2639 T3-14 k data from N2646 T2-13
3.	2N Pb/Te	N	Internal memo by R.W. Fritts
4.	SiGe (78/22) t = 0	N	Publication by V. Raag, 11th IECEC
5.	Same as 4 t = 5 yrs.	N	Same as 4
6.	TPM-217	P	Extensive internal experimentation for S and ρ. Comparative measurement at Resalab for k Pulse diffusivity at Battelle for k Pulse diffusivity at Sandia for k
7.	2P Pb/Te	P	Same as No. 3
8.	SiGe (78/22) t = 0	P	Same as No. 4
9.	Same as 8 t = 5 years	P	Same as No. 4
10.	Adv. SiGe (63/37)	P	Publication by R.K. Pisharody and L.P. Garvey, 13th IECEC – Sample 2

FIGURE II-1: COUPLE PERFORMANCE PROGRAM

(I-2)

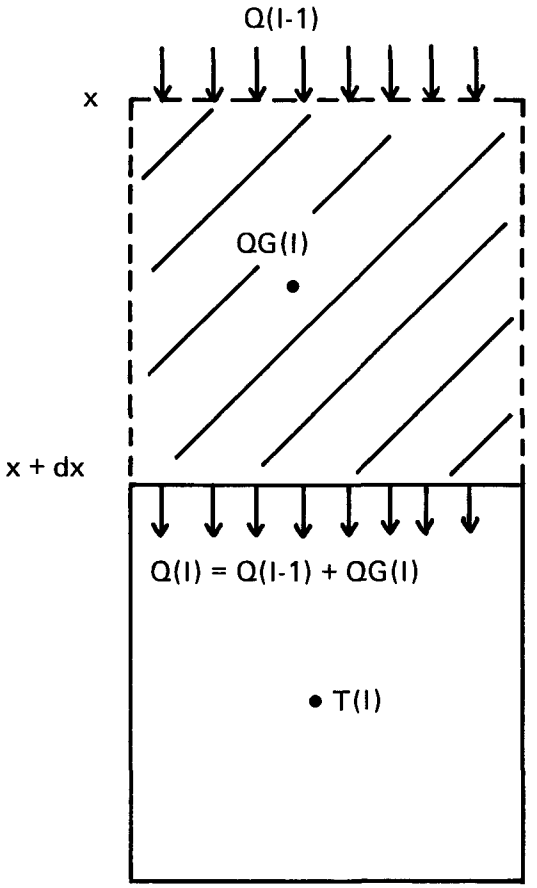

FIGURE II-2: GRAPHICAL REPRESENTATION OF THE COMPUTATION OF HEAT FLUXES

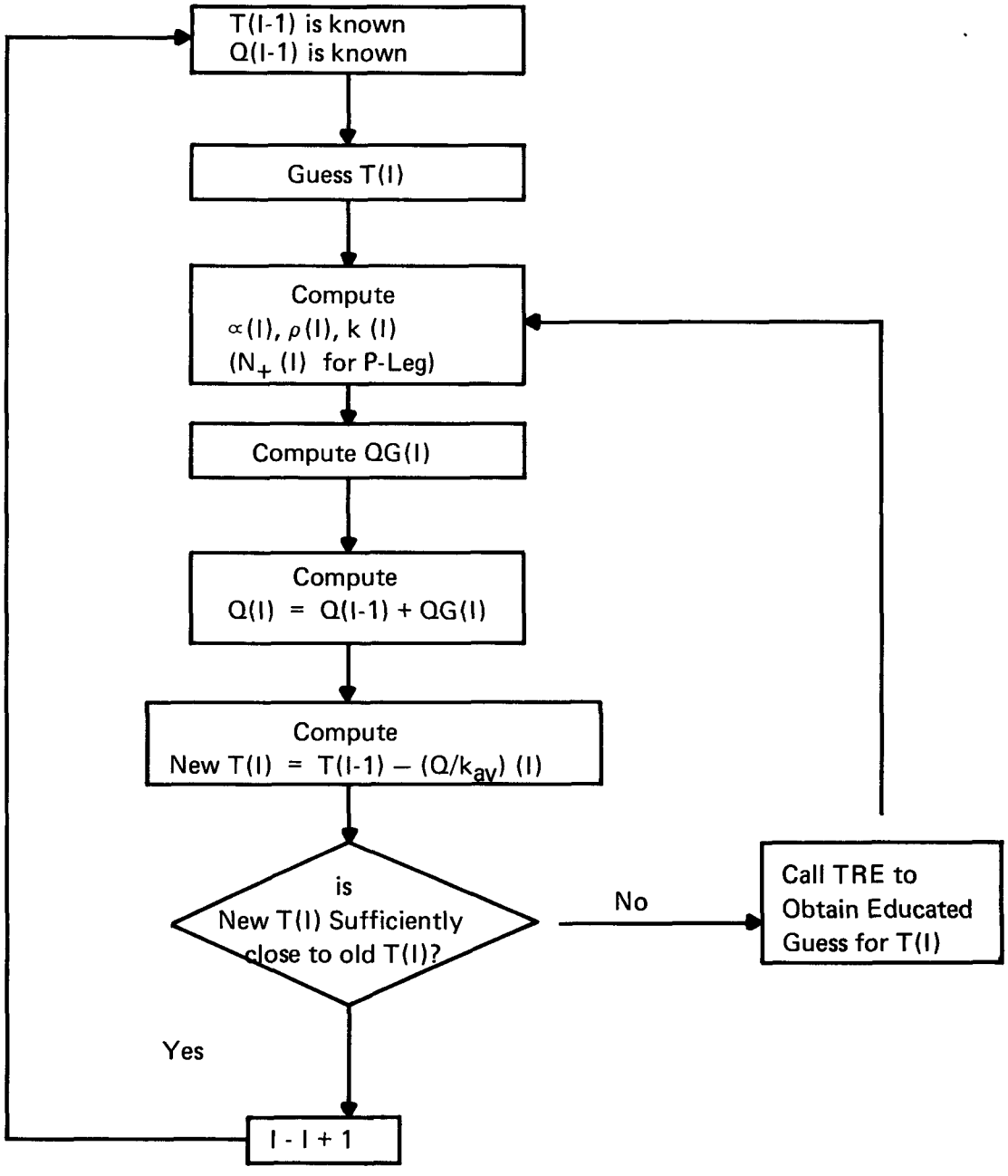

FIGURE II-3: FLOW CHART ILLUSTRATING FORWARD INTEGRATION PROCEDURE

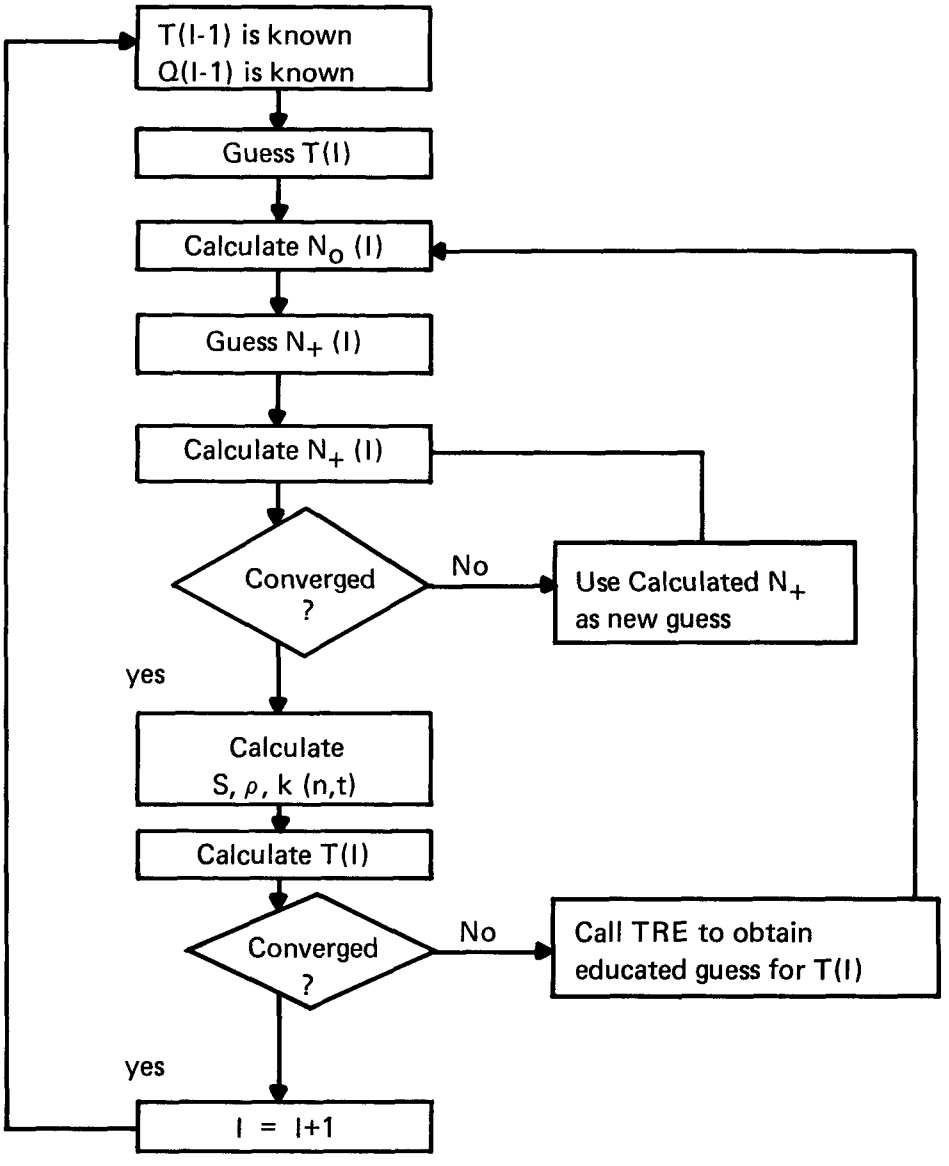

FIGURE II-4: FLOW CHART FOR P-LEG SOLUTION

2. Seebeck coefficient and electrical resistivity models for the P-leg have been verified. Figure II-8 shows comparisons between the numerical model and several of the most recent tests conducted. For single element tests, seebeck coefficient predictions fall within 3% of measured values fairly consistently while electrical resistivity falls within 9%.

3. A study was performed to determine a comparison of the selenides with respect to other state-of-the-art materials, e.g. Silicon Germanium and Lead Telluride systems. This was accomplished by calculating maximum attainable thermoelectric efficiency for various operating temperature intervals, with all thermal and electrical contact resistances set to 0. The results, which are shown in Figure II-9, indicate a number of things. First, the selenide materials offer the potential for far superior performance over the Silicon Germanium systems. Second, the Silicon Germanium system has as a characteristic an unavoidable and predictable degradation mechanism that brings about a significant loss in efficiency over a five year period. Third, a lead telluride-selenide segmented N-leg offers additional significant performance gains to the selenide systems. The curve titled M-9 BOL has been included to show what level of performance has been attainable to date. Ideally, M-9 performance should have fallen near the curve entitled $NdSe_x$/TPM-217.

   The presence of electrical contact resistances and high resistances in the N-leg are responsible for holding the performance down.

   Figures II-10 and II-11 focus entirely on the selenides. These curves represent maximum attainable efficiencies for the conditions cited. Several interesting points can be made from these plots. First, the variation of T_{HN} has a stronger effect on performance for couples with $NdSe_x$ N-legs than for couples with $GdSe_x$ N-legs. Similarly, performance is more sensitive to the temperature interval of the P-leg than to the temperature interval of any of the N-legs. This is an indication that the P-leg is the largest contributor in any selenide couple thought of to date. Also, it indicates that a $NdSe_x$ N-leg plays a larger role than a $GdSe_x$ N-leg. These curves represent what should be attainable levels of performance.

4. It has been used to generate the SN-1 leg designs, which will be used in M-22R. It has also been used to generate designs for $NdSe_x$ N-legs.

5. A study was conducted to determine how sensitive overall performance is to variations of various controllable parameters, e.g. thermoelectric element dimensions, hardware and contact resistances and thermoelectric material properties. The purpose of the sensitivity study was to answer the question: How much variability can be accepted from couple to couple and still be within the limits of acceptable performance? The information for the study was obtained by making a series of computations which involved perturbing one parameter while holding the others fixed[2] and observing the effects on relevant performance parameters, e.g. thermoelectric efficiency, P-leg T_H, N-leg T_{seg} and leg resistance. For all calculations, heat flux per couple and the load voltage were constrained to fixed values in order to simulate a module environment.

---

2) Note: In actuality, these parameters are not completely independent of one another so that it is impossible to vary one parameter and fix the others. However, the degree of dependency is low.

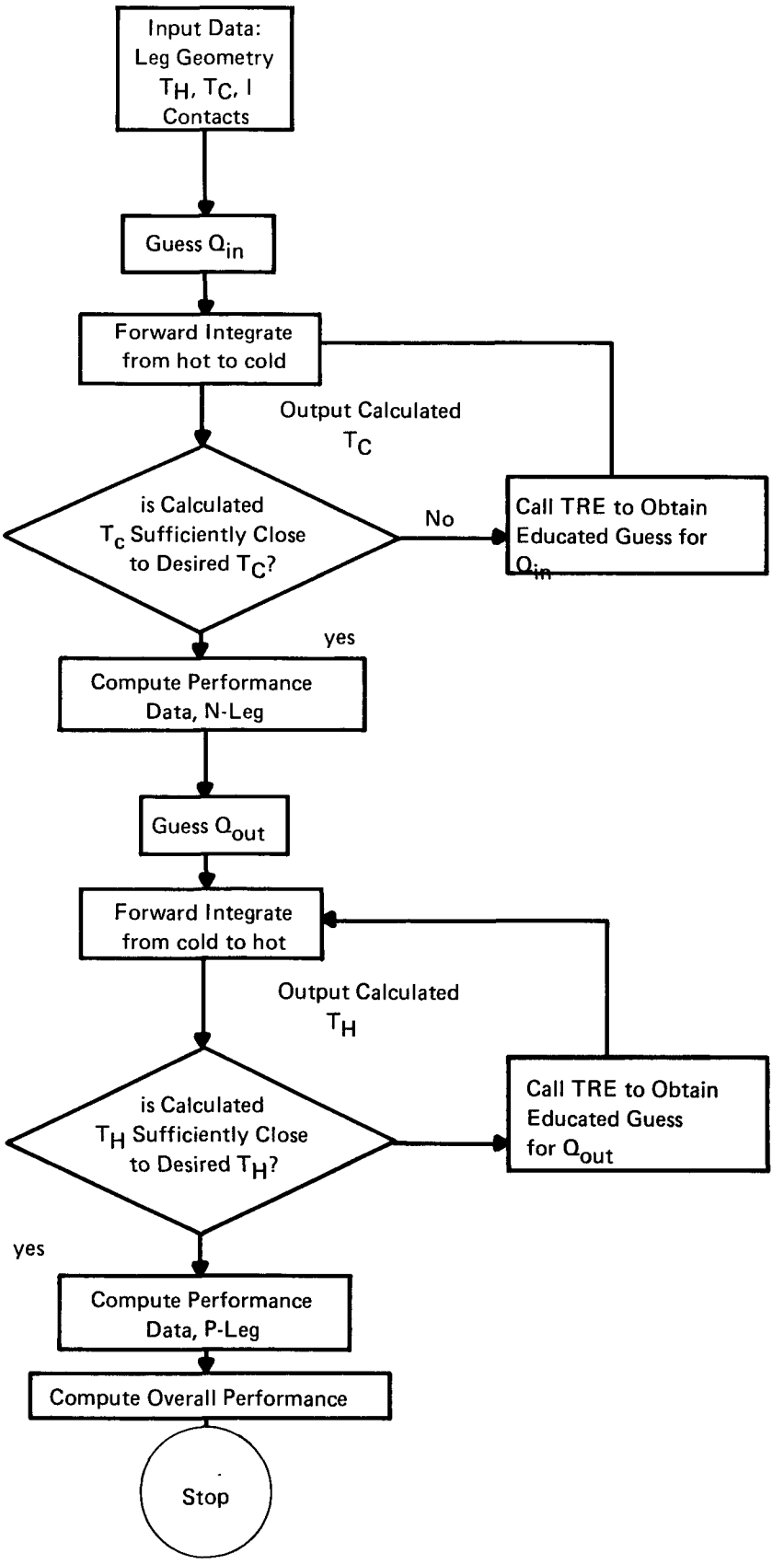

FIGURE II-5: A GENERAL FLOW CHART FOR PROGRAM COUPLE 1

Couple 1, Exe. 7, 5-JUN-79
Enter Parameters: 0,1,1,5,1
Increments: .2, .1
No. of N, P Leg Segments: 1, 1
N Leg thermal contacts – hot to cold: 0,0
N Leg Elec. contacts – hot to cold: 0, 0
P Leg Thermal contacts – cold to hot: 0, 0
P Leg elec. contacts – cold to hot: 0, 0
THN, THP, TON, TOP, I, ECC, Y: 1227, 1227, 127, 127, 55., 30., .0136
N Leg segments – N, D, L, Mat, Rext: 30, .942, .394, 4, 1.0
P Leg segments – N, D, L, Mat: 30, .444, .394, 2
1, .100
%FRSAPR floating divide check PC = 6502
%FRSAPR floating overflow PC = 6507

N-LEG SOLUTION

X	T (X)	K (X)	RHO (X)	ALPH (X)	Q (X)
.000	♦♦♦♦♦	2.00	15.00	100.0	22.78
.035	♦♦♦♦♦	2.12	14.17	116.6	22.27
.069	♦♦♦♦♦	2.24	13.42	131.7	21.37
.104	999.6	2.36	12.73	145.5	20.62
.138	936.1	2.48	12.09	158.2	19.99
.173	877.4	2.61	11.50	169.9	19.46
.207	822.8	2.74	10.96	180.8	19.01
.242	771.8	2.87	10.45	191.0	18.63
.276	723.9	3.01	9.97	200.6	18.30
.311	679.0	3.15	9.52	209.6	18.03
.345	636.6	3.30	9.10	218.1	17.79
.380	596.6	3.45	8.70	226.1	17.59
.414	558.7	3.61	8.32	233.7	17.42
.449	522.7	3.77	7.96	240.9	17.27
.483	488.6	3.94	7.62	247.7	17.15
.518	456.1	4.11	7.29	254.2	17.05
.552	425.1	4.30	6.98	260.4	16.96
.587	395.6	4.49	6.69	266.3	16.89
.621	367.4	4.68	6.40	271.9	16.83
.656	340.4	4.89	6.13	277.3	16.79
.690	314.7	5.10	5.88	282.5	16.75
.725	290.1	5.33	5.63	287.4	16.73
.759	266.5	5.56	5.40	292.1	16.71
.794	244.0	5.80	5.17	296.6	16.69
.828	222.4	6.06	4.95	300.9	16.69
.863	201.7	6.32	4.75	305.1	16.69

FIGURE II-6: SAMPLE PROBLEM 2 SOLUTION

N-LEG SOLUTION (Continued)

X	T (X)	K (X)	RHO (X)	ALPH (X)	Q (X)	
.897	181.8	6.60	4.55	309.0	16.69	
.932	162.8	6.88	4.36	312.8	16.70	
.966	144.5	7.18	4.18	316.5	16.71	
♦♦♦♦	127.1	7.50	4.00	320.0	16.72	
♦♦♦♦	535.0	4.27	8.08	238.4	22.78	Integrated Averages

SEG. NO	THOT	TCOLD
1	1227.0	127.1

POUT = 7.2500
QIN = 30.969
RES = 1.80
EFF = .2341

P-LEG SOLUTION

X	T (X)	EN (X)	K (X)	RHO (X)	ALPH (X)	Q (X)
.000	127.0	.099	25.00	2.50	200.0	♦♦♦♦♦
.035	149.0	.111	23.70	2.37	200.0	♦♦♦♦♦
.069	171.9	.123	22.48	2.25	200.0	♦♦♦♦♦
.104	195.6	.136	21.34	2.13	200.0	♦♦♦♦♦
.138	220.2	.149	20.28	2.03	200.0	♦♦♦♦♦
.173	245.7	.162	19.28	1.93	200.0	♦♦♦♦♦
.207	272.1	.176	18.34	1.83	200.0	♦♦♦♦♦
.242	299.6	.191	17.47	1.75	200.0	♦♦♦♦♦
.276	328.0	.206	16.64	1.66	200.0	♦♦♦♦♦
.311	357.5	.221	15.86	1.59	200.0	♦♦♦♦♦
.345	388.0	.237	15.13	1.51	200.0	♦♦♦♦♦
.380	419.7	.253	14.44	1.44	200.0	♦♦♦♦♦
.414	452.5	.270	13.78	1.38	200.0	♦♦♦♦♦
.449	486.5	.288	13.17	1.32	200.0	♦♦♦♦♦
.483	521.7	.306	12.58	1.26	200.0	♦♦♦♦♦
.518	558.1	.324	12.03	1.20	200.0	♦♦♦♦♦
.552	595.9	.343	11.51	1.15	200.0	♦♦♦♦♦
.587	635.0	.363	11.01	1.10	200.0	♦♦♦♦♦
.621	675.5	.384	10.54	1.05	200.0	♦♦♦♦♦
.656	717.4	.405	10.10	1.01	200.0	♦♦♦♦♦
.690	760.8	.427	9.67	0.97	200.0	♦♦♦♦♦

FIGURE II-6: SAMPLE PROBLEM 2 SOLUTION (Continued)

P-LEG SOLUTION (Continued)

X	T (X)	EN (X)	K (X)	RHO (X)	ALPH (X)	Q (X)
.725	805.8	.450	9.27	0.93	200.0	♦♦♦♦♦
.759	852.3	.473	8.89	0.89	200.0	♦♦♦♦♦
.794	900.5	.498	8.52	0.85	200.0	♦♦♦♦♦
.828	950.3	.524	8.17	0.82	200.0	♦♦♦♦♦
.863	♦♦♦♦♦	.551	7.84	0.78	200.0	
.897	♦♦♦♦♦	.580	7.53	0.75	200.0	
.932	♦♦♦♦♦	.610	7.23	0.72	200.0	
.966	♦♦♦♦♦	.643	6.94	0.69	200.0	
♦♦♦♦						
♦♦♦♦	585.2	.338	13.43	1.34	200.0	

SEG. NO	THOT	TCOLD
1	1227.0	127.0

POUT = 7.9994
QIN = 28.032
RES = 1.35
ENC = .0991
ENH = .6784
EFF = .28537

POUT = ♦♦♦♦♦♦♦
QTOT = 59.001
T.E. EFF = .25846 → η = 25.8%

ECC = 46.92128 → Ecc per Couple = $\frac{46.92}{168}$ = .279V → Load Resistance = $\frac{.279V}{54.6A}$ = 5.12 mr

AMPS = 54.60000 → I = 54.6 Amps

FIGURE II-6: SAMPLE PROBLEM 2 SOLUTION (Continued)

Maximum Thermoelectric Efficiency = 26%

Load Resistance = 51 mΩ

Current Flow = 55 A

FIGURE II-7: THE EXACT SOLUTION CORRESPONDING TO THE APPROXIMATE SOLUTION OF FIGURE 5

A. Single Element Tests

Test Name	Temperature Interval (°C)	IL/A (A/cm)	Seebeck Coef (μV/°C)		Resistivity (mΩ-cm)	
			Measured	Predicted	Measured	Predicted
ATT 591	900/150	10.8	--	241	--	6.67
ATT 592	900/150	10.8	220	241	6.10	6.67
ATT 593	900/150	10.8	220	241	6.10	6.67
ATT 594	900/150	10.8	233	241	6.40	6.67
ATT 595	900/150	10.8	241	241	7.00	6.67
ATT 596	900/150	10.8	234	241	7.10	6.67
CC1	800/200	0.60	288	283	16.6	14.2
"	800/200	4.71	277	270	12.0	10.6
"	800/200	9.42	260	258	9.27	8.46
"	800/200	14.61	247	246	7.56	7.06
"	800/200	18.85	240	239	6.66	6.27
ATT 600	900/164	16.51	235	239	5.71	6.19

B. Multi-Element Tests

Test Name	Temperature Interval (°C)	IL/A (A/cm)	Seebeck Coef (μV/°C)		Resistivity (mΩ-cm)	
			Measured	Predicted	Measured	Predicted
M-21	913/160	13.4	211	245	6.76	6.91
ATT 590	850/150	6.94	218	243	7.61	7.23

FIGURE II-8: A COMPARISON OF THE P-LEG NUMERICAL MODEL WITH EXPERIMENT

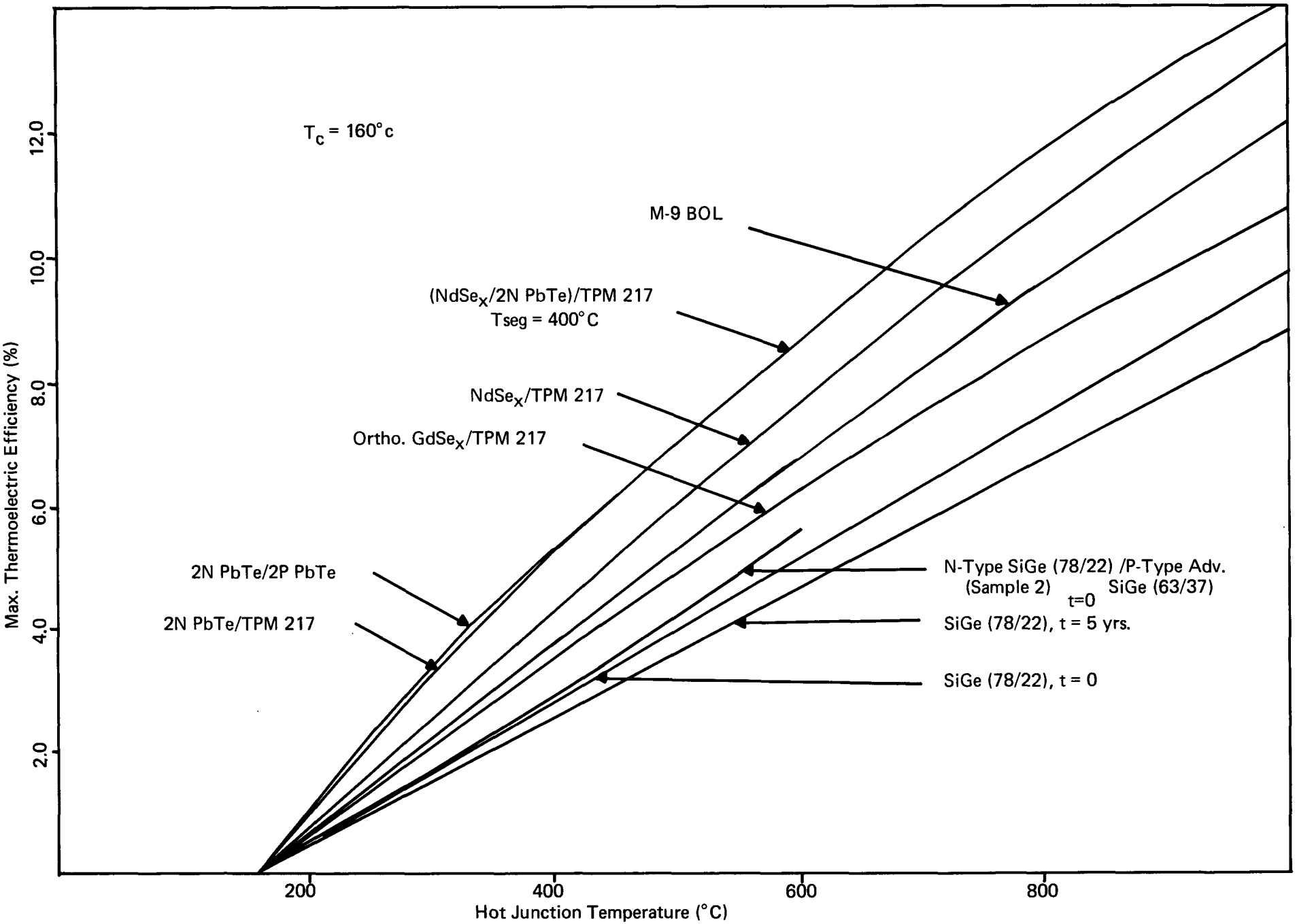

FIGURE II-9: A COMPARISON OF POTENTIALS FOR VARIOUS THERMOELECTRIC MATERIAL PAIRS

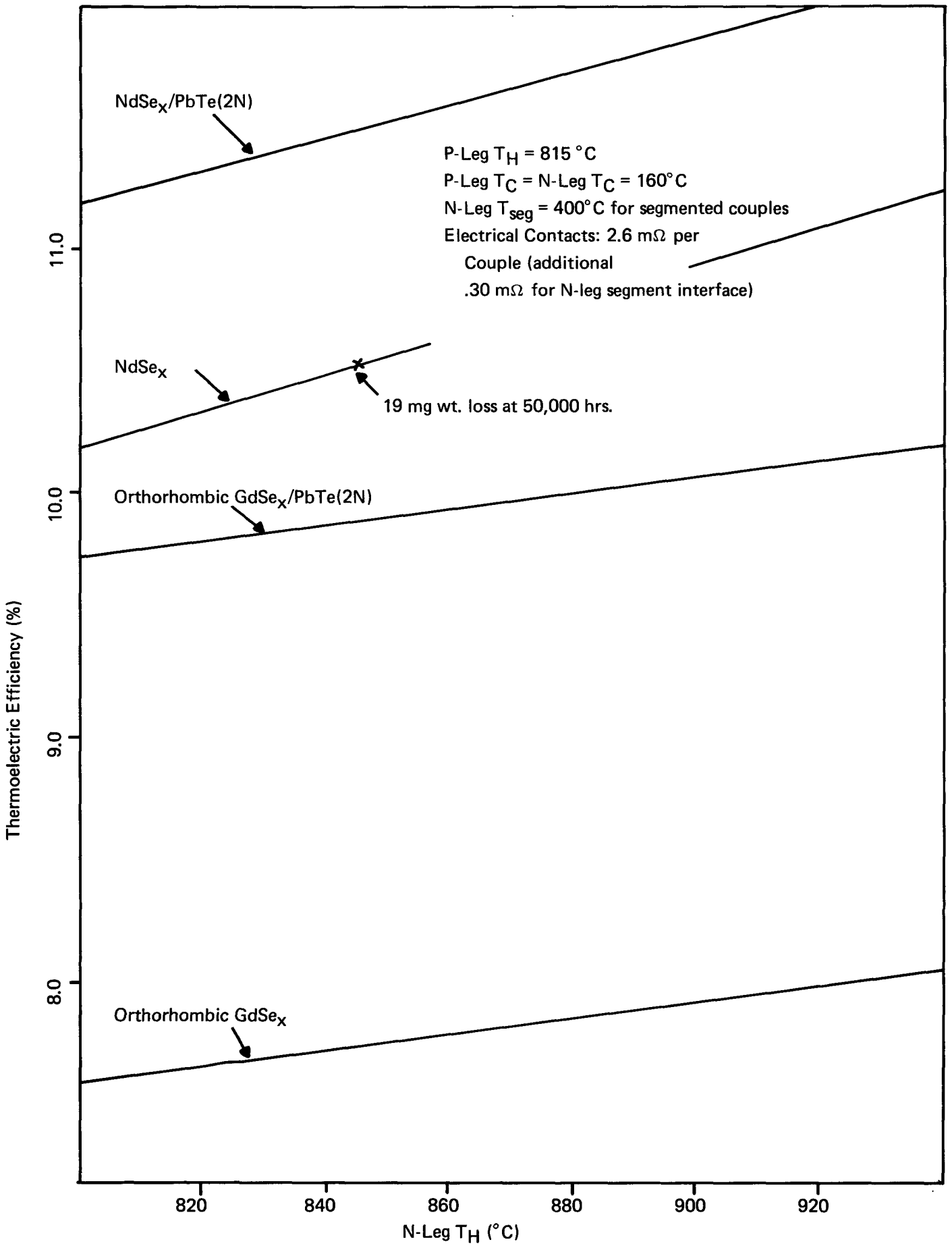

FIGURE II-10: THERMOELECTRIC EFFICIENCY VS. N-LEG HOT JUNCTION TEMPERATURE

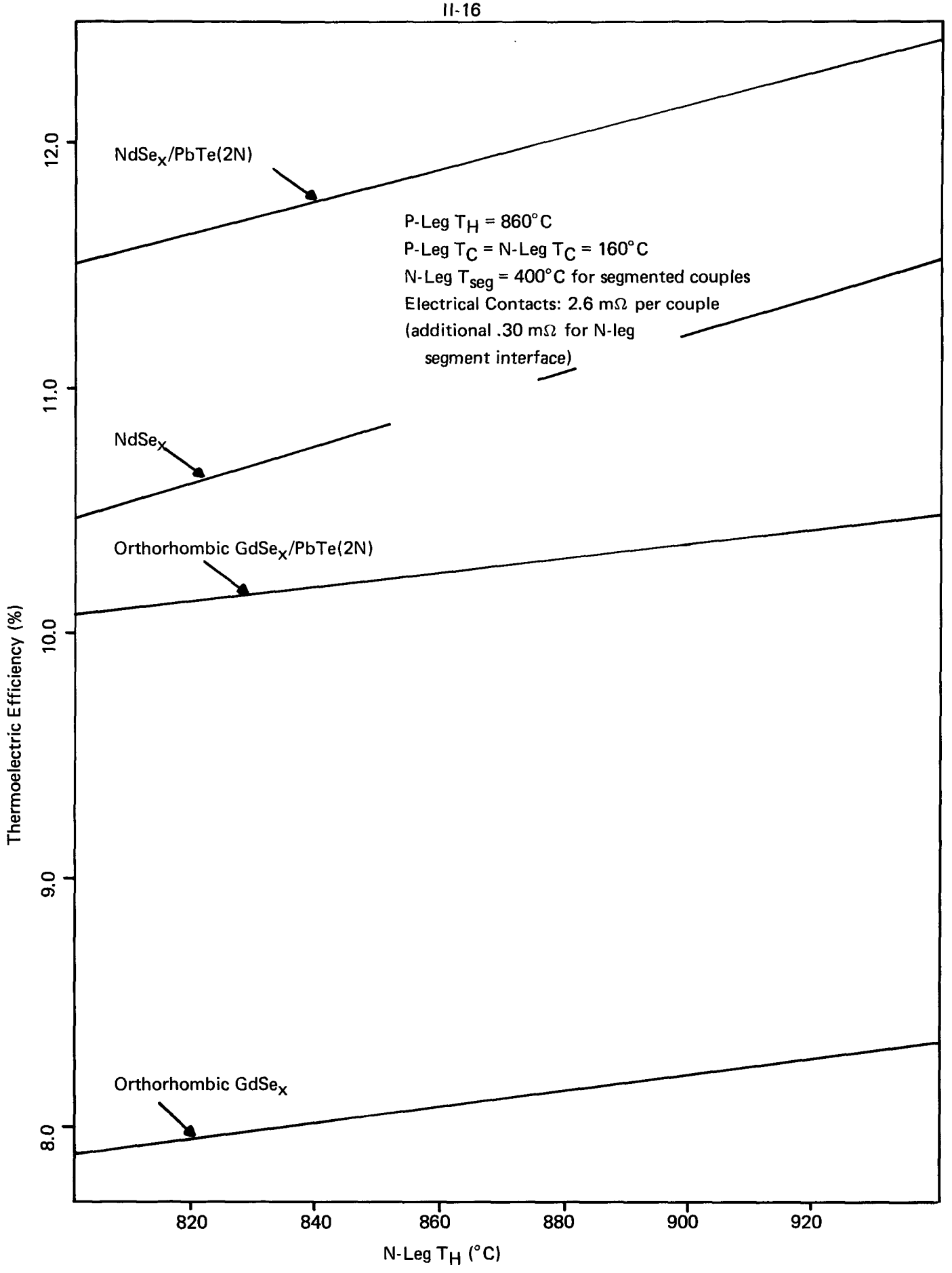

FIGURE II-11: THERMOELECTRIC EFFICIENCY VS. N-LEG HOT JUNCTION TEMPERATURE

B. EFFECTS OF POINT CONTACTS ON THE ELECTRICAL BEHAVIOR OF TPM-217

Since P-leg carrier concentration is dependent upon current density, the occurrence of point contacts at either end of the leg could have a significant effect on its electrical behavior. A study to evaluate this effect was started but has not been completed. The following approach was taken.

An axisymmetric configuration was assumed. A one-dimensional resistivity distribution comparable to that of a P-leg operating at 860/160°C was imposed across the solution plane. The current density distribution was obtained with the use of a two-dimensional heat conduction program.

The only cases run thus far have been for constriction at the hot end of the leg. Three (3) solutions have been obtained: no constriction, constriction over 50% of the diameter, and constriction over 90% of the diameter. The results have not been analyzed, but a plot of the 50% solution is shown in Figure II-13. Since the carrier concentration throughout the P-leg is tied to the cold end, it is suspected that constriction at the cold end would be a more serious problem than constriction at the hot end. Post test observations of Module M-21 and other single-element tests have shown this to be a real possibility.

C. HEAT FLOW THROUGH A CONVERTER

1. Bypass Heat Flow Through a Converter

This calculation was made for the SN-1 design. The objective was to determine the magnitude of the heat flux flowing around the elements and through the Hi-Fi thermal insulation and through the P-leg slurry wrap. The details of the calculation are shown in Figure II-14. The bypass heat flux total of 221.5 W is higher than older estimates because the smaller N-leg diameter for the segmented design has affected an increase in bypass area. This figure represents approximately 11% of the total available heat flux.

2. Thermal Resistance of Cold End Hardware

A thermal resistance calculation was made for the SN-1 reference design cold end hardware. Details of the calculation are shown in Figures II-15, and II-16. The compression springs have not been included in the model. They were found to have a sufficiently high resistance so as not to be significant. The resistance figure 7.2°C/W has been confirmed experimentally. Note that this does not include contact resistances but represents only the resistance of the hardware itself.

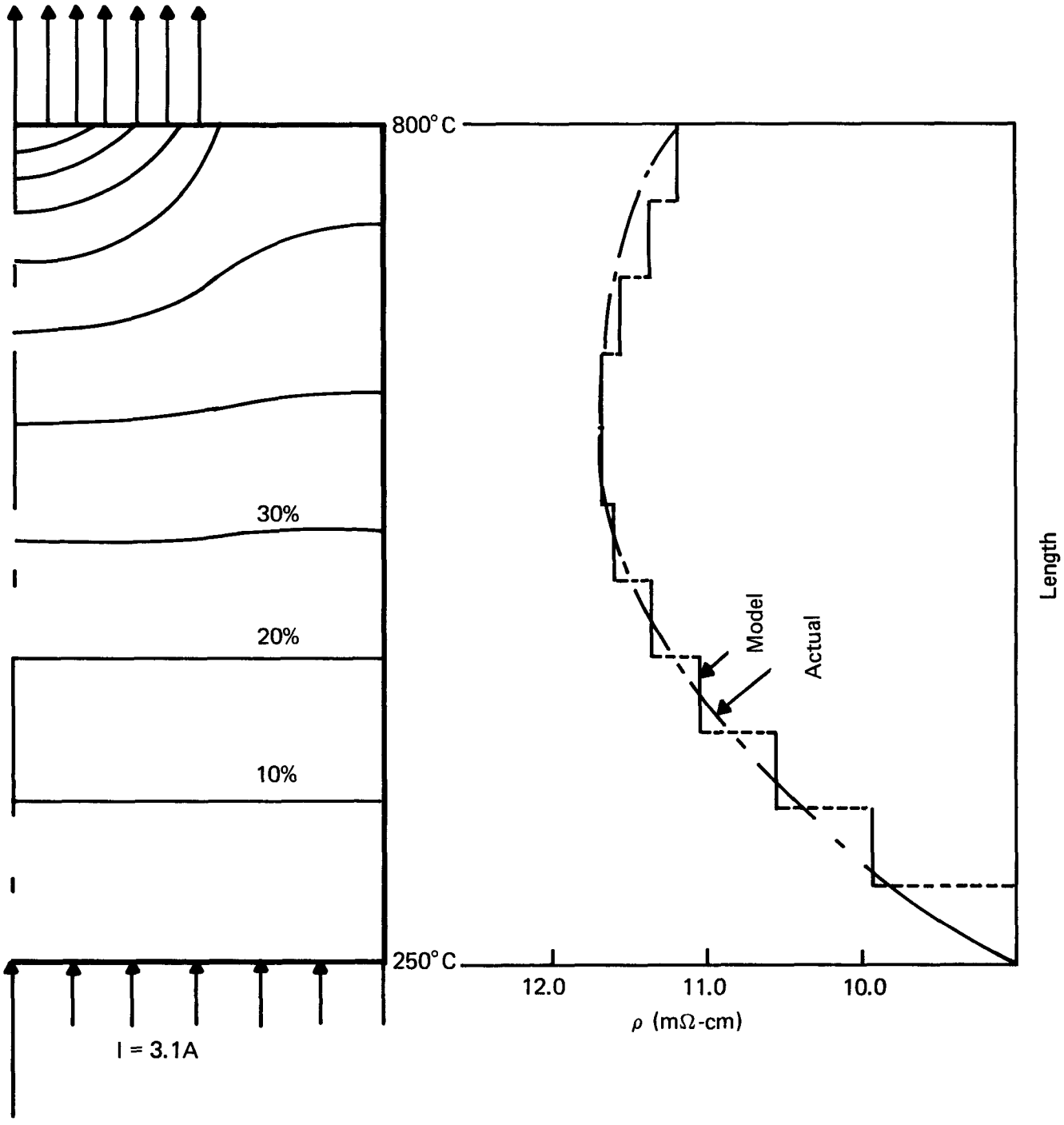

FIGURE II-13: P-LEG EQUIPOTENTIAL LINES FOR 75% CONSTRICTION AND RESISTIVITY PROFILE USED IN CALCULATION

The calculation of the bypass in the HiFi paper is based on the following assumptions:

- Width of insulation for two (2) rings
  (from TES/3M Interface Drawing, No. SIG 116001)

= 2 [3.00 + 2(.12)] = 6.48 inches

- Average diameter of Insulation
  - Distance across POCO hot frame flats = 8.117 inches
  - Hot strap thickness x 2 = 0.136 inches
  - 1/2 leg length x 2 = 3.300 inches

  8.553 inches

- Cut-outs for legs
  - N-Leg Diameter = .200
  - P-Leg Diameter (with .025 thick wrap) = 0.310
  - 336 Couples

Heat Flow Area = $\pi(8.553)\ (6.48) - \pi/4\ [(200)^2 + (.310)^2]\ 336$

= $174.1 - 35.9 = 138.2\ in^2$

- Thermal conductivity of HiFi paper (15% compression) measurements at Dynatech R/D Co. at 0% compression and 30% compression are .015 and .013 BTU/hr-ft-°F respectively; therefore, the value of .014 BTU/hr-ft-°F will be used for 15% compression. The amount of compression of 15% was selected based on insulation compliance measurements performed at 3M.
- Assumed hot frame temperature = 960°C
- Assumed cold strap temperature = 160°C
- $Q_{Bypass\ (hiFi)} = K\ A\ \frac{\Delta T}{\Delta X}$

$$\therefore\ Q_{Bypass\ (hiFi)} = \frac{(.014)\ (138.2)\ (860 - 160)\ (12)\ (1.8)}{(144)\quad (0.3)\quad (3.413)} = 198.4\ W(t)$$

- Bypass in Wrap
  - From Dynatech R/D Co. measurements

$$k_{wrap} = .030\ \frac{BTU}{hr\text{-}ft\text{-}^\circ F}$$

$$\therefore\ Q_{wrap} = \frac{336}{144}\ \frac{\pi}{4}\ (.310^2 - .260^2)\ (.030)\ \frac{(860 - 160)}{0.3}\ \frac{(12)\ (1.8)}{(3.413)} = 23.1\ W(t)$$

- Total converter bypass = 198.4 + 23.1 = 221.5 W(t)

FIGURE II-14: CALCULATION OF BYPASS HEAT FLOW WITHIN THE S/N-1 CONVERTER

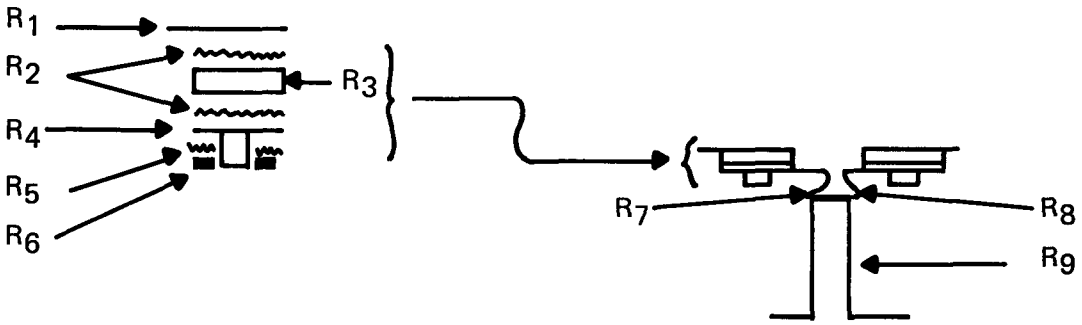

$$Re = \sum_{i=1}^{7} Ri$$

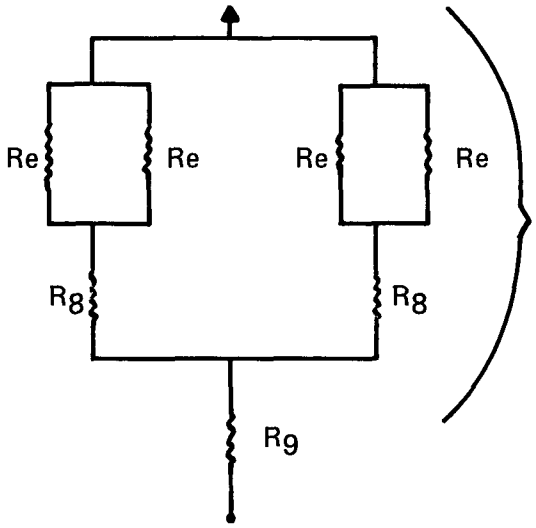

$$R_{tot} = R_9 + \left[\frac{R_8 + \frac{Re}{2}}{2} \right]$$

FIGURE II-15: COLD END HARDWARE
ONE-DIMENSIONAL HEAT FLOW MODEL

D. CHARACTERIZATION OF DYNAMIC RESPONSE

An effort was initiated with an independent support group within 3M to conduct a study to characterize the mechanical behavior of a converter ring in a dynamic environment. A mutual decision was made to use a lumped parameter model that would be analyzed by ANSYS, a general purpose finite-element structural analysis program. The effort was broken into two (2) sections: natural response and forced response. To date, the first of these has been completed.

A sketch of the lumped parameter model is given in Figure II-17. The masses of one half of each spring and of all of the cold frame segments were lumped into the outer housing, and the mass of everything else was lumped into the hot ring. The compression springs were given both axial and lateral stiffness. The lateral stiffnesses were calculated from an equation given by Wahl in Vol. 2 of The Shock and Vibration Handbook by Harris and Crede. Figure II-18A describes the calculation.

The first phase of the study was to determine the natural frequencies for any resonance peaks that lie in the same range of the frequency domain as the JPL signal specifications. This determination was carried out without any damping included in the model. As a check on the accuracy of the numerical solution, the natural frequencies of three (3) simple mode shapes were calculated. The modes that were examined by hand are described in Figure II-17 and the calculations themselves are shown in Figure II-18B. The natural frequencies for pure torsion and for pure longitudinal motion are identical.

The agreement between ANSYS and the hand calculations was to within 2%, so that the output looks sound.

A total of nine mode shapes were identified between 0 and 1200 cps. Of these, the first three were pure rigid body motions. Presently it is not known which of these modes are the most important. The forced response solution, which has not been obtained, would indicate that.

E. THERMAL EXPANSION CALCULATIONS

Thermal expansion calculations were performed for radial and longitudinal directions in a converter ring of the SN-1 design. There is no circumferential expansion. The details of the calculations are shown in Figures II-19 and II-20. Notice from Figure II-19 that in order to simulate radial expansion for a full ring, it is necessary to overcompress an eighteen-couple assembly by 0.017 in. at room temperature.

F. APPLIED STRESS VARIATIONS

It is necessary to understand the force-displacement characteristics of the new cold end hardware so that the effect of thermal expansion, creep and tolerance variations in contact pressure can be determined. A summary of the forces on a thermoelectric element is given by a force balance on the thermoelectric leg and surrounding insulation (Figure II-21).

1. Calculate R for one rail of one cold frame segment:

$R = (R^{A/L})^{-1}$

Refer to Fig. 1 for meanings of R_1, R_2, R_3, R_4, R_5

	R W/cm-K	L_1 (cm)	L_2 (cm)	A (cm^2)	L (cm)	R (°C/W)
R_1	3.98	–	–	.456	.0267	.0147
R_2	.346	–	–	.456	.0102	.0646
R_3	2.30	–	–	.456	.0787	.0750
R_4	3.98	–	–	.456	.0254	.0140
R_5	.346	–	–	.350	.0051	.0413
R_6	3.98	–	–	.350	.0533	.0383
R_7	3.98	1.016	.0533	.0542	.794	3.68
R_8	.346	1.14	.356	.406	.005	.0356
R_9	1.71	2.11	.356	.750	1.02	.7953

$Re = R_1 + R_2 + R_3 + R_4 + R_5 + R_6 + R_7 = 3.93°C/W$

$$R_{tot} = Rg + \left(\frac{R_8 + \frac{Re}{2}}{} \right) = 1.80°C/W$$

2. Calculate heat flux through one rail of one cold frame segment:

$$Q \cong \frac{(1126\ W/ring)}{(168\ Couples/ring)} \times (2\ Couples/rail) = 13.4W$$

∴ Expected $\Delta T = QR = 24.1°C$

3. Now, what is the thermal resistance based on the heat flux through a single element:

$$R = \Delta T/Q = \frac{24.1°C}{3.35\ W/Element} = 7.19°C/W$$

This figure is an acceptable thermal resistance. (The goal is 7°C/W ± 3°C/W).

FIGURE II-16: CALCULATION OF COLD END HARDWARE THERMAL RESISTANCE

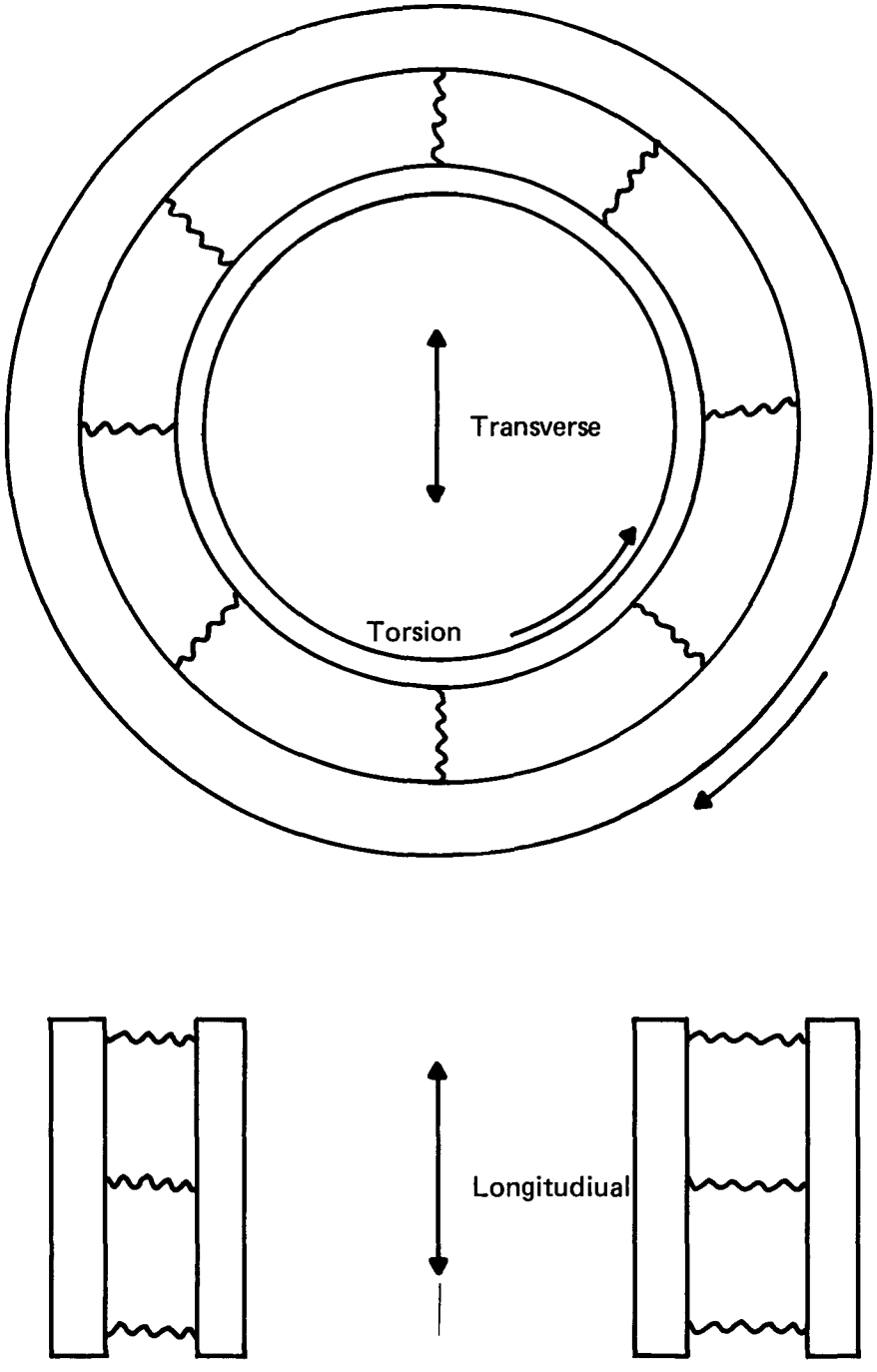

FIGURE II-17: A SKETCH OF THE LUMPED PARAMETER MODEL

$$K_L = \frac{10^6 d^4}{(_L nD\ (.204h_s^2 + .265D^2)}\ ,\ \frac{\text{lbs}}{\text{in.}}\ *$$

where n = Number of active coils
d = Wire diameter, [in]
ST = Axial deflection due to F, [in]
L_o = Free length, [in]
C_L = A factor, see graph below
D = Wire diameter, [in]
h_s = Operating height, [in]

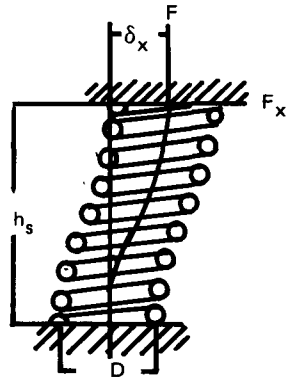

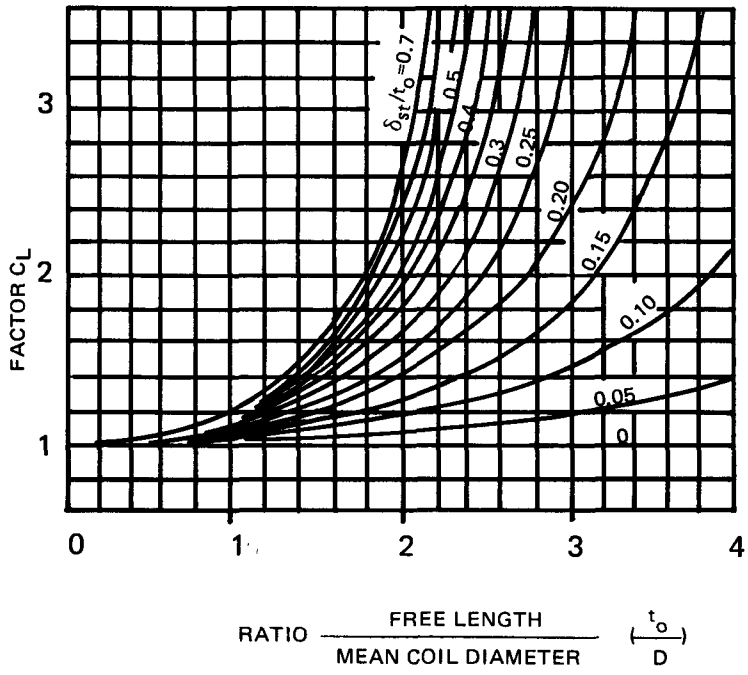

Lateral stiffnesses for SN-1 springs

N-leg = 46.4 lbs./in. = 38% of axial stiffness

P-leg = 17.2 lbs./in. = 17% of axial stiffness

FIGURE II-18A: CALCULATION OF LATERAL STIFFNESS OF A COMPRESSION SPRING

* Only valid for steel springs with $E = 30 \cdot 10^6$ psi and $G = 11.5 \cdot 10^6$ psi

1. Assumptions

Axial Spring Constants: N-Leg = 115.0 lbf/in.
P-Leg = 94.4 lbf/in.

Lateral Spring Constants: N-Leg= 46.4 lbf/in.
P-Leg = 17.2 lbf/in.

Mass of inner ring = 4.61 lbm

2. A. Lateral Motion of Inner Ring

K_a for 6-couple = $K_{a6} = 6(K_{aN} + K_{aP}) = 6\ (115 + 94.4) = 1256$ lbf/in.

K_L for 6-couple = $K_{L6} = 6(K_{LN} + K_{LP}) = 6(46.4 + 17.2) = 382$ lbf/in.

K_a for half of converter = $K_{a6}\left[1 + \sum_{i=1}^{7} 2\text{Cos}^2\ (\theta_{i-1} + 12.86°)\right]$, $\theta_o = 0°$

$= 7.00\ K_{a6} = 8795$ lbf/in.

Similarly, K_L for half of converter = $7.00\ K_{L6} = 2671$ lbf/in.

∴ K for entire converter = 2(8795 + 2671) = 22,932 lbf/in.

∴ $\omega_N = \sqrt{\dfrac{(22{,}932\ \text{lbf/in.})\ (12\ \text{in/ft})\ (32.2\ \text{lbm/slug})}{(4.61\ \text{lbm})}}$

$= 1386$ /s = 221 Hz

B. Torsional Motion and Longitudinal Motion of Inner Ring

K for entire converter = $28\ K_{L6} = 10{,}696$ lbf/in.

∴ $\omega_N = \sqrt{\dfrac{(10{,}696)\ (12)\ (32.2)}{(4.61)}}$ = 947 /s = 151 Hz

FIGURE II-18B: CALCULATION OF TWO RESONANT FREQUENCIES

A. Full connector ring.

1. Estimation of change in stack height.
   Temp. of hot frame = 860 + 25 = 885°C
   ΔD Hot Frame = (8.09 • 10^{-6}/°C) (885 - 20) (8.117 in.) = + .057 in.
   Temp. of cold frame - 150 - 25 = 125°C
   ΔD cold frame = (13.0 • 10^{-6}/°F) (125 - 20°C) (1.80°F/°C) (10.159 in.) = + .025 in.
   $\therefore\Delta$ Stack height = ½ (.025 - .057) = -.016 in.
   $\therefore$ the stack height decreases by .016 in.

2. Estimation of change in spring height:
   a) N-Leg
      T Hot strap = ½(885 + 860) = 875
      ΔL Hot strap = (30 • 10^{-7}/°F) (873 - 20°C) (1.80°F/°C) (.1 in.) = + .0005 in.
      Tn-leg = ½ (860 + 160) = 510
      ΔL N-Leg - (10 • 10^{-6}/°C) (510 - 20°C) (.3 in.) = + .0015
      ΔL cold strap, follower = (10 • 10^{-6}/°F) (150 - 20°C) (1.80°F/°C) (.011 + 021 in.)
      = + .0001 Negligible
      ΔL BeO disc = (5.5 • 10^{-6}/°C) (150 - 20°C) (.030 in.) = .00002 - Negligible
      $\therefore\Delta$L spring = ΔStack ht. — $\Sigma\Delta$ L's
      = -.016 — .0005 — .0015
      = -.018 in.
      $\therefore$ the operating N-Leg spring height decreases by .018 in. during heat-up in a full converter ring.

   b) P-Leg
      ΔL Hot strap = (30 • 10^{-7}/°F) (873 - 20) (1.80) (.068) = .0003 in.
      ΔL P-Leg = (20 • 10^{-6}/°C) (510 - 20) (0.30) = .0029 in.
      $\therefore\Delta$ L spring = -.016 -.0003 -.0029
      = -.019
      $\therefore$ The operating P-Leg spring height decreases by .019 in. during heat-up in a full converter ring.

B. Eighteen couple module

1. Estimation of change in stack height.
   Temp. of hot frame = 885°C
   ΔL Hot frame =(8.09 - 10^{-6}/°C) (885 - 20) (1.250 in.) = .0087 in.
   Temp. of tantalum pins = ½ (885 + 125°C) = 505°C
   ΔL pins = (3.60 • 10^{-6}/°F) (505 - 20°C) (1.80) (3.22 in.) = .0101 in.
   $\therefore\Delta$ Stack height = .0101 — .0087 = + .0014 in.
   $\therefore$ The stack height increases by .0014 in.

FIGURE II-19: CALCULATION OF THERMAL EXPANSION ALONG THE STACK

2. Estimation of change in spring height.
   a) N-Leg
      As before, Δ L Hot strap = .0005 in.
      Δ L N-Leg = .0015 in.
      $\therefore\Delta$ L spring = .0014 -.0005 -.0015 = -.001 in.
      $\therefore$ The N-leg spring length decreases by .001 in. in an eighteen couple module during heat-up.

   b) P-Leg
      As before, Δ L Hot strap = .0003 in.
      Δ L P-leg = .0029 in.
      $\therefore\Delta$ L spring = .0014 -.0003 -.0029 = -.002
      The P-leg spring length decreases by .002 in. in an eighteen couple module during heat-up.

FIGURE II-19: CALCULATION OF THERMAL EXPANSION ALONG THE STACK (Continued)

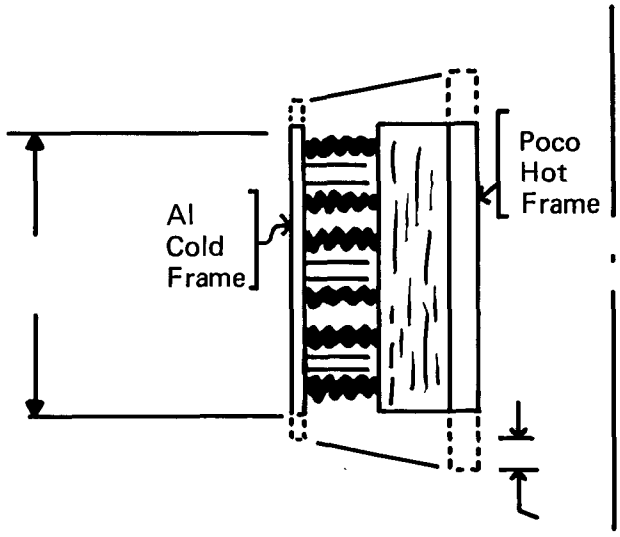

* Solid lines indicate configuration at T_{ref}

Dotted lines indicate configuration at operating temperatures

Assume: Hot Frame Temperature = 885°C
Cold Frame Temperature = 125°C

$$= \quad POCO\ (T_H - T_{ref})L - \quad A1\ (T_C - T_{ref})\ L \qquad /2$$

$$= \quad (8.09\ 10^{-6}/°C)\ (885 - 20)\ (3'') - (13.0\ 10^{-6}/°C)\ (125 - 20)\ (3'') \qquad /2$$

$$= \quad .008 \text{ in.}$$

FIGURE II-20: THERMAL EXPANSION NORMAL TO THE STACK

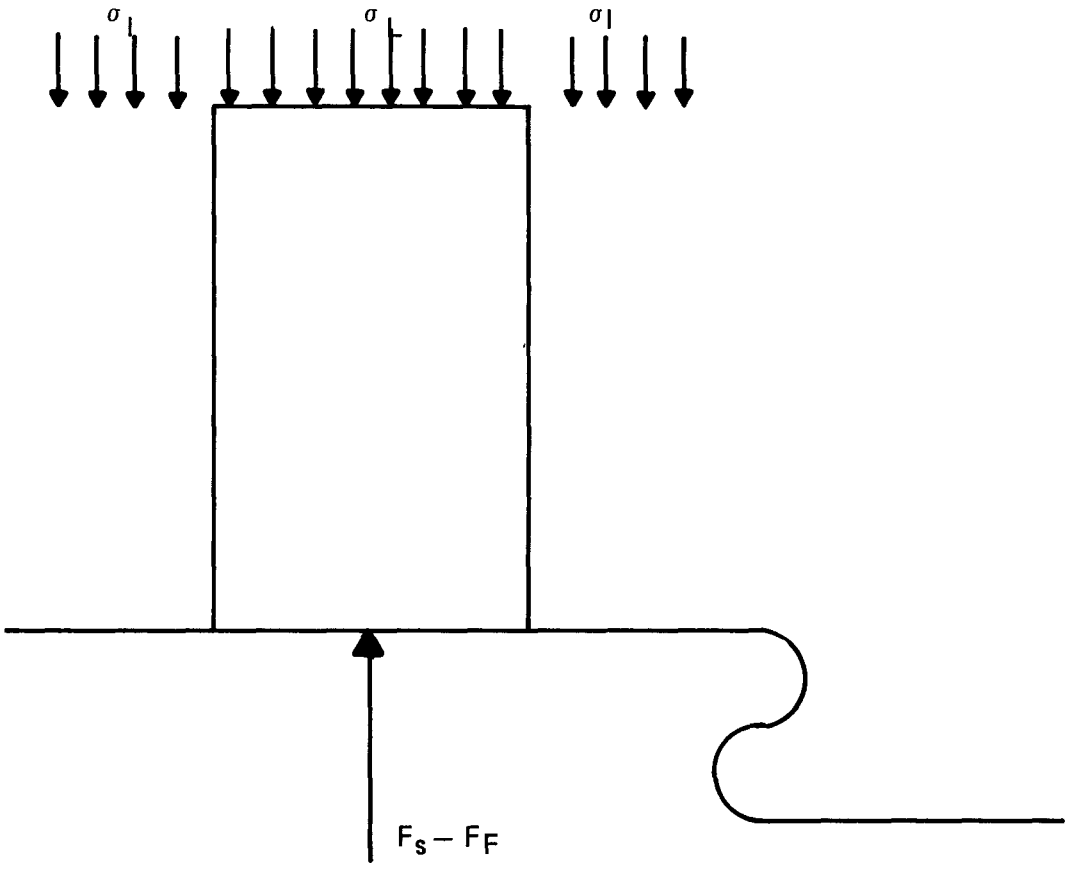

FIGURE II-21: FORCE BALANCE ON LEG AND SURROUNDING INSULATION

$$F_{TOT} = F_s - F_F = F_L + F_I = \sigma_L A_L + \sigma_I A_I \quad (7)$$

$$\therefore F_L = \frac{1}{A_L} (F_s - F_F - \sigma_I A_I) \quad (8)$$

where

$$F_s = F_{si} - K(L-L_i)$$

where F_s = Spring Force
F_{si} = Initial Spring Force (Nominal Compression)
F_F = Effective Spring/Friction Force of Follower
F_L = Net Force on Leg
F_I = Net Force on Insulation Surrounding Leg
σ_I = Stress on Insulation as a Result of Compression
σ_L = Net Stress or Contact Pressure on Thermoelectric Leg
K = Spring Constant of Follower Spring
L = Length of Follower Spring
L_i = Initial Length of Follower Spring (Nominal Compression)
A_I = Cross-Sectional Area of Thermal Insulation Associated with one Thermoelectric Leg
A_L = Cross-Sectional Area of Thermoelectric Leg

The stress on the insulation as a function of compression was measured using a special enclosing fixture and an Instron mechanical test machine. These data are shown plotted in Figure II-22 and a least squares curve fit to the data is given by:

$$\sigma_I = a_1 + a_2\epsilon_I + a_3\epsilon_I^2 + a_4\epsilon_I^3 + a_5\epsilon_I^4 \quad (9)$$

where $\epsilon_I = 1 - L_I/L_o$ (10)

where L_I = Length of Insulation (Between Hot and Cold Straps)

L_o = Unstressed Insulation Thickness

The measurements of the force-displacement characteristics of the follower were obtained in a spring test device. A typical force-displacement curve is shown in Figure II-23. The spring characteristics of the follower spring are obtained from QC measurements which are routinely performed on the springs. All of the components of the force balance described in equation (8) are thus combined and the results are shown in Figure II-24 as a function of follower deflection. Follower deflection will either occur from thermal expansion, P-element creep or sublimation. The actual compression of the follower spring at assembly is a function of the tolerance stack-up of components in the N- or P-leg stack. The effects for the extreme tolerance stack-up conditions are shown in Figures II-25 and II-26.

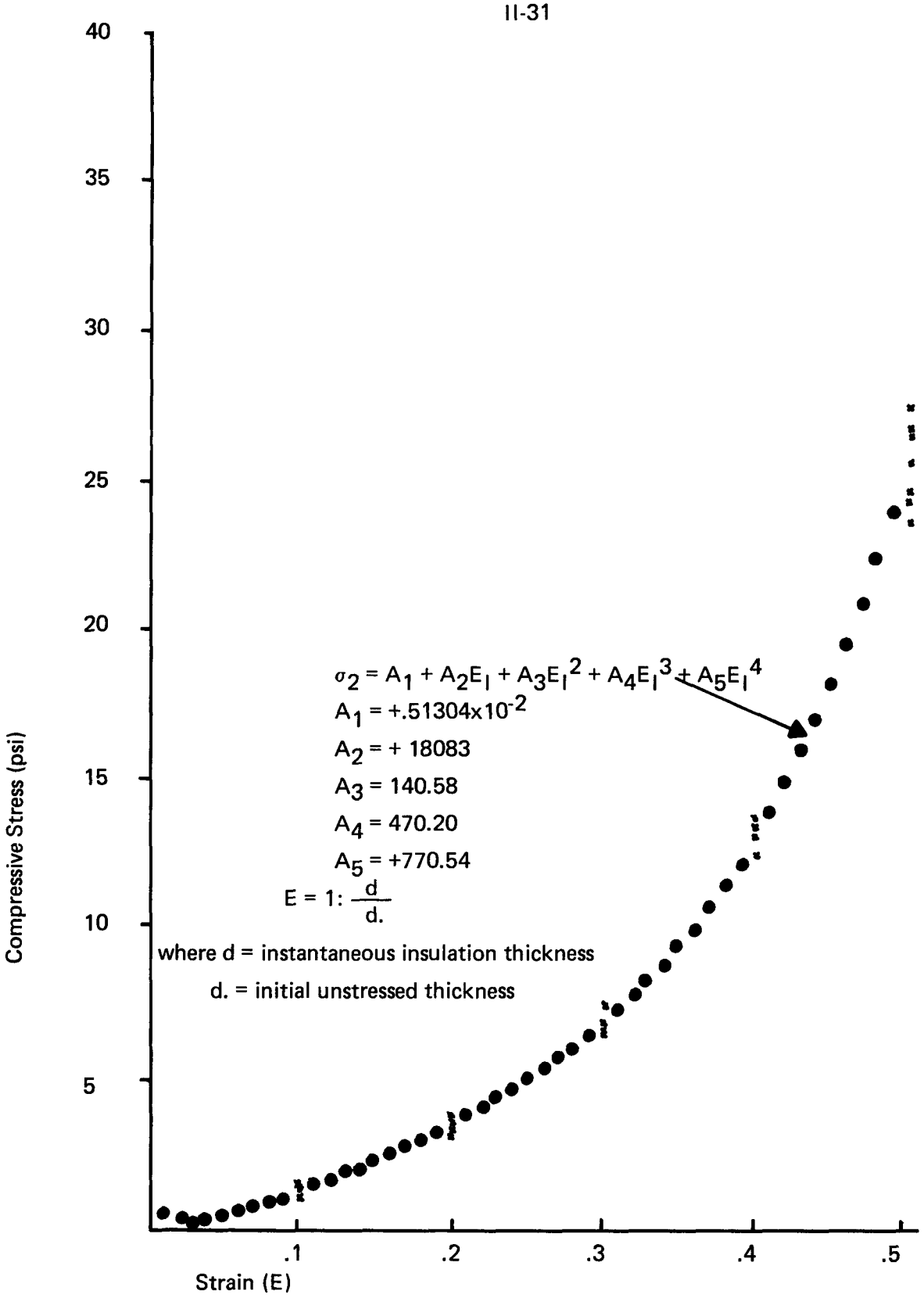

FIGURE II-22: STRESS VS. STRAIN DATA
LAYERED Hi-Fi 660 PAPER
1" THICK TEST SECTIONS NOMINALLY
4TH ORDER POLYNOMIAL FIT

It can be seen that the minimum value for N-leg contact pressure at 10 mils deflection is about 200 psi and the minimum value for contact pressure on the P-leg at 30 mils deflection is about 30 psi. These values should be the maximum amount as a result of thermal expansion and/or creep/sublimation. Measurements have shown that this will still be an acceptable amount of contact pressure for each of the elements.

G. N-LEG THERMAL STRESS ANALYSIS

In order to get some indication of the role of thermal stresses in N-leg cracking, a study was initiated to characterize them. It was decided that a numerical study would be the best way to study the problem. ANSYS, the same general purpose program used for dynamic characterization, has been used thus far. To date only one solution has been obtained. The problem treated was an unsegmented cubic $GdSe_x$ N-leg with a one-dimensional temperature profile. The results obtained are being studied and verification of the results is being sought.

It has not yet been possible to study the effects of the transformation process on the thermal stresses in the N-legs because the orthorhombic material has not been characterized for mechanical properties. In addition to characterizing the orthorhombic material, $NdSe_x$ and (2N) PbTe need to be characterized.

H. CALCULATION OF THE MAXIMUM STRESS LEVEL IN THE POCO HOT RING

An estimate of the maximum stress in the graphite hot ring was determined by the following procedure (refer to Figure II-27).

1. Treat one-half of a ring

2. Neglect facets and pinholes (treat as a hemi-cylinder) and solve for reaction forces. These reactions correspond to the internal compressive stress in the system.

3. Using this stress as the applied stress, calculate the maximum stress using a concentration factor that is obtained from standard graphs available in the literature.

The results obtained indicates that $\sigma max = 3279$ psi. Since the compressive strength of graphite AFX-Q1 is 22,000 psi, there is a safety margin of 6.7 inherent in the design.

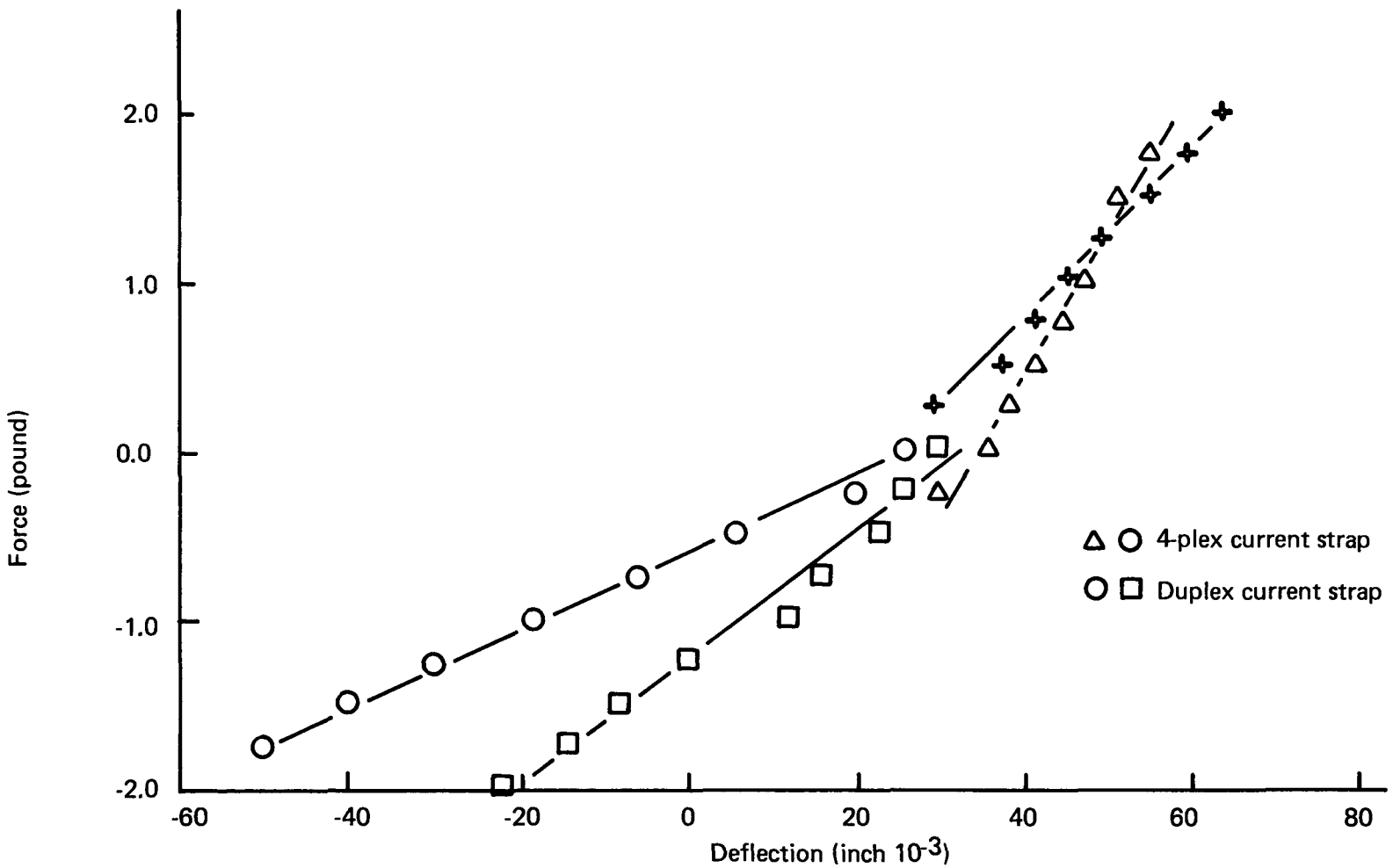

FIGURE II-23: COMPLETE COLD END ASSEMBLY FORCE VS. DEFLECTION

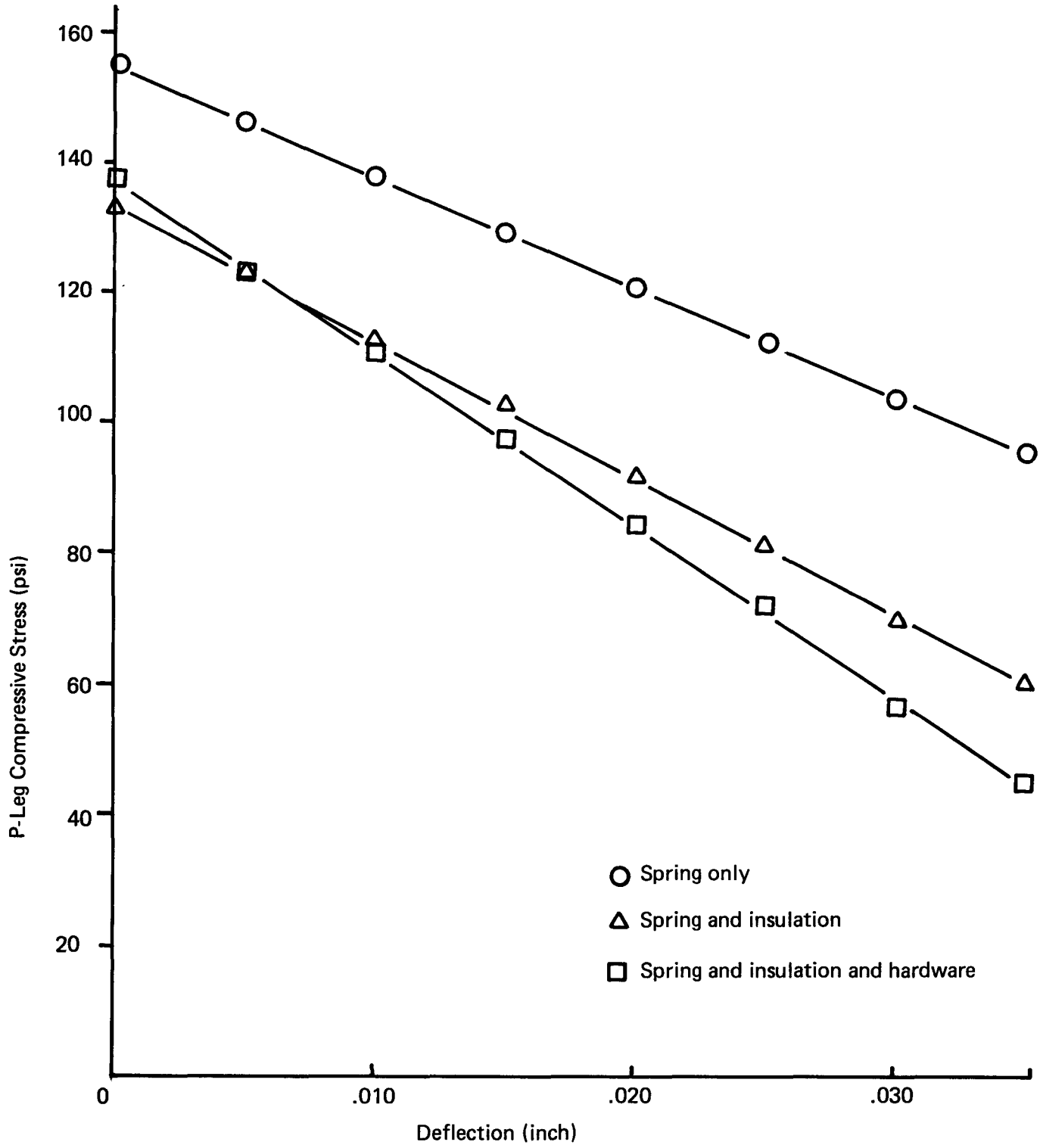

FIGURE II-24: INDIVIDUAL COMPONENTS OF FORCE BALANCE ON THERMOELECTRIC LEG

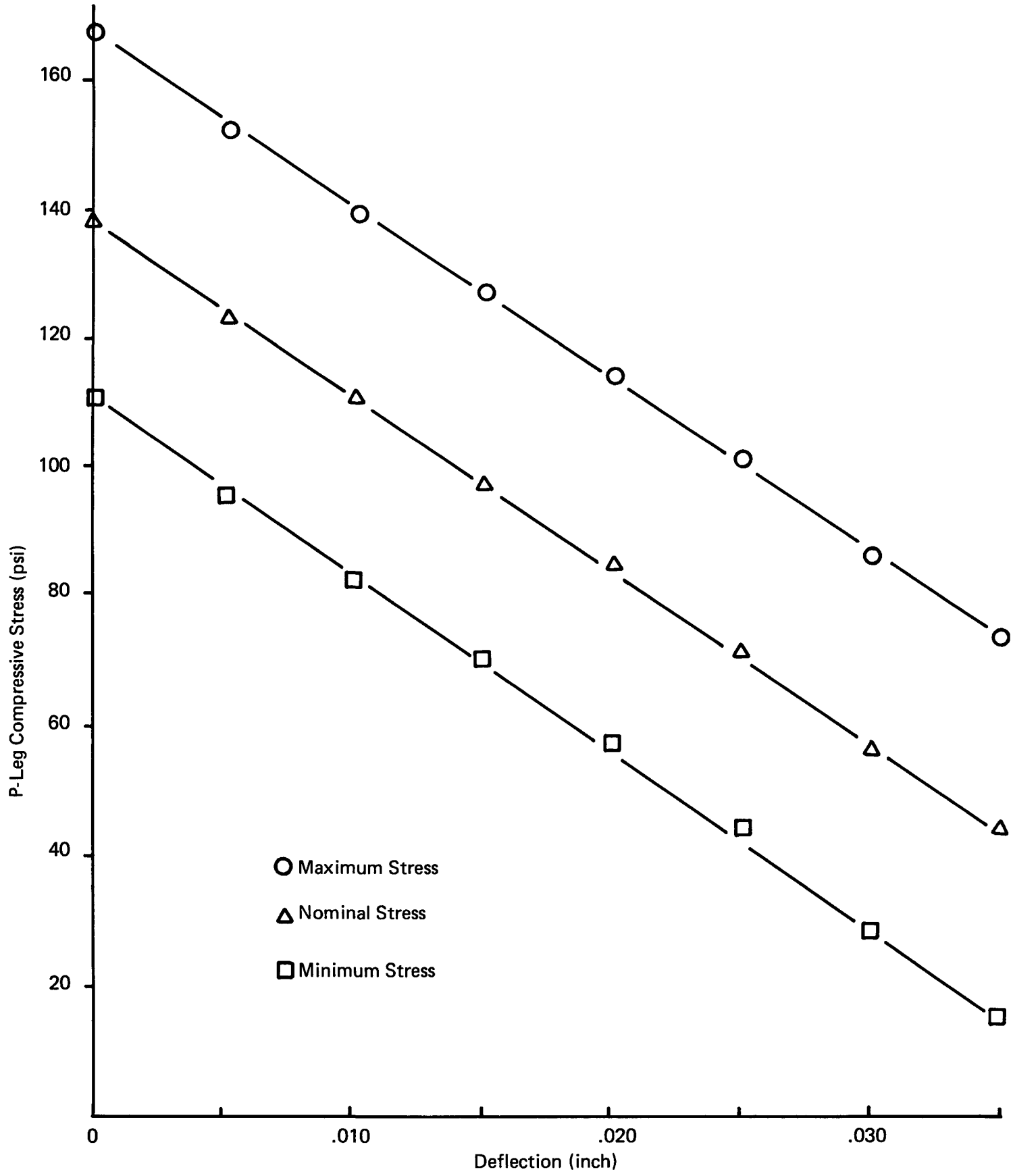

FIGURE II-25: P-LEG COMPRESSIVE STRESS VS. DEFLECTION

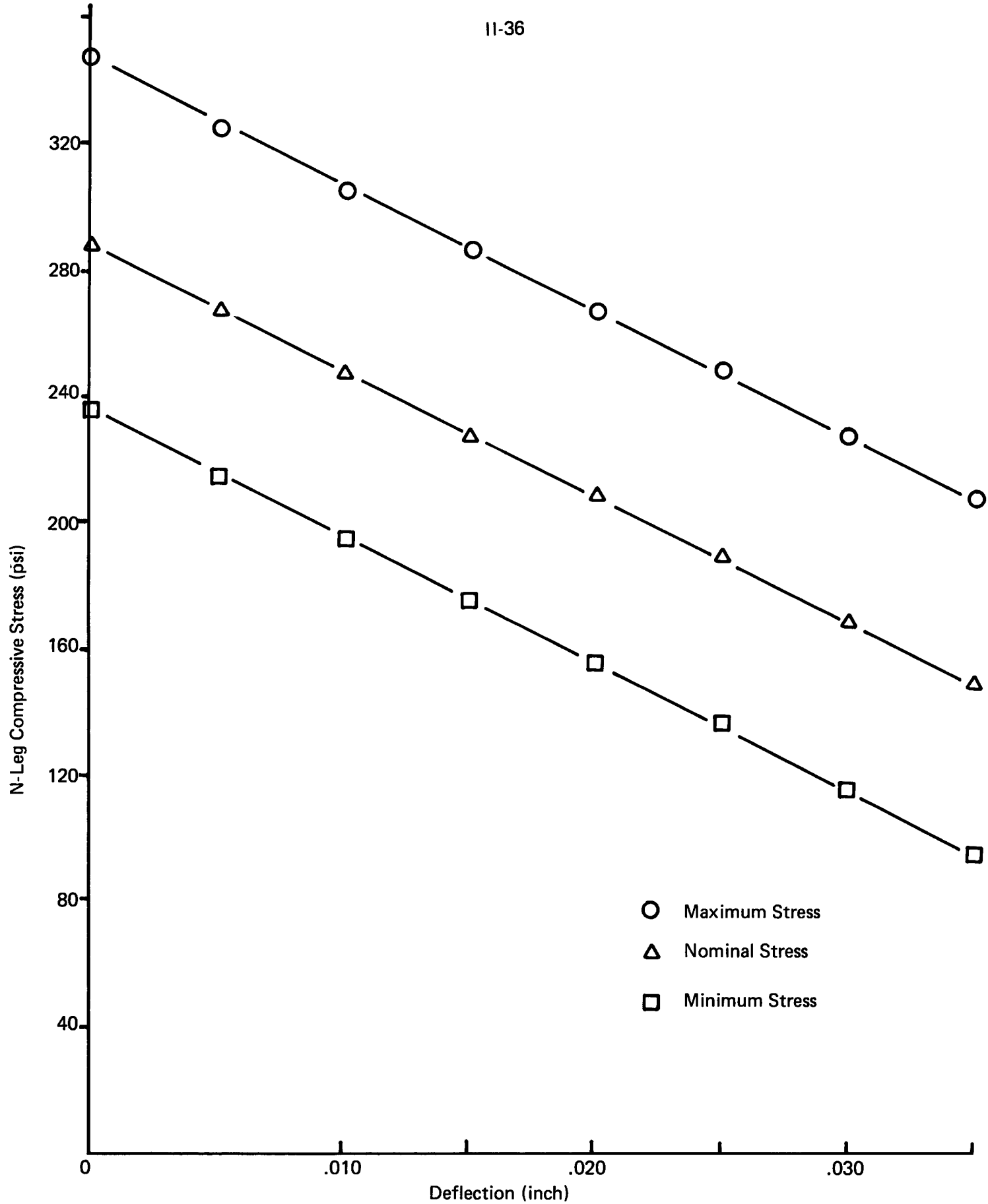

FIGURE II-26: N-LEG COMPRESSIVE STRESS VS. DEFLECTION

Use one-half of the ring and neglect facets and pin-holes:

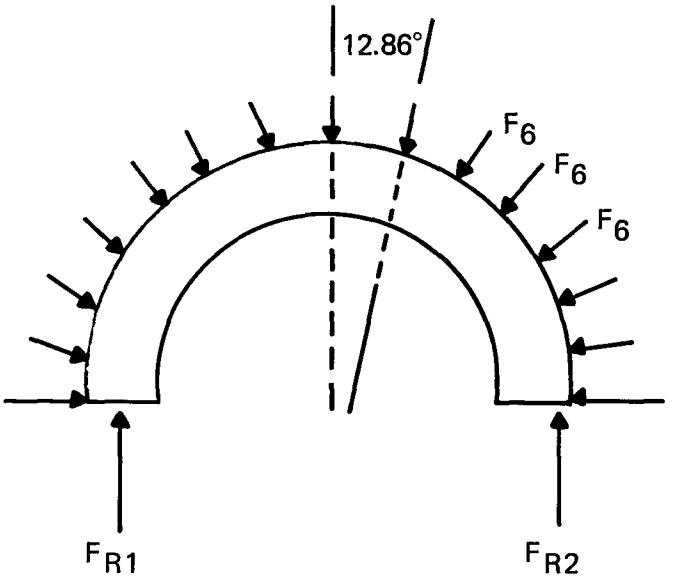

1. Calculate engineering stress (neglect holes and facets).

Cross-sectional area = 3.00 in. x .230'' = .690 in^2

F_6 = 6 (23.4) + 6 (8.5) = 191.4 lbs.

$F_{RT} = F_{R1} + F_{R2}$

$F_{RT} = F_6 [1 + \sum_{i=1}^{7} 2 \text{ Cos } (\Theta_{i-1} + 12.86°)]$, $\Theta_o = o°$

= 7.88 F_6

= 1508 lbs.

From symetry, $F_{R1} = F_{R2} = \frac{1508}{2} = 754$ lbs.

$\therefore \gamma e = \frac{754 \text{ lbs.}}{.690 in^2} = 1093$ psi

FIGURE II-27: FREE BODY DIAGRAM FOR CALCULATING ENGINEERING STRESS IN RING

2. Account for pin-holes through assignment of a stress concentration factor. Various graphs appearing in "Stress Concentration Factors" by Peterson, Wiley Interscience, 1974 were used in arriving at a rough estimate of 3. See Figure 2 for pin-hole layout.

   ∴ Estimated maximum stress in Graphite hot ring = 3(1093) = 3279 psi

3. Compare w/Compressive strength of AFX-Q1 Graphite (POCO)
   Temp - 22,000 psi

   ∴ Estimated safety margin = $\frac{22000}{3289}$ = 6.71

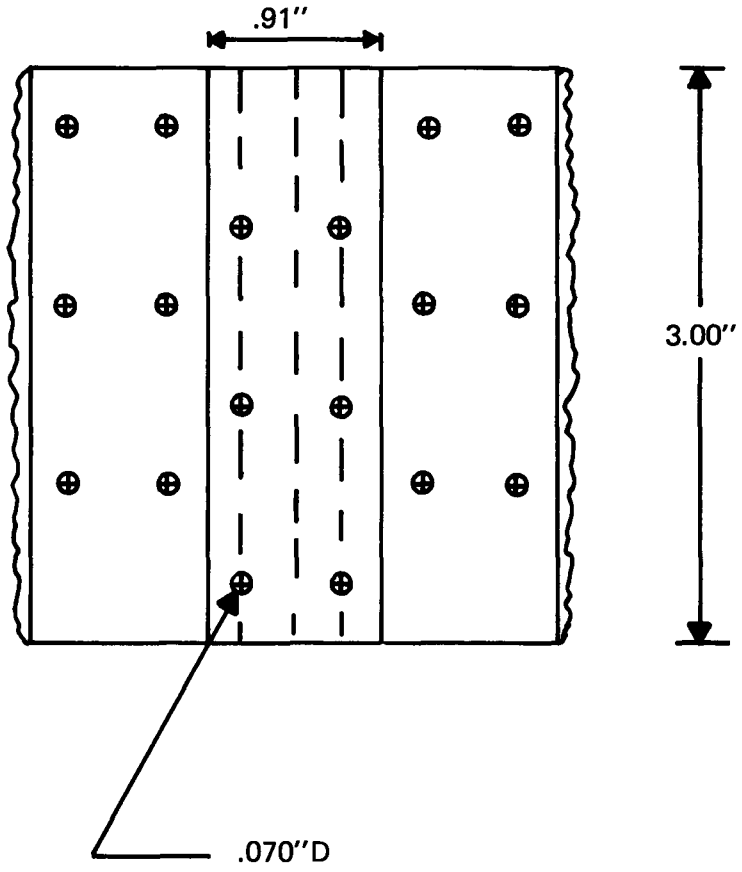

FIGURE II-27: Continued
PIN HOLE LAYOUT

III. SYSTEM TESTING

A. SPRING LOAD RELAXATION

A compilation of spring load relaxation data appears in Figure III-1. In the course of 20,000 hours of exposure, M-7 springs experienced an almost complete loss of load. This degree of load relaxation was far in excess of existing load relaxation vs. time data available in the literature. Springs from other modules had higher than expected load losses, though none were as dramatically high as M-7. The fundamental differences between the conditions in which the module springs and the literature springs were tested were that the module springs were operated in an oxygen free environment (either vacuum or inert backfill, depending on the module) and were also subjected to Selenium vapor. Spring tests described in the literature took place in air.

A series of load relaxation tests were planned and run. These tests, which were intended to be diagnostic tests, are described and their results displayed in Table III-1. The air data is in acceptable agreement with the literature, and the vacuum plus Selenium data is in good agreement with the module data. Comparison of the vacuum only data with the vacuum plus Selenium data indicates that the presence of Selenium is not the key. This conclusion has been backed up by a number of chemical analyses. X-ray flourescence tests were conducted to obtain an overall Selenium content measurement, and whereas there was Selenium present on all springs, there was no correlation between Selenium pickup and load relaxation. Oak Ridge Labs determined that all of the Selenium pickup occurs at the surface in the form of a very thin film of Iron Selenide. The fact that this film is not a contributor to load relaxation was demonstrated with dip tests performed at 3M.

Microhardness tests performed by both 3M and Oak Ridge showed that hardness changes occurred throughout the cross-sections of the springs. Also, metallographic analysis performed by Oak Ridge showed grain enlargement throughout the crossection, an observation consistent with the microhardness tests.

It is important to mention that M-7 springs were slightly under designed with respect to load relaxation considerations. It is estimated that the BOL corrected stress in the N-leg springs was 130 ksi. This could be the reason why M-7 springs relaxed more than other modules, but at this point enough information to make this statement conclusively is not available. It appears that one reason all module springs relaxed more than expected was that the absence of oxygen seemed to accelerate load relaxation rate, but again, at present there is not enough information to explain why this occurs.

The observation of grain enlargement in the module springs that were examined indicates that the operating temperature was too high for ASTM A-401 Cr-Si steel, the material used for modules M-7 through M-18. Presently, 17-7 PH stainless steel is being used for module springs. Test data indicates that 17-7 relaxes only about 50% as much as Cr-Si under identical conditions and test durations. Even though 17-7 shows superior performance with respect to Cr-Si, other materials are being looked into, e.g. Inconel X, MP-35N and Elgiloy. To date springs of these materials have not been tested, but designs have been made and springs have been ordered for continuation under the Technology Program.

B. CONVERTER TO HOUSING INTERFACIAL ΔT

A number of tests have been conducted to characterize the thermal resistance of the interface between the cold frame segment and the outer housing. For all experiments, the outer housing was modeled by a 6064 A1 chill block tailored to match the convex surface of the cold frame segment and polished to a 16 μ" RMS surface finish. Temperature drops across the interface were measured with teflon insulated .003" D Iron-Constantan thermocouples embedded .030 in. from the interface on either side. The results are compiled in Tables III-2 and III-3. The contact pressures shown in the table correspond to the use of six 24 lb. N-leg springs and six 8.5 lb. P-leg springs.

A few conclusions can be drawn from these results. First, the change from 2024 to 6061 A1 apparently has no effect on thermal resistance at the interface. Second, the presence of a ductile intermediate layer in test number 3 significantly reduces the thermal resistance. The relatively wide spread in the data could be attributed to a number of things: differences in mean temperature, variability in degree of oxidation of the aluminum surfaces from test to test, and large uncertaintly ($\pm$ 10%) in the contact pressure.

Thermal resistance with an intermediate ductile layer needs to be better characterized. Presently the effect of the ductile layer on the variability of thermal resistance is not but needs to be known.

C. COLD END HARDWARE THERMAL RESISTANCE

A number of tests have been conducted to study the magnitude and reproducibility of the thermal resistance of the SN-1 cold hardware. These measurements were made along with the cold end interfacial ΔT measurements. All specimens were X-rayed before the test in order to provide some indication of bond quality. The results, which are displayed in Figure 4, show that whereas there does seem to be some correlation between bond quality and thermal resistance, it isn't strong enough to warrant using X-rays alone as a QC inspection tool. (This is not to say that X-ray couldn't be used for detecting grossly flawed assemblies). In any event, the data indicates that reproducibility of thermal resistance is not a problem.

D. CHEMICAL COMPATIBILITY OF NICKEL HOT JUNCTION ELECTRODES WITH GdSe

Nickel, as a T_{HJ} electrode for $GdSe_x$, was proposed as a substitute for the gadolinium foil being used. Unpublished postmortum findings indicated gadolinium will be completely converted to various gadolinium selenides before Galileo EOM. As a result of these findings, the following evaluation program was initiated:

Objectives:

- Study the effect of P-TPM-217 sublimation suppression on nickel hot junction electrode.
- Study the compatibility of nickel/$GdSe_x$ under simulated module conditions.

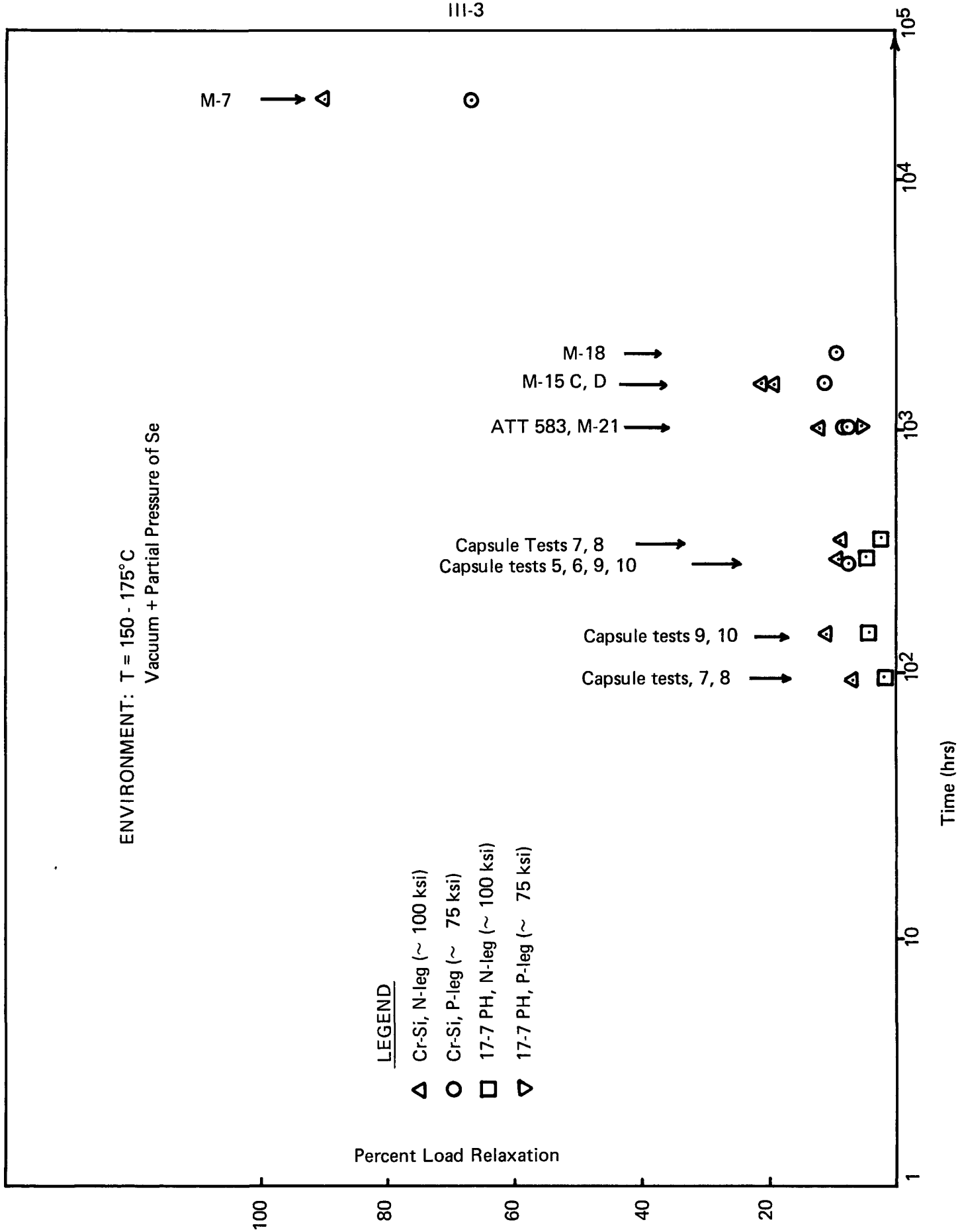

FIGURE III-1: A COMPILATION OF LOAD RELAXATION DATA

TABLE III-1

A COMPILATION OF LOAD RELAXATION DATA

Material	Corrected Stress (ksi)	Temperature (°C)	Environment	Duration (hrs)	% Load Loss	No. of Springs
Cr-Si	100	150	Air	274	4.6	6
302 Stainless	100	150	Air	274	5.9	6
17-7 PH (R.T. Set)	100	150	Air	274	3.1	6
17-7 PH (H.T. Set)	100	150	Air	274	2.9	6
Cr-Si	73.4	179	Vacuum + Se	283	8.0	6
17-7 PH (R.T. Set)	85.1	179	Vacuum + Se	283	7.0	6
Cr-Si	100	175	Vacuum + Se	360	8.3	12
17-7 PH (R.T. Set)	100	175	Vacuum + Se	360	3.1	12
Cr-Si	100	175	Vacuum	300	9.1	12
17-7 PH (R.T. Set)	100	175	Vacuum	300	4.3	12

TABLE III-2

COMPILATION OF INTERFACIAL ΔT RESULTS

Test No.	Segment Material	Intermediate Material	Contact Pressure (Psi)	Mean Temperature (°C)	Heat Flux (W)	Mean ΔT (°C)	No. of ΔT Readings	Contact Resistance (°C/W)
1	2024-T7	None	65.0	142	26.7	5.8	1	.217
2	6061-T6	None	65.0	119	35.4	7.7	1	.218
3	6061-T6	.001 Sn foil	65.0	236	32.6	5.2	3	.160
4	6061-T6	None	65.0	58.1	49.9	12.8	3	.257
5	6061-T6	None	65.0	47.7	53.8	19.0	3	.353
6	6061-T6	None	65.0	128	40.4	11.3	2	.280
7	6061-T6	None	65.0	133	41.2	9.3	1	.226
8	6061-T6	None	65.0	139	37.0	7.8	1	.211

TABLE III-3

COMPILATION OF COLD END HARDWARE THERMAL RESISTANCE DATA

Assembly No.	Thermal Resistance (°C/W)	Bond Quality
1	5.04	Good
2	7.08	Poor
3	7.92	Fair
4	6.40	Poor
5	6.42	Good
6	6.22	Poor

Technical Approach:

- Accelerated operation simulating module conditions (TPM-217 material lost to approximate that lost during 50,000 hours).

- Post-test evaluation to include: physical, visual and chemical techniques to measure foreign material uptake by the nickel.

Matrix:

1.	Fixtures	– 12-station with module hardware.
2.	T/E Materials	– Copper bonded partition or non-partitioned .260" dia. TPM-217 W-T_h/Ag-T_c sputtered .300" dia. $GdSe_x$.
3.	Electrodes	– W-Re, TPM-217 .027" nickel pressure engaged to $GdSe_x$.
4.	Compression Pressure	– Module specifications.
5.	Atmosphere	– Vacuum 10^{-6}-10^{-7} torr.
6.	Insulation	– Fiberfrax H-blanket.
7.	Temperature	– T_h as close to 900°C as possible.
8.	Time	– 160 hours (1 test). >1000 hours (1 test).
9.	Current	– 5 amps.

Analytical Evaluation Techniques:

- Metallurgical.
- Visual.
- Physical – weight loss TPM-217.
- Chemical/Instrumental – (1) Trace emission spectroscopy.
  (2) Qualitative microprobe.

Thermodynamic Considerations:

The following reactions were considered in the evaluation of the nickel – Gd_2Se_3 system:

1. $Ni_{(S)} + Se_{(S)} \xrightarrow{900°C} NiSe_{(S)}$ — ΔH = -10 k-cal/mol; ΔS = -2.3 cal/mol-deg; ΔG = -7.3 k-cal/mol

(2) $2NiSe_{(S)} \xrightarrow{900°C} 2Ni_{(S)} + 2Se_{(S)}$ — ΔH = 20 k-cal/mol; ΔS = -4.6 cal/mol-deg

(3) $2Se_{(S)} \xrightarrow{685°C} Se_{2(g)}$ — ΔH_{Se2} = 22.81 k-cal/mol

(Equation $\log_{10} P_{torr} = 8.0886 - \frac{4989.5}{T}$ was used for these calculations) * — (S → G); ΔS_{Se2} = 23.8 cal/mol-deg (S → G)

* Andier N. Nesmeyanov, Vapor Pressure of the Elements, USSR Academy of Sciences, p. 331, 1961.

(4) $2Gd_{(S)} + 3Se_{(S)} \xrightarrow{900°C} Gd_2Se_{3\,(S)}$ $\Delta H = -255$ k-cal/mol
$\Delta S = -7.2$ cal/mol-deg
$\Delta G = -246$ k-cal/mol

(5) $Gd_2Se_{3\,(S)} + Ni_{(S)} \xrightarrow{900°C} NiSe_{(S)} + 2GdSe_{(S)}$ $\Delta H = 27$ k-cal/mol
$\Delta S = -12.1$ cal/mol-deg
$\Delta G = 38.2$ k-cal/mol

Combining the data from equation 2 and 3, the partial pressure of $Se_{2(g)}$, over $NiSe_{(S)}$ at 900°C was found to be 0.1 torr. This value is substantially higher than previous Knudsen cell data on Gd_2Se_3 from which the partial pressure of $Se_{2(g)}$ over Gd_2Se_3 at 900°C was found to be 10^{-8} torr.

From the above thermodynamic consideration, the nickel–Gd_2Se_3 system is judged to be compatible.

Experimental Results:

- Black deposit of Ta-Se on Ta gimbal.
- Nickel foil free from foreign materials.
- Moly current strap as pretest.
- Ta gimbal/Ni foil/$GdSe_x$ all bonded together.
- No nickel diffusion into $GdSe_x$.
- TPM-217 weight loss ~60 mg.
- Absolute Seebeck coefficient varied accordingly:

Time	μv/°C
BOT 2 hr	205
14 hr	197
50 hr	195
EoT 160 hr	202

- Contact resistance of nickel foil $< 1m\Omega$.

Conclusions:

Based on the above experimental and thermodynamic results, nickel and Gd_2Se_3 are judged to be compatible.

TABLE III-4

	Component	Observations/Results
1.	Ta Cone Heater	As pretest: No evidence of selenization nor oxidation.
2.	Al_2O_3/Moly strap	As pretest: No evidence of selenization nor oxidation.
3.	Ta Gimbal	Microprobe analysis showed the uniformly distributed black deposit to be TaSe. No evidence of oxidation was detected. The gimbal was bonded to the nickel foil which was bonded to the $GdSe_x$ element.
4.	Ni Foil	As pretest: Microprobe analysis of the surface indicated the foil to be free of foreign material. The foil was bonded to the Ta and the $GdSe_x$.
5.	$GdSe_x$	Metallurgical examination indicated the Ni-$GdSe_x$ interface was continuous and void-free. No evidence of nickel inclusions were detected. TPM-217 deposits were detected on the T_{CJ} 1/4 of element. Trace emission spectrographic analysis indicated < 30 ppm Ni in the $GdSe_x$. This value represents the lower limit of detectibility for the ES method.
6.	TPM-217	Severely erroded/rilled at T_{HJ}: weight loss = 60 mg.

E. POCO GRAPHITE ADSORPTION/DESORPTION TESTS

Objective:

To determine the gas adsorption rates for Poco AXF-Q1 exposed to various atmosphere conditions.

Summary:

Adsorption/desorption experiments run with Poco AXF-Q1 exposed to 42% RH lab air and boiling water showed identical results. For a flight converter utilizing two (2) 500g Poco rings, the expected gas adsorption during assembly and subsequent gas desorption during processing would be approximately 25 mg.

Experimental Results:

The rate of gas adsorption in 42% RH lab air was measured. After inital processing according to MSI 2012, the weight gain was measured in air on an analytical balance. The rate of gas adsorption in air plateaued within thirty minutes and remained constant throughout the 216 hour test duration. These data are plotted in Figure III-2. The Poco AXF-Q1 adsorbed 25 micro grams of gas/gram of Poco during this experiment.

The effect of soaking Poco AXF-Q1 in boiling distilled water on the rate of gas adsorption in 42% RH lab air was also studies. The sequence for this study was:

- Soak Poco from the initial gas adsorption in lab air experiment
- Air dry Poco
- Process Poco as per MSI 2012
- Measure rate of gas adsorption in 42% RH lab air

The weight gain, after the soaking and air drying but prior to processing, was 123 μg/g Poco. This is only a five fold increase over the 42% RH lab air adsorption.

As with the initial gas adsorption experiment, the rate of gas adsorption in air plateaued within thirty minutes and remained constant throughout the 216 hour test duration. The data were identical to that for the initial gas adsorption experiment. The data are shown in Figure III-2.

The data in Figure III-2 show that the adsorption/desorption cycles are reversible. In addition, these data from this study are consistent with previously published outgassing studies.[1]

---

1. C.A. Alexander, Outgassing of Space Quality Carbons and Graphite BMI-X-682, 7/12/77.

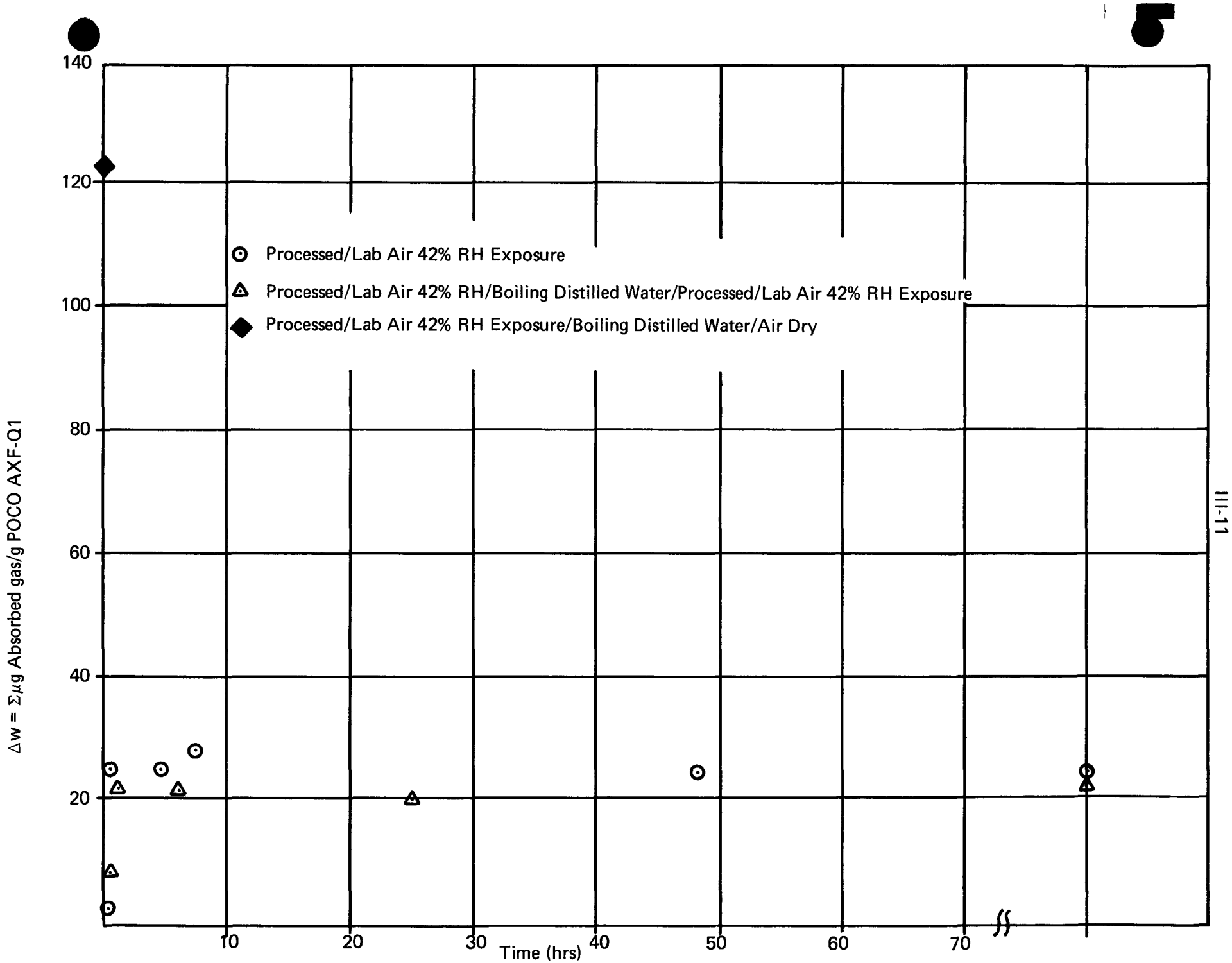

FIGURE III-2: POCO AXF-Q1 ADSORPTION: VARIOUS EXPOSURES

F. STORAGE CONDITIONS: SPUTTERED GdSe

As a result of the deleterious effects of the static vacuum/water vapor environment on M-12 $GdSe_x$ elements, a simple controlled experiment was initiated. Briefly this experiment involved two phases:

Phase I:

- Limiting the available water vapor (1 ml) within a storage container under a static vacuum environment.
- Exposing two Ni and Ag sputtered N-$GdSe_x$ elements plus copper foil to the above environment.

Phase II:

- Eliminating water vapor from the same storage container.
- Exposing a Ni and Ag sputtered N-$GdSe_x$ element plus copper foil to the water vapor free static vacuum environment.

Results:

Phase I:

Within two days, both elements had started expanding and the copper foil was blackened. After a 14 day exposure, the elements and foil were completely crumbled and blackened respectively. Most likely, the available water vapor in the static vacuum environment reacted with the $GdSe_x$ producing an oxyselenate and releasing H_2Se which subsequently reacted with the copper foil.

Phase II:

After eight-four days, the $GdSe_x$ and copper foil were as pretest with respect to:

- Weight (to <0.5 mg)
- Physical dimensions
- Appearance of Ag and Ni sputtercoats
- Appearance of foil surface
- Room temperature electrical resistance measurements

A table of the Phase II data is presented in Table III-5.

Conclusions:

Static vacuum storage of highly reactive Ag sputtered $GdSe_x$ is safe provided water vapor is absent.

This storage method can be accomplished in portable evacuable containers containing activated molecular sieves.

TABLE III-5

N-$GdSe_x$:

	Pre-Test	Post-Test
Weight (g)	2.7935_6	2.7936_0
Physical Dimensions	0.305L; 0.315D	0.305L; 0.315D
Appearance	Shiny and clean	Shiny and clean
Room Temp. Electrical Resistance		
1) Total mΩ as is	9.99 lot $\bar{X}$	9.3
2) Total mΩ deflashed	– –	8.1
3) Contact Ni mΩ as is	3.22 lot $\bar{X}$	1.85
4) Contact Ni mΩ deflashed	– –	1.35
5) Contact Ag mΩ as is	0.46	0.19
6) Contact Ag mΩ deflashed	– –	0.22

Foil:

Weight (gm)	2.380	2.378
Appearance	Shiny and clean	Shiny and clean

G. TESTING TO OBTAIN RELIABILITY DATA BASE

It was recognized that available data accumulated on selenide thermoelectric materials had limited applicability for predicting EOM power characteristics of the flight RTG for the Galileo Mission. This observation was valid because a reference design had not been selected to allow reliability testing; hence, no valid reliability data base existed. The lack of an acceptable data base coupled with the time restriction after a thermoelectric design baseline was selected mandated a form of accelerated testing.

The demonstration test program was to be formulated in two (2) phases. The accelerated test phase consisted of ten (10) 18-couple modules which were to be used to establish a relationship between acceleration factor and test conditions - the first phase. A designed experiment to determine empirically the rate of power degradation with varying stress levels of module hot and cold end temperatures and current was prepared and a summary description follows as Attachment 13. From the results of this first phase of testing, a simple polynominal equation of the following form

$$dP/dt = B_o + B_1T_h + B_2T_c + B_3I_L \qquad \text{(first order terms)}$$

$$+ B_{12}T_hT_c + B_{13}T_hI_L + B_{23}T_cI_L \qquad \text{(two factor interaction terms)}$$

$$+ B_{11}T_h^2 + B_{22}T_c^2 + B_{33}I_L^2 \qquad \text{(second order terms)}$$

$$+ B_{123}T_hT_cI_L \qquad \text{(three factor interaction term)}$$

would be generated using least squares multiple non-linear regression techniques. Also a theoretical investigation would be made after post test analysis of the test modules to determine why the response was affected and to construct a basic mechanistic model and an estimation of the parameter of this model. The expression for the mechanistic model would be of the form:

$$W = [N_o\,(T_c) + b\,I_L]^4\; e^{-B/T_h}$$

while W represents loss in the P-leg due to sublimation effects

N, b and B = parameters

e = base of the natural log

Both of these formulas would be used to establish a relationship between the desired acceleration factor of 12 for time vs. power degradation.

The second or reliability phase of the test program would consist of eight (8) eighteen-couple modules operated at an acceleration factor of twelve to verify performance over the 50,000 hour space mission in about 4,000 hours. In both phases the eighteen-couple modules would be fully instrumented as three (3) quasi-independent six-couple modules, i.e., six-couple current, open and closed circuit voltages as well as individual leg hot and cold end temperatures and voltages were to be monitored.

Computer programs were prepared to enable the data acquisition system to collect data on a programmed time interval basis for storage in the data collection system. Programs to print out parametric data on command from reduction of the stored raw data were also prepared.

The assumption was made that other potential failure mechanisms such as (1) long term effect of N-leg element cracking, (2) reduction of element contact pressure due to spring relaxation, (3) loss of sublimation wrap seal of P-legs, and (4) selenium deposition and chemical attack on the other module materials would be resolved by the time of the design freeze.

Satisfactory operation of the twenty-four (24) quasi-independent six-couple modules at the 12x acceleration factor would demonstrate 0.95 reliability at 70% confidence level on an attributes basis for the time frame of the test.

ATTACHMENT TO SECTION III

ATTACHMENT 13

Testing to Obtain Reliability Data Base

A description of a designed experiment to determine empirically the rate of power degradation with varying stress levels of hot and cold end temperatures and current and maximize the information for data reduction was prepared. This description follows.

To adequately describe the degradation empirically it was recommended that a test matrix be utilized that would include not only variation in T_h but also in independent variables T_c, cold end temperature, and I_L, load current. The object of such a test program would be to get better definition of output power changes with excursions in these independent variables.

The informational data available from such a series of tests will make SIG/Galileo power prediction procedures more accurate since it is possible that T_h, T_c and I_L may vary outside the design limits over the mission time frame. Such excursions in hot and cold end temperatures and current can occur because of the following considerations:

1) Fuel Decay.
2) Insulation degradation.
3) Heat pipe performance degradation.
4) Emissive coating degradation.
5) Solar and planetary IR fluxes variation.
6) SIG/RTG vehicle orientation.
7) Degradation of conductivity in one of the leg current paths could lead to increased current in the parellel leg.

A review of the best procedures for a designed experiment to achieve the maximum information and efficiency of observations for most meaningful data analysis was made.

Some of the considerations involved in design of experiments are briefly summarized in the following paragraphs.

A planned designed experiment should incorporate the following basic concepts: randomization, replication and orthogonality.

Randomization in a design means to conduct the order of experimental runs in a random (not systematic) fashion. Randomization of test order eliminates or balances out the effects of extraneous or undesirable systematic variation. The effect of such randomization is to make it legitimate to analyze the results as if they were independent.

Replication is the repetition of an experimental run. In the analysis of experimental results it is important to have an estimate of experimental error (i.e., random error). To replicate requires the preparation of two or more independent samples treated as nearly alike as possible. It is common practice to obtain an estimate of the experimental error variance when only quantitative variables are involved by replicating the center point of the design. This is accomplished by setting the variables at their center levels and making several independent observations at these settings. These center points are worked into the random order of performing the entire experiment.

Orthogonality in a design implies that the estimates of the main effects and interactions are uncorrelated with each other. Designs having this property insure that if a systematic change occurs corresponding to any one of the effects, the change will be associated with that effect alone.

Factorial Experimental Designs

Factorial experiment designs are superior to one factor at a time experimentation in many respects.

1. The effects of several factors in the same set of experiments can be studied simultaneously.

2. The effect of each factor at all levels of the other factors can be tested and whether or not this effect changes as other factors change.

3. Tests can be made for the effects of the factors separately (the main effects) and also for joint effects of two or more factors combined (interaction effects).

4. It is possible to obtain a more complete picture of what is happening over the entire "experimental region of interest" than would be obtained by varying each of the factors one at a time while keeping the others constant.

5. Every judgement made about the effects of the factors is based on all the observations accumulated in the entire set of experiments, not merely on a few selected observations. Thus, factorial experiments are more sensitive in the detection of small effects.

Scaling Coding of the Independent Variables

It is very desirable to "standardize" or "code" the levels of the independent variables. The coded variables are often much easier to manipulate, analyze and interpret than the original variables. When the factor is continuous such as temperature or current, a suitable coding procedure can be imposed on the original levels of the factor and refer to the levels as the high level a +1 and the low level as -1. The midpoint or center point is 0.

Rotatability

For a rotatable design, the variance of the estimated response is constant at a given distance in any direction from the origin (center) of the design in the K - dimensional factor space defined by the independent variables. For k = 3 the α value for rotatability is $2^{3/4} = 1.682$.

Investigation of the response function include empirical studies aimes at how the controlled variable affect the response by means of simple polynominal equations of the following form:

Response (change in power as a function of time)

$= B_o$ (constant term)

$+ B_1 T_h + B_2 T_c + B_3 I_L$ (first order terms)

$+ B_{12} T_h T_c + B_{13} T_h I_L + B_{23} T_c I_L$ (two factor interaction terms)

$+ B_{11} T_h^2 + B_{22} T_c^2 + B_{33} I_L^2$ (second order terms)

$+ B_{123} T_h T_c I_L$ (three factor interaction term)

Also a theoretical investigation will be made to determine why the response is affected and the construction of a basic mechanistic model and the estimation of the parameters in the model. A proposed model is as follows:

$$W = (N_o (T_c) + bI_L)^4 e - B/T_h$$

where W represents loss in the P-leg due to sublimation effects

N_o, b, Bb — parameters

E — base of natural log.

In order to determine these coefficients for T_h, T_c and I_L through analysis of variance (ANOVA) techniques, it is recommended that a central composite second order design constructed from three main pieces, each of which comprise a set of points be used.

1) The 2^k vertices of a k - dimensional "cube" or factorial design.

2) The 2 k vertices of a k — dimensional "star" including.

3) A number, N_o, of "center points."

No. of Variables (factors)	K	3
No. of parameters to be estimated (K $\pm$ 1) (k + 2)/2 for a full second order design		10
No. of runs (ecluding No.)	$2^k + 2k$	14
No. of center points		6
Recommended No. of runs		18
Actual No. of runs for proposed design		30

Composite Design for k = 3 Variables

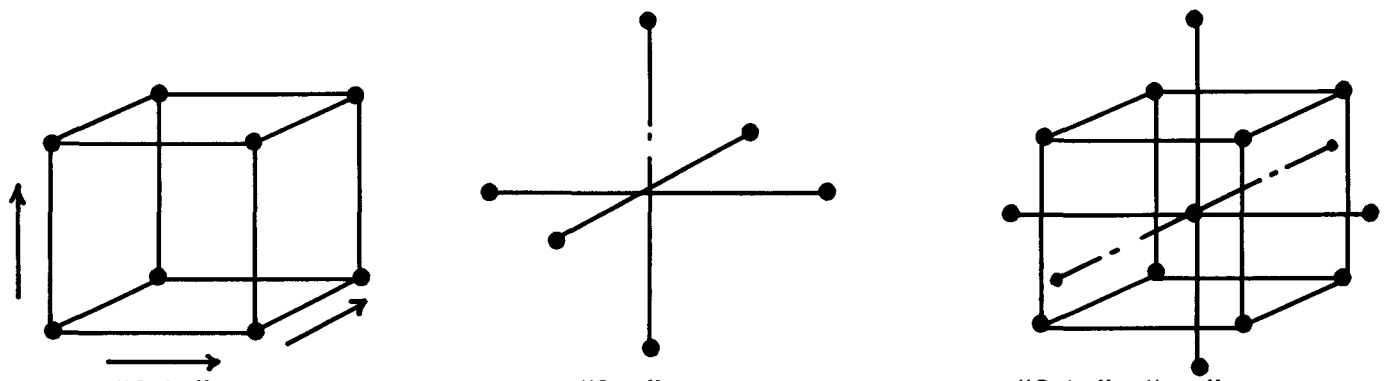

FIGURE 13-1

Based on the above considerations, it was recommended that in addition to the five accelerated test modules M-25 to M-29 initially in the program an additional identical series of five-eighteen couple modules having flight system hardware configuration would have to have been added to the program to expand the reliability data base. These ten eighteen couple modules would each be connected electrically as three six couple sets to permit variation in current loading. The physical constraints of the eighteen couple hardware arrangement would require that T_h and T_c operate at a fixed temperature for a given module. The range of operating conditions would be as shown in Table 13-1.

TABLE 13-1

Symbol	Description	Range	$-\alpha$	-1	0	$+1$	$+\alpha$
T_h	Hot End Temp.	800-976°C	800	836	888	940	976
T_c	Cold End Temp.	125-175°C	125	135	150	165	175
I	Load Current	6.25-15.35	6.25	8.1	10.8	13.5	15.35

The lower limit for the range of hot end temperature, T_h, is selected as 800°C in order to increase the scope of the reliability data base and for projection of longer converter life at a lower hot end temperature. The upper limit for the hot end temperature is chosen as 976°C as the limit for temperature under which degradation processes will remain the same as at lower temperatures even though proceeding at an accelerated rate.

The cold end temperature, T_c, range is chosen to increase the reliability data base. The current range is based on a lower limit of possible ΔT operation of 650°C and an upper limit of twice rated current at 230 watts of power at 30 volts.

Figure 13-2 shows the proposed composite design in representative visual form.

All ten eighteen-couple modules will be fully instrumented as three quasi-independent six-couple modules i.e., six couple current, open and closed circuit voltages as well as individual leg hot and cold end temperatures and voltages will be monitored. The data will be collected on a programmed time interval basis and stored in the data acquisition system. The parametric data as summarized will be available on a command printout basis.

Post test analysis of the modules subjected to the accelerated stress levels of the test matrix will add information to enhance the development of a given parameter versus probability as a function of various environment conditions. Least squares regression analysis techniques may be applied as applicable to the variables data to determine trend analysis.

Results of the analyses and test of each component may be collected and integrated into a single assessment report. The assessment report will identify failure modes, experience with failures and will aid in prediction of converter performance to end-of-mission time.

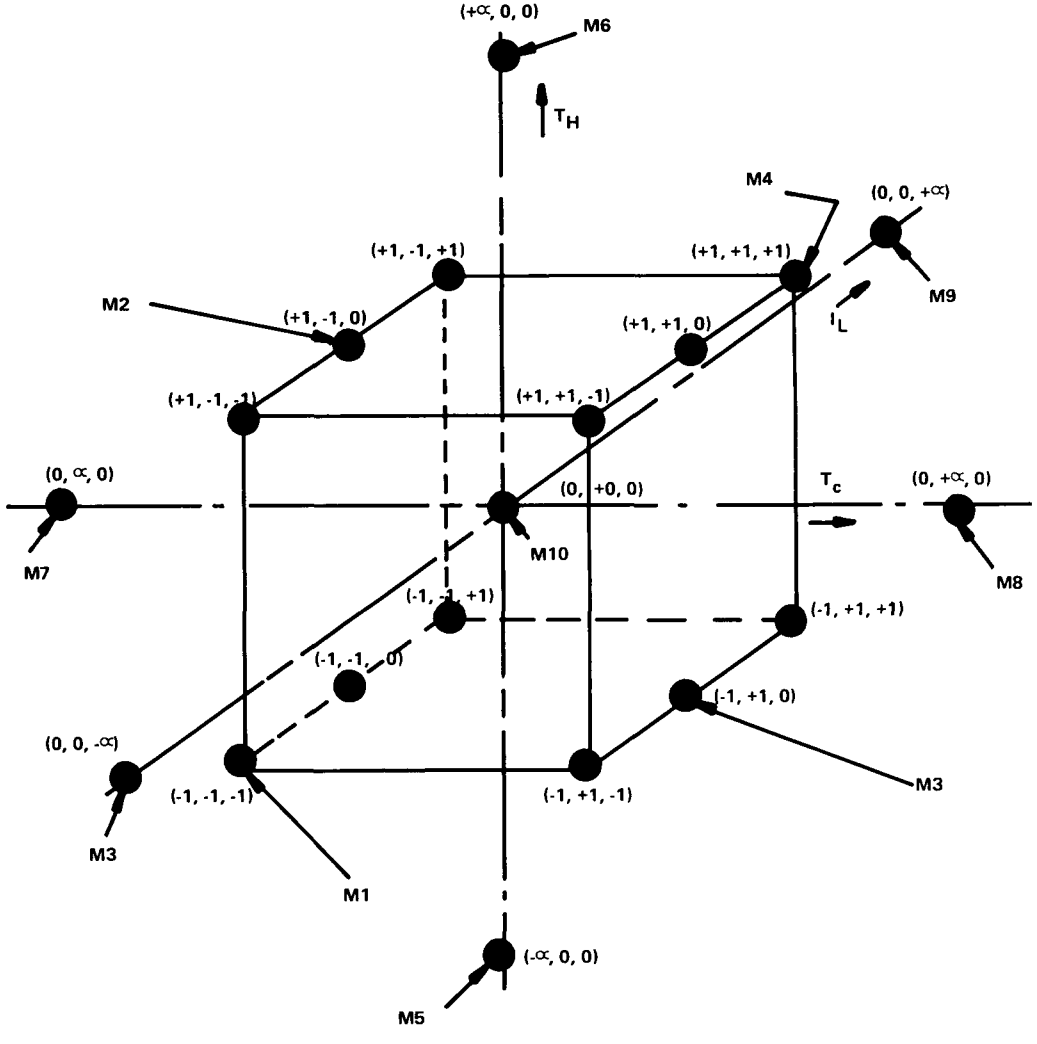

SYMBOL	DESCRIPTION	RANGE	$-\alpha$	-1	0	+1	$+\alpha$
T_h	HOT END TEMP.	800–976°C	800	836	888	940	976
T_c	COLD END TEMP.	125–175°C	125	135	150	165	175
I	LOAD CURRENT	6.25–15.35	6.25	8.1	10.8	13.5	15.35

FIGURE 13-2: TEST MATRIX

TEST NO.		MATRIX MODULE	PROGRAM MODULE	T_h	T_c	I_L
1		M-1-1	M25A-1	-1	-1	-1
2		M-2-1	M25B-1	+1	-1	-1
3		M-3-1	M26A-1	-1	+1	-1
4	2^3	M-4-1	M26B-1	+1	+1	-1
5	FACTO-	M-1-2	M25A-2	-1	-1	+1
6	RIAL	M-2-2	M25B-2	+1	-1	+1
7		M-3-2	M26A-2	-1	+1	+1
8		M-4-2	M26B-2	+1	+1	+1
9		M-1-3	M25A-1	-1	-1	0
10	I_L	M-2-3	M25B-3	+1	-1	0
11	CENTER	M-3-3	M25A-3	-1	+1	0
	POINTS					
12		M-4-3	M26B-3	+1	+1	0
13		M-5-1	M27A-1	$-\alpha$	0	0
14	α	M-6-1	M27B-1	$+\alpha$	0	0
15	POINTS	M-7-1	M28A-1	0	$-\alpha$	0
16	FOR 2ND	M-8-1	M28B-1	0	$+\alpha$	0
17	ORDER	M-9-1	M29A-1	0	0	$-\alpha$
18	EFFECTS	M-9-2	M29A2	0	0	$+\alpha$
19		M-9-3	M29A-3	0	0	0
20	MATRIX	M-10-1	M29B-1	0	0	0
21	CENTER	M-10-2	M29B-2	0	0	0
22	POINTS	M-10-3	M29B-3	0	0	0
23		M-5-2	M27A-2	$-\alpha$	0	0
24		M-5-3	M27A-3	$-\alpha$	0	0
25		M-6-2	M27B-2	$+\alpha$	0	0
26	REPLI-	M-6-3	M27B-3	$+\alpha$	0	0
27	CATE	M-7-2	M28A-2	0	$-\alpha$	0
28	POINTS	M-7-3	M28A-3	0	$-\alpha$	0
29		M-8-2	M28B-2	0	$+\alpha$	0
30		M-8-3	M28B-3	0	$+\alpha$	0

MODULE NO._____ ATT NO._____ DATA STORED – DATE_____ TIME_____

DATA ACCESSED – DATE_____ TIME_____

–	VARIABLE – – – – – – – – –	UNITS	SECTION – 1	SECTION – 2	SECTION – 3
IM	Current Measured	AMPS			
IML	Current Matched Load	AMPS			
EC	Voltage-Closed Circuit	VOLTS			
ED	Voltage – Open Circuit	VOLTS			
POM	Power Out - Measured	WATTS			
POM/C	Power Out – Measured/Couple	WATTS			
PON	Power Out Normalized	WATTS			
PON/C	Power Out Normalized/couple	WATTS			
R1	Resistance Total Internal	MILLIOHMS			
THOT	Temp. Hot End Average	DEG C			
T COLD	Temp. Cold End Average	DEG C			
T DELTA	Temp Range Average	DEG C			
SPA	Seebeck Voltage – P-Leg Average	UV/DEG C			
SNA	Seebeck Voltage – N-Leg Average	UV/DEG C			
RIPA	Resistance – P-Leg Average	MILLIOHMS			
RINA	Resistance – N-Leg Average	MILLIOHMS			
R%XPA	% Extr. Res. P-Leg Average	PERCENT			
R%XNA	% Extr. Res. N-Leg Average	PERCENT			
THB	Temperature Hot Block	DEG C			
TCF	Temperature Cold Front	DEG C			
T SHOE	Temperature Shoe	DEG C			
PIM	Power In Measured	WATTS			
VAC	Vacuum	U TORR			

FIGURE 13-3: SUMMARY PRINTOUT

MODULE NO._____ ATT NO._____ DATA STORED – DATE_____ TIME_____

DATA ACCESSED – DATE_____ TIME_____

SET	VARIABLE – – – – – – – – – –	UNITS	SECTION – 1	SECTION – 2	SECTION – 3
P SET 1	T HOT	DEG C			
	T COLD	DEG C			
	S BAR	UV/DEG C			
	RI	MILLOHOMS			
	R%X	PERCENT			
N SET 1	T HOT	DEG C			
	T COLD	DEG C			
	S BAR	UV/DEG C			
	RI	MILLIOHMS			
	R%X	PERCENT			
P SET 2	T HOT	DEG C			
	T COLD	DEG C			
	S BAR	UV/DEG C			
	RI	MILLIOHMS			
	R%X	PERCENT			
N SET 2	T HOT	DEG C			
	T COLD	DEG C			
S	S BAR	UV/DEG C			
	RI	MILLIOHMS			
	R%X	PERCENT			
P SET 3	T HOT	DEG C			
	T COLD	DEG C			
	S BAR	UV/DEG C			
	RI	MILLIOHMS			
	R%X	PERCENT			
N SET 3	T HOT	DEG C			
	T COLD	DEG C			
	S BAR	UV/DEG C			
	RI	MILLIOHMS			
	R%X	PERCENT			

FIGURE 13-4: DETAILED PRINTOUT

IV. MANUFACTURING

The manufacturing objectives at the start of the Galileo Program were to build seven (7) SN converters consisting of two (2) rings of 168-couples in each ring and sixteen (16) test modules of 18-couples each. This was to be done over a period of approximately thirty-six (36) months.

Planning and scheduling were started utilizing designs and experience from the Technology Program as the base line. CRAM (Critical Resources Allocation Method), a form of network analysis for scheduling manufacturing of SN-1 was instituted during this program.

Make and buy decisions and vendor selection were based on prior development of the hardware during the Technology Program. During the planning stage, the long lead time items were identified so that the raw materials or unfinished goods could be identified. It was also planned that materials would be certified where ever possible in this program.

A. HOT FRAME AND HEATER BLOCKS

The material used is a high purity, high density graphite supplied by POCO, identified as POCO AFX-Q1. This material was specified for Galileo; it had been used in modules and GDS-I. This is a single source item. Experience in the past and discussions with POCO indicate that delivery of three (3) or more size 8-1/4" x 8-1/4" x 3-1/4" graphite blocks of the quality required might take a year. This is the largest size in width (8-1/4") that can be produced by their equipment. Apparently the yield rate for graphite blocks of the size and quality needed for Galileo is quite low, and the elapsed time to process such blocks is sixteen (16) to twenty (20) weeks.

Experience has shown that as much as three (3) runs have been required to obtain blocks of the required size and quality. Approval was granted to start early procurement of graphite blocks. POCO was to machine two (2) rings from two (2) blocks for SN-1. Due to schedule considerations and providing for a second machining source of graphite, a local vendor machined two (2) rings for SN-2 or back-up for SN-1 if needed, because of schedule or damage. Ultrasonic scan charts for eight (8) graphite blocks, SN-3, SN-4, SN-5 and SN-6, were delivered to 3M for review. They were found acceptable by QC, but further work was held due to Galileo stop work order. Some of these blocks are or will be used for heater blocks for modules in the Technology Program. Larger blocks are required because of the use of larger diameter heaters in the Technology Program. Prior to final assembly, the graphite goes through a cleaning process which includes a high temperature vacuum bakeout procedure.

B. CERAMIC PINS

The ceramic pins used to locate the P-legs on the hot straps were made of alumina rod cut to length.

C. Platinum Strips

Platinum strips .0005" thick and die cut to provide holes under the N-leg gimbal and match the outside contour of the hot current straps were designed. There was a minor problem trying to develop a die to cut .0005" thick platinum without tearing or burring. This had apparently been solved when the stop work order was received.

D. HOT CURRENT STRAPS – GIMBALS

The hot current straps were machined from molybdenum sheets. The gimbals are machined from molybdenum then finish machined to match the hot straps. The set is identified and marked. The hot straps are then sent to St. Louis, MO, for alumina plasma spray coating on the bottom surface which contacts the platinum and graphite. Some time and effort was spent with various potential suppliers in selecting a vendor. Additional effort was spent to develop a corner treatment chamfer/radius so that the spray coating would bond to the lower corner and bond for some distance up the sides to reduce cracking and chipping. Coating on the corners and sides would reduce the potential for shorts caused by platinum touching the bare molybdenum. If small conductive particles touched the graphite or platinum and the bare hot straps, shorts could also result. By spray coating up the sides approximately .015" or more, this could reduce a potential problem. After spray coating, the alumina is finish ground to flatness and dimension. The bare top surface is also cleaned or sanded with fine grit polishing cloth or paper to remove oxides and over spray from the spraying and grinding steps. This provides a clean, flat contact surface for the legs. Prior to final assembly, the parts go through an ultrasonic solvent cleaning process.

E. PLATINUM AND NICKEL FOIL DISCS

Platinum foil .0005 thick and nickel foil .005 thick was procured. The discs could be stamped out in house or by one of several local stamping houses specializing in small precision parts. The parts were cleaned in an ultrasonic solvent cleaner.

F. SUPPORT OF LEG MANUFACTURE

1. Gadolinium

A study and planning exercise was undertaken with various responsible people to determine needs and schedules for specific amounts of gadolinium foil and pellets. Yield rates based on GDS-I, quantity of units to be built for testing and shipping, dates units were to be on test or shipped, all entered into the gadolinium schedule and quantity requirements list.

No gadolinium foil was shipped to 3M from Ames Lab, as the design was changed and gadolinium foil eliminated.

The following quantity of gadolinum pellets was received from Ames Laboratory:

July 10, 1978	460 grams
August 29, 1978	2167 grams
October 10, 1978	1105 grams
November 21, 1978	1288 grams
December 13, 1978	2433 grams
January 30, 1979	2059 grams
Total:	9512 grams

The stop work order was issued for the Galileo Program and Ames Lab made no more gadolinium pellet shipments for the Galileo Program.

2. Tungsten 25% Rhenium Alloy for P-Leg Hot End Cap

In the technology development phase, a Tungsten 25% Rhenium alloy .002 thick foil was used on the P-leg hot end. As testing progressed, data collected indicated that some sort of barrier would be needed on the P-leg. An astro quartz slurry wrap was tried. It became apparent that the wrap should go beyond the end of the P-leg material so that subsequent shrinkage would not leave a gap at the leg material Tungsten-25% Rhenium foil cap interface. A proposed design was a .020" thick cap with a shoulder; the minor diameter to be .010" to .015" thick and the major or flange diameter to be .005 to .010 thick. The minor diameter to be the same diameter as the P-leg material element. The major diameter to be .320" or approximately .025" on the side for the wrap to butt against. The cap would also have a blind hole .005" to .010" deep for location over the ceramic pin. Various attempts were made to produce such a cap. Obtaining .020" thick material in sufficient quantity was a problem.

Making the caps from rods was very time consuming, costly and resulted in a low yield. It did give some pieces for the first cut tests. Powder metallurgy, because of the small total requirements, did not appear a feasible solution in the opinion of some powder metallurgy houses. They mentioned the development and engineering time and costs plus tooling. A purchase order was issued to Rhenium Alloys of Cleveland, OH, to make a small number, 50 to 200, by whatever method they deemed suitable. After about six months, they were able to make about fifty, which appeared to be usable for testing.

A few square inches of .020" thick sheet was obtained. This was given to a local supplier, who tried various machining techniques. We were able to order .020" thick foil from H. Cross and Schwartzkopf. We obtained some material but there were delays in delivery. We attempted to find other sources of Tungsten 25% Rhenium, contacting DoE, ORNL, Sandia and various other agencies. We contacted ThermoElectron who had a small amount and would try to make caps for us. They were able to develop a process after about eight weeks that would yield about fifty caps each week. Due to the Galileo stop work order, our purchase order with Thermo-Electron was cancelled.

Knight Tool, a local supplier, was able to develop a method of making caps at about 200 a week. Some of the foil received was pure Tungsten. It shattered when punched and did not pass electrical conductivity screening tests. It was returned and the supplier replaced it as soon as he could in partial shipments. The method that made acceptable parts at the least cost and largest weekly quantity delivery required punching discs, EDM (Electro Discharge Machining) the flange and the blind locating hole.

G. COLD END HARDWARE – SUB-ASSEMBLY COLD FRAME SEGMENTS

The cold frame segments are made of 6061-T6 Aluminum. Aluminum plate 4" thick and multiples of 12" in length and width are the basic starting material. The plate is cut into 12 inch square sections. The center is cut out and the corners are cut off, leaving a rough ring. The ring is machined on a numerical controlled mill; then cut up into segments. Some study was given to making the cold frame segments from small pieces of bar stock approximately ¾" x 1¼" x 4".

The cold frame segments for SN-1 and SN-2 were machined from a large plate by numerical control tape milling machines. The segments were electroless nickel plated in order to provide a surface for soldering the copper flexible follower. Another benefit of the electroless nickel plate is burr reduction; the plating process etches and smooths the fine burrs, rounds/breaks sharp corners. It also provides a surface which reduces the potential for twist locks to turn up chips and burrs when installed.

H. TWIST LOCKS

The twist locks are machined from 6061-T6 Aluminum bar stock, slotted and sides trimmed in a press. The twist locks are electroless nickel plated to reduce burr and/or chip generation from the spring end or the edge of the retainer step of the cold frame segment.

I. COLD FRAME SEGMENT

Work was being done in attempting to tin plate the base of the cold frame segment which is in contact with the finned housing. At the time of the stop work order, no parts had been tin plated meeting a design objective or an acceptable level. The alternative method was to use tin foil which was intended to be used in SN-1.

J. COPPER FOIL FLEXIBLE FOLLOWERS/COLD CURRENT STRAPS

The SN-1 design flexible follower was made up of fourteen (14) layers of .0015 thick ETP copper foil (CDA 110).

A copper foil sheet is photo etched or chemically milled so that the excess copper is removed, leaving a chain of seven (7) pieces attached to each other by small tabs. The chain is then accordion folded, using a fixture to locate the holes or outer edges, resulting in one (1) piece seven (7) layers thick. The ends of the seven (7) layer folded part are spot welded with one (1) small spot in order to maintain alignment during the bonding assembly. During the development of this part, it was found that in trying to spot weld the large required areas, the spot welds were of poor quality, generally burr holes and pits in the spot welded area. The seven (7) layer parts or in the case of the flexible follower, two (2) seven (7) layer stacks are placed in a bonding fixture in an inert atmosphere (Argon). The fixture is heated and pressure applied which results in the part being bonded to two (2), three (3) or four (4) places, depending on the part design. The areas not bonded are flexible and each leaf or layer can be flexed which makes the part more flexible than if it were one (1) piece the same thickness. The same process is used to make cold current straps. The flexible followers are fourteen (14) layers thick and two (2) seven (7) layer stacks used. The cold current straps are seven (7) layers thick and one (1) seven (7) layer stack is used. The tabs used in folding the layers are trimmed away after bonding. It is important that the copper parts be clean, and be kept clean after the photo etch or chemical milling process so as not to become oxidized. It is also important that in the bonding process, especially when heating up, that there be no oxygen present. Use of inert gas or vacuum is required. Oxides on the copper affect bonding quality, strength and the area of bond.

The copper foil bonding operation was developed and bench tested in the lab. Acceptable parts were made for tests and modules. The operation was scaled up primarily through the use of several sets of tooling, moved and set up in a short run production facility. The operation was set up, with test and pilot runs being made, but had not gone into full scale production when the Galileo stop work order was issued. This operation has since been dismantled and the equipment returned to the lab.

K. SPRING RETAINER BUTTONS

The spring retainer buttons are made of ETP copper bar stock on a lathe. The function of this part is to locate the cold current strap end of the Helical coil spring.

L. BeO DISCS

The beryllium oxide discs act as an electrical insulator, but a thermal conductor in the cold end sub-assembly.

These parts are a long lead time item and promised delivery dates are not always kept, nor do the suppliers always meet all specifications. For these reasons, purchase orders were placed with several suppliers. At the time of the order, it was not known what type of solder or braze material was to be used; the discs were specified only with molybdenum mangenese coating with nickel plating on both sides.

The coating was specified so that at least a .007" wide band at the circumference would not be coated. This was to prevent solder from running to the edge of the beryllium oxide disc.

Some of the BeO discs were dished so they would not bond properly to the cold current straps or copper spring retainer buttons with the specified amount of solder.

M. COLD CURRENT STRAP SUB-ASSEMBLY

All the parts were cleaned ultrasonically in Freon solvent. Solder preforms made from .0015 thick solder ribbon are used on each side of the BeO disc. The Molybdenum-Manganese coated area is fluxed with a minute drop of flux on each side. The parts are loaded into a solder fixture. The cold current strap is placed in position with the solder preform then the fluxed BeO disc is loaded with the copper spring retainer. The fixture is placed into a quartz tube in a tube furnace hooked up to a vacuum system, pumped down and heated up. When the piece parts reach the prescribed temperature, the heat is turned off, the quartz tube removed from the furnace and allowed to cool with the vacuum system operating.

N. COLD FRAME SEGMENT AND FLEXIBLE FOLLOWER SOLDER SUB-ASSEMBLY

The cold frame segment and copper foil followers are cleaned ultrasonically with Freon solvent. The cold frame segment with electroless nickel plate is fluxed, a solder preform is placed on the rail then the fourteen (14) layer copper foil flexible follower is placed on the rail with a fixture. The fixture is placed in a quartz tube hooked up to a vacuum system, evacuated and placed in a tube furnace and heated up to the prescribed temperature. When the parts reach temperature, the

furnace is shut-off, the tube removed and allowed to cool down while under vacuum. After cooling, a rivet is installed through the copper follower into the cold frame segment to give added assurance that the follower and segment will not separate, which could result in legs being displaced. After riveting, the assembly is placed in a fixture to form an "S" shape on each side of the rail. After forming the double loops on all followers on a segment, it is placed in another fixture so the cold current straps can be soldered to the follower.

The previous cold current soldered sub-assembly is now located with solder preforms so that the appropriate spring retainers protrude through the holes in the flexible followers. The sub-assemblies are soldered together in a vacuum to make up the cold end sub-assembly.

O. INVESTIGATION OF ULTRASONIC WELDING OF COLD END HARDWARE

A parallel effort was undertaken to bond cold end hardware ultrasonically in addition to the pressure-temperature bond method. Investigation was not completed due to the stop work order. From the work that was done, it appears that the layers of copper foils could be ultrasonically bonded to each other and to the copper buttons, spring retainers and P-leg discs. The copper to copper ultrasonic bond did not appear to be a major problem. The next step was to ultrasonically bond copper to aluminum.

In the SN-1 design, the aluminum is electroless nickel plated, a solder, 10% tin, 88% lead, 2% silver with flux in a vacuum is used to make the copper to aluminum bond. The ultrasonic weld would eliminate flux and the electroless nickel plate. Preliminary work and samples indicated feasibility and a successful weld could be made.

P. FINAL ASSEMBLY

Assembly tooling was redesigned and modified from GDS-I. Bars and clamps were used on the outside of the cold frame segments and rings. The GDS-I design used threaded rods and bosses. A partial dummy assembly was put together which indicated some additional changes and modifications to be made to the final assembly tooling. Due to the stop work order, a practice assembly of SN-1 was never accomplished.

Q. EQUIPMENT

At the initial planning, it was thought that the housing would be a cylinder which could be loaded in a normal size clean bench. After the program started, it was determined that the housing would have fins, possibly 24" to 30" long and up to 30" in diameter. After consultation with 3M Engineering it was decided that 3M would purchase and install ceiling mounted vertical laminar flow clean air modules. The modules were installed, inspected and certified to class 100. This allowed work to take place under them in a space approximately 6 ft. by 12 ft. by 7½ ft. high.

R. SPECIAL PROCESSING AND SHIPPING CONTAINERS

Special large stainless steel vacuum processing containers which when mounted on supports and packaged in special crates could also be used as shipping containers. The opening in Teledyne's vacuum chamber (submarine) limited the size of the processing-shipping container which also limited the size of the external housing of SN-1.

V. QUALITY ENGINEERING AND CONTROL

A. QUALITY ASSURANCE

The SIG/Galileo Quality Assurance Program Plan was completed and submitted to DoE (Report No. MMM-2864-0011). MSI-2008 and 2009 P-leg and N-leg materials fabrication specifications, Q.A. Standard Instructions and processing check sheets were completed and submitted to DoE. Inspection of all hardware and material ordered prior to the stop work order was completed

B. CONFIGURATION MANAGEMENT

The 3M computer programming department investigated and identified a computer system to maintain records for configuration management control.

C. DoE ACCEPTANCE

The acceptance data package description was completed and made an appendix to the QA Program Plan.

D. NON-DESTRUCTIVE TESTING PLAN

The NDT plan was completed and incorporated in the QA Program Plan.

VI. RELIABILITY

A. RELIABILITY

Reliability – The system of activities established to provide the level of reliability (probability that the equipment will perform adequately its intended function for the specified interval under-stated conditions) in the 3M Selenide Converter technology program to meet the needs of the user. The essential reliability tasks worked on are outlined as follows:

- Reliability Requirements

  1) Determine
  2) Study and Analyze
  3) Promote through review of engineering, design, and manufacturing documents, specifications and drawings.

- Design Review

  1) Inherent reliability is established and determined by the basic design
  2) Determine the design factors which can be used as indices of quality and reliability of components and systems
  3) Prepare FMECA for system

- Test Objectives

  1) Establish methods for measuring and correlating design factors as related to quality and reliability of the system. i.e., acceptable value and range for each pertinent factor
  2) Establish methods for assessing reliability determined within stated confidence limits from tests
  3) Document test objective, independent and dependent variables, test conditions and methodology for obtaining, storing and recording data

- Evaluation and Assessment

  1) Analysis of Variance (ANOVA) techniques (least squares regression analysis) for separating variabilities in collection of observations into components or sources
  2) Develop model to predict long term performance
  3) Verify reliability prediction by applicable tests using accelerated conditions as applicable to the stated time frame

- Failure Reporting System – The purpose of the failure reporting system is to ensure that all failures occurring during the program from material receiving inspection through performance testing of module designs are recorded and used for product improvement.

A preliminary Program Plan for the Galileo Mission to delineate the specific tasks in the reliability area during design development, fabrication and test of deliverable thermoelectric converters for use in the Galileo Mission was submitted to DoE in January 1979. (Reference Report Number MMM-2864-0035).

A Thermoelectric Converter Failure Mode Effects and Criticality Analysis, FMECA, was prepared to identify the failure areas which could result in loss of electrical power during the mission. The purpose of the FMECA was to assure that all possible failure modes of the converter system, parts, manufacturing process or quality control system have been addressed. Summarizing, the purpose of the FMECA was to identify potential and known failure modes; identify the causes and effects of such failure modes; prioritize the identified failure modes according to frequency of occurrence, severity and detection; and provide for problem follow-up and corrective action. The criteria for FMECA Analysis is listed in Attachment 14.

A preliminary copy of the FMECA is included as attachment 14.

A system failure mode logic diagram was prepared to indicate logical combinations of failure modes leading to converter failure as identified by the FMECA and provide a basis for allocating the failure probabilities of the system to the component failure modes. Included in this work were Fault Tree Analyses made of the P and N-legs. These diagrams are included in the appendix. These system and component diagrams were developed to identify causative events and their logical relationships to a specified undesired event or failure mode. The technique identifies the failures through the causational events and their logical relationship, beginning at the undesired or top event and proceeding downward through the various operational modes and subsystems to the component level. The definition of the logical relationships between these causational events allows the quantitative analysis of the probability of the undesired event using the basic rules of probability.

The reliability effort also extended to contributions made to post test analysis (PTA) made of operational modules removed from test. Computer programs of the module data were obtained which reduced the data to individual leg parametric performance. Thus, individual leg performance could be easily compared and correlated with observations made on PTA disassemblies.

A failure reporting system was proposed to ensure that all failures occurring during the program from material receiving inspection through acceptance testing of the converter are recorded and utilized for product improvement.

Quality control would report deviations and failures during material receiving, during fabrication and production of converters; Reliability would perform this function for acceptance testing. The form used for reporting would be that shown on the following page entitled the "Failure Report Form".

A Failure Review Board (FRB) or Committee composed of members representing the different work areas of the program as shown in the Work Interface Chart would receive the failure report. The FRB analyzes the failed item, determines the appropriate corrective action for recommendation to DoE. After appropriate action has been determined, the Failure Review Board Coordinator initiates the action, monitors its progress, and schedules an audit follow-up. After the action and audit are completed, the Coordinator forwards a verification notice and the corrective action findings to the FRB, which in turn completes the "Failure Review Report". The block diagram of the failure reporting system and the Failure Review Report form are shown on the following pages.

FAILURE REPORT FORM DATE _____

REPORT NO. _____

ITEM NAME _____ ITEM DRAWING NO. _____

DATE OF FAILURE _____

FAILURE DESCRIPTION _____

APPLICABLE SPECIFICATION _____

DEVIATION _____

RELIABILITY

QA

FIGURE 4

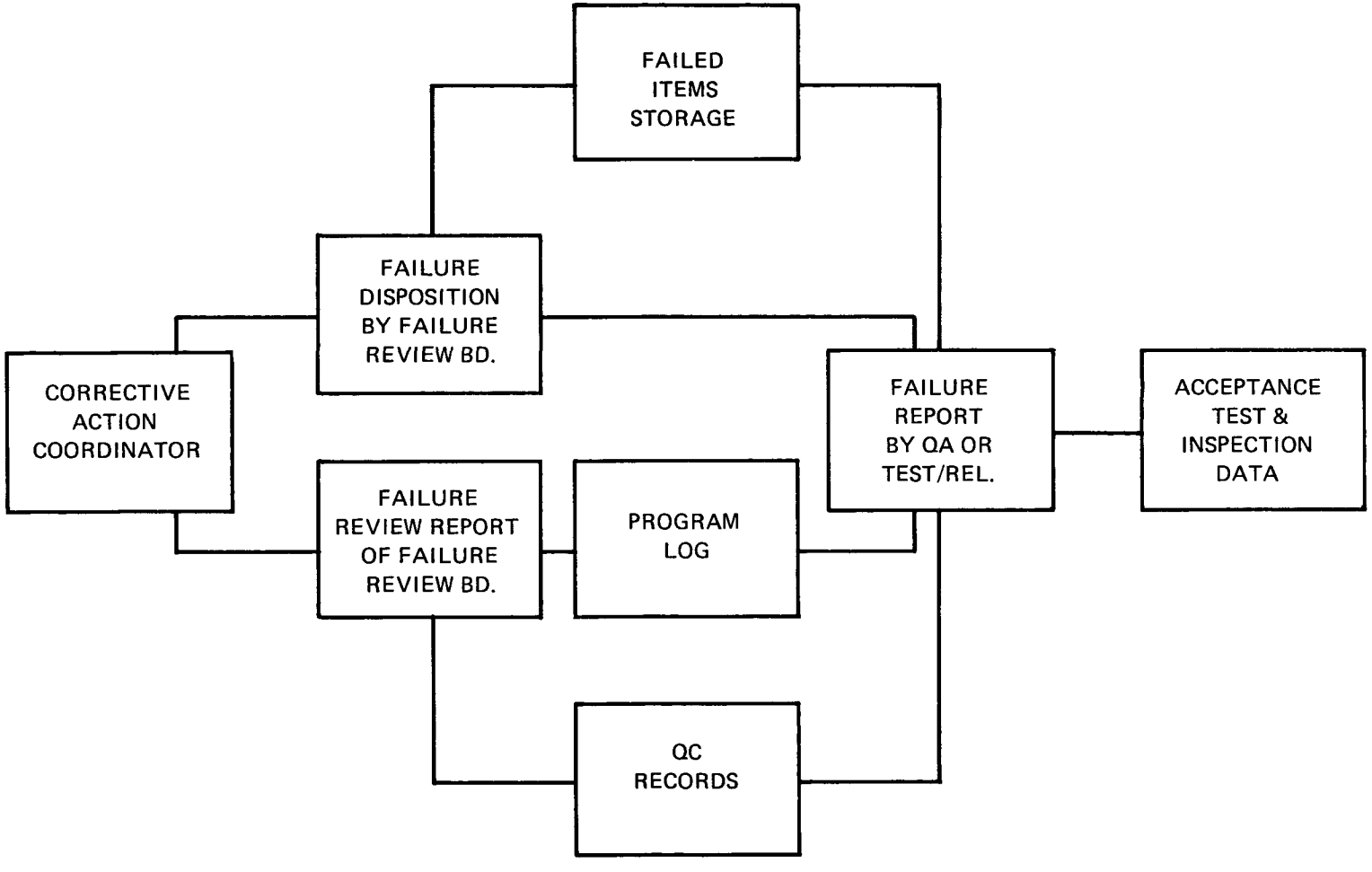

FIGURE 5: FLOW PLAN FOR FAILURE REPORTING AND REVIEW SYSTEM

FAILURE REVIEW REPORT

DATE_____

REPORT NO._____

ITEM NAME_____ ITEM DRAWING NO._____

DATE OF FAILURE_____

FAILURE DESCRIPTION_____

FAILURE ANALYSIS_____

CORRECTIVE ACTION_____

CORRECTIVE ACTION EFFECTIVE ON_____

DSN_____ REL_____

MAT'L_____ PROG._____

MFG_____ SYS._____

QA_____

FIGURE 6

ATTACHMENT TO SECTION VI

ATTACHMENT 14

Criteria For FMECA Analysis

1) Assumed Failure Mode

Description of each possible failure mode anticipated. The question to be considered is "Could It?" as opposed to "Will it?"

2) Assumed Cause of Failure

Listing of all causes assignable to each failure mode. Care will be taken to assure that the list is inclusive so that remedial effort will be aimed at all pertinent causes.

3) Effect on Mission Performance

In as far as is possible, expressing the effect in terms of converter power output change.

4) Probability of Failure Mode Occurrence

The probability of occurrence is evaluated on a "0.1" to "10" scale. As an example, a "0.1" indicates a very improbable occurrence, whereas "10" would indicate a very probable occurrence.

5) Severity of Failure Mode Occurrence

The severity or estimated consequence of the failure is evaluated on a "0.1" to "10" scale. A "0.1" indicates a minor nuisance, whereas a "10" indicates a severe total failure of mission power.

6) Detection of Failure Mode Occurrence

The number assigned here is based on the estimated probability that a potential problem can be detected while corrective action can be taken. A "0.1" indicates a high probability that the failure would be detected, while a "10" indicates a low probability that the failure would be detected.

7) Risk Priority Number

The product of the numbers for probability, severity, and detection previously evaluated for a specific failure mode provides an indicator of the relative priority or criticality of the failure mode.

8) Proposed Course of Action

A brief description of the correction action recommended including those responsible for resolution.

From the risk priority number, a criticality analysis rating becomes readily apparent as an indication of areas of emphasis for improved reliability.

TABLE 14-1: 1 FAILURE MODE EFFECTS AND CRITICALITY ANALYSIS (FMECA)

ITEM		ASSUMED FAILURE MODE	ASSUMED CAUSE OF FAILURE	EFFECT ON MISSION PERFORMANCE	COMPENSATING PROVISIONS	FAILURE MODE OCCURRENCE			RISK PRIORITY NO.	PROPOSED COURSE OF ACTION
DESCRIPTION	DETAIL					PROBABILITY OF	SEVERITY OF	DETECTION OF		
1. HOT END HARDWARE	A. SPACER (POCO GRAPHITE MATERIAL)	1. CRACKING. 2. BREAKING OR SPALLING 3. SHATTERING	DYNAMIC VIBRATION AND HANDLING INITIATE HIGH STRESSES WHICH CAUSE FAILURE DUE TO INHERENT MATERIAL DEFECTS.	LOSS OF A PORTION OR ALL OF CONVERTOR OUTPUT POWER.	MOST LIKELY TYPE OF CRACK WOULD HAVE MINOR EFFECT.	.2 .2 .1	1 5 10	10 7 .1	2 7 .1	Q.C. PROGRAM
	B. HOT SHOE FOIL	1. ELECTRICAL SHORT CIRCUIT TO SPACER.	DYNAMIC VIBRATION CAUSES GIMBAL TO TOUCH FOIL AND/OR SPACER.	VARIES FROM REDUCTION IN OUTPUT TO TOTAL LOSS OF GENERATOR OUTPUT. A SHORT TO GROUND COULD POSSIBLY PRODUCE AN UNDESIRABLE CONDITION FOR THE LOAD.		1	1	10	10	Q.C. PROGRAM REQUEST ELECTRICAL FLOATING GENERATOR FRAME.
	C. HOT END CURRENT STRAP INSULATION $A1_2^0_3$	1. ELECTRICAL SHORT CIRCUIT TO HOT SHOE.	IMPURITIES, METAL PARTICLES, CRACKED INSULATION, THERMAL CYCLING.	REDUCED OUTPUT FROM THE AFFECTED ELEMENTS. INCREASED HOT SPACER TEMPERATURE MAY CAUSE EXCESSIVE HEATING OF THE OTHER ELEMENTS.	MOST LIKELY TYPE OF CRACK WOULD HAVE MINOR EFFECT.	.1	2	1	.2	
		2. TRANSVERSE CRACK SEPARATES HOT END INSULATION INTO TWO OR MORE PIECES.	EXCESSIVE COEFFICIENT OF FRICTION AND STRESSES DUE TO THERMAL CYCLING.	EXCESSIVE RELATIVE MOTION CAUSES AN INCREASE IN HOT JUNCTION RESISTANCE.		.1	2	9	1.8	
	D. CERAMIC PIN	1. SHEARED, CRACKED OR BROKEN PIN CAUSING SHIFTING OF CURRENT STRAP.	DYNAMIC VIBRATION AND STRESSES DUE TO THERMAL CYCLING.	REDUCED OUTPUT FROM THE AFFECTED ELEMENTS		1	1	10	10	Q.C. PROGRAM
	E. HOT END CURRENT STRAP	HIGH ELECTRICAL RESISTANCE ON OPEN CIRCUIT OF CURRENT STRAP OR ELEMENTS.	1. FOREIGN MATERIAL DURING ASSEMBLY.	REDUCED OUTPUT DUE TO EXCESSIVE RESISTANCE.	WOULD BE DETECTED DURING CHECKOUT AND PROCESSING	.1	2	1	.2	ASSEMBLE CONVERTOR IN CONTROLLED AREA.
			2. THERMAL INSULATION WORKS INTO THE AREA BETWEEN THE ELEMENT AND CURRENT STRAP AND/OR GIMBAL THERMAL CYCLING AND/OR VIBRATION.	REDUCED OUTPUT FROM THE AFFECTED ELEMENTS. INCREASED HOT SPACON TEMPERATURE MAY CAUSE EXCESSIVE HEATING OF THE OTHER ELEMENTS		.1	2	8	1.6	

TABLE 14-2: 2 FAILURE MODE EFFECTS AND CRITICALITY ANALYSIS (FMECA)

ITEM DESCRIPTION	ITEM DETAIL	ASSUMED FAILURE MODE	ASSUMED CAUSE OF FAILURE	EFFECT ON MISSION PERFORMANCE	COMPENSATING PROVISIONS	FAILURE MODE OCCURRENCE PROBABILITY OF	FAILURE MODE OCCURRENCE SEVERITY OF	FAILURE MODE OCCURRENCE DETECTION OF	RISK PRIORITY NO.	PROPOSED COURSE OF ACTION
2. THERMO-ELECTRIC ELEMENT	A. N-TYPE LEG	1. CRACKING	1. THERMAL CYCLING.	SPRING PRESSURE MAY MAINTAIN NEARLY CONSTANT OUTPUT, BUT SENSITIVITY TO SHOCK AND VIBRATION WILL BE INCREASED.		1	1	9	9	LIMIT THE NUMBER OF THERMAL CYCLES
			2. IMPROPER FABRICATION OF ELEMENT.		WOULD BE FOUND IN QC CHECKS.	.1	1	9	.9	Q.C. PROGRAM
			3. IMPROPER ASSEMBLY OF GENERATOR.			.1	1	9	.9	
			4. EXCESSIVE STRESS EXERTED ON ELEMENT DURING FABRICATION OR INSPECTION.			.1	1	9	.9	
			5. TRANSFORMATION OF MATERIAL			10	1	9	90	
			6. EXCESSIVE CURRENT BECAUSE HIGH RESISTANCE IN ONE LEG CIRCUITS.			1	1	10	10	
		2. CHANGE IN DOPING LEVEL.	1. OXYGEN IN SYSTEM CAUSED BY OUT—GASSING OF INSULATION	GRADUAL REDUCTION GENERATOR OUTPUT POWER. EXTENT OF REDUCTION WILL BE LIMITED.	INSULATION PROCESSING CONTROL.	.1	5	2	1	Q.C. PROGRAM
			2. CAUSED BY FAILURE OF SEAL DURING TERRESTRIAL OPERATION.			.1	10	1	1	
		3. EXCESSIVE RESISTANCE	1. IMPROPER FABRICATION OF COLD END BOND AND/OR SPATTERING.	HIGH GENERATOR RESISTANCE. INCREASED SENSITIVITY TO VIBRATION.	SPRING PRESSURE PREVENTS COMPLETE FAILURE. THIS CONDITION COULD POSSIBLY BE DETECTED BY ULTRASONIC MEASUREMENT TECHNIQUE, RESISTANCE VERSUS LENGTH MEASUREMENT, AND/OR PULL TEST.	.1	1	9	.9	Q.C. PROGRAM
			2. POOR ELEMENT ALIGNMENT DURING ASSEMBLY.	LOW OUTPUT POWER DUE TO HIGH GENERATOR RESISTANCE.	WOULD BE DETECTED DURING PROCESSING.	1	2	4	8	MODULE TESTS TO IDENTIFY PROBLEMS.
			3. CONTAMINATION FROM TEG MATERIALS.	LOW OUTPUT POWER	WOULD BE DETECTED DURING PROCESSING.	1	1	10	10	MODULE TESTS TO IDENTIFY PROBLEMS.
			4. OXIDATION OF INTERFACES.			1	2	4	8	

TABLE 14-3: 3 FAILURE MODE EFFECTS AND CRITICALITY ANALYSIS (FMECA)

ITEM		ASSUMED FAILURE MODE	ASSUMED CAUSE OF FAILURE	EFFECT ON MISSION PERFORMANCE	COMPEN-SATING PROVISIONS	FAILURE MODE OCCURRENCE			RISK PRIOR-ITY NO.	PROPOSED COURSE OF ACTION
DES-CRIP-TION	DETAIL					PROBA-BILITY OF	SEVER-ITY OF	DETEC-TION OF		
2. THER-MO-ELE-CTRIC ELE-MENT	B. P-TYPE LEG	A. CRACKING AT THE COLD JUNCTION.	1. THERMAL CYCLING THROUGH THE MA-TERIAL'S TRAN-SITION.	SPRING PRESSURE MAY MAINTAIN NEARLY CONSTANT OUTPUT, BUT SENSITIVITY TO SHOCK AND VIBRA-TION WILL BE INCREA-SED.		2	3	10	60	LIMIT THE NUM-BER OF TEMP-ERATURE CYCLES.
			2. OPERATING THE MATERIAL BELOW ITS TEMPERATURE RANGE.			1	3	10	30	DESIGN CONVER-TER NOT TO OPER-ATE IN THIS RANGE.
			3. EXCESSIVE STRESS EXERTED ON ELE-MENT DURING ASSEMBLY.			.1	3	1	.3	Q.C. PROGRAM
			4. IMPROPER BONDING OF ELEMENT COLD CONTACT.			.1	3	1	.3	
		B. SUBLIMATION	1. EXCESSIVE OPERA-TING TEMPERATURE, CHANGING DOPANT DISTRIBUTION.	NO SHORT-TERM EFFECTS, LONG-TERM COPPER GROWTH AT PARTITION AND COLD END. CONDENSATION OF SUBLIMATION PRO-DUCT ON INSULATION INCREASES THERMAL LOSS OR ELECTRICAL SHORT. COPPER GROWTH COULD CAUSE ELECTRICAL SHORTING.	THE ELECTRICAL PROPERTIES OF THE MATERIAL ARE NOT AFFECTED.	3	3	9	81	Q.C. PROGRAM
			2. EXCESSIVE OPERA-TING CURRENT BE-CAUSE OF FAILURE OF ADJACENT LEG IN PARALLEL SET CAUSING CHANGE IN DOPANT DISTRI-BUTION.			1	8	10	80	
			3. FAILURE OF WRAP.			3	8	9	216	
			4. LOSS OF WRAP CON-TACT SEAL AT HOT JUNCTION FOIL FOR INTERFACE.			5	8	8	320	
			5. OXYGEN IN SYSTEM.			.1	3	2	.6	
		C. CHANGE IN DOPANT LEVEL	1. OXYGEN IN SYSTEM.	REDUCTION IN CON-VERTER OUTPUT	SEEBECK COEFFIENT AND RESISTANCE OF LEG WILL RE-TURN TO NORMAL WHEN OXYGEN IS GONE.	.1	1	2	.2	
			2. CONTAMINATION FROM GENERATOR MATERIALS.			.1	1	10	1	COMPATIBILITY PROGRAM
		D. EXCESSIVE RESISTANCE	1. POOR ELEMENT ALI-GNMENT DURING ASSEMBLY	REDUCTION IN CON-VERTER OUTPUT		1	1	1	1	
			2. CONTAMINATION FROM TEG ASSEMB-BLY MATERIAL.			.1	1	10	1	
			3. CONTAMINATION FROM WRAP PAR-TICLES.			1	5	10	50	
			4. OXIDATION OF INTERFACES			1	2	4	8	

TABLE 14-4: 4 FAILURE MODE EFFECTS AND CRITICALITY ANALYSIS (FMECA)

ITEM DESCRIPTION	ITEM DETAIL	ASSUMED FAILURE MODE	ASSUMED CAUSE OF FAILURE	EFFECT ON MISSION PERFORMANCE	COMPENSATING PROVISIONS	FAILURE MODE OCCURRENCE PROBABILITY OF	FAILURE MODE OCCURRENCE SEVERITY OF	FAILURE MODE OCCURRENCE DETECTION OF	RISK PRIORITY NO.	PROPOSED COURSE OF ACTION
3. COLD END HARDWARE	A. FOIL COLD STRAP	1. POOR THERMAL CONTACT IN FOLLOWER RAIL ASSEMBLY.	POOR BONDS AT JOINING SURFACES.	INCREASES THERMAL IMPEDANCE, CAUSES HIGHER JUNCTION TEMPERATURES, RESULTS IN REDUCED POWER OUTPUT.	RIVETS ADDED TO BONDS	.1	2	2	4	Q.C. PROGRAM
		2. HOLES FORMED IN COLD STRAP.	CORROSION OF COLD STRAPS.			8	7	10	560	
		3. TEARING OF ONE OR MORE CURRENT STRAPS.	VIBRATION		TESTS SHOW ADEQUATE DESIGN.	.5	7	10	35	Q.C. PROGRAM
		4. LOSS OF FREEDOM OF FOIL COLD STRAP.	1. BONDING ON STIFFENING OF COLD STRAP LAYERS.	INCREASE OF COLD JUNCTION TEMPERATURE DUE TO REDUCTION IN THE FORCE WITH CONSEQUENT LOSS OF POWER.	LONG TERM ACCELERATED COMPONENT EVALUATION.	2	5	10	100	Q.C. PROGRAM
			2. BLOCKING OF COLD FOLLOWER ACTION BY THERMAL INSULATION AGING.			.5	5	10	25	
	B. BERYLIA OXIDE DISC INSULATION	1. ELECTRICAL SHORT CIRCUIT.	1. IMPURITIES, METAL PARTICLES, CRACKED INSULATION, THERMAL CYCLING.			2	2	1	4	Q.C. PROGRAM
			2. FOREIGN MATERIAL DEPOSITED ACROSS JOINT.			7	5	10	350	COMPATIBILITY PROGRAM
			3. CRACKING OF INSULATION.			.1	3	10	3	
	C. SPRINGS	A. REDUCTION IN SPRING FORCE.	CHANGE OF MATERIAL PROPERTIES WITH TIME AT OPERATING TEMPERATURE.	INCREASED ELECTRICAL RESISTANCE REDUCES OUTPUT. INCREASED THERMAL IMPEDANCE INCREASES TEMPERATURE OF HOT AND COLD JUNCTION.	TESTING MAKES UNLIKELY	6	8	10	480	Q.C. PROGRAM
		B. BROKEN SPRING	IMPROPER MANUFACTURING.	LOSS OF AT LEAST A PORTION OF GENERATOR OUTPUT.	SERIES-PARALLEL CONNECTION REDUCES THE CHANGE OF COMPLETE FAILURE.	.1	2	10	2	Q.C. PROGRAM
	D. INTERCONNECTIONS	1. ELECTRICAL OPEN CIRCUIT	1. EXCESSIVE FLEXURE WHICH HAS WEAKENED THE WIRE AND CONNECTION.	BREAKAGE RESULTS IN THE LOSS OF AT LEAST A PORTION OF GENERATOR OUTPUT. VIBRATION SENSITIVITY IS INCREASED.	STRANDED WIRE PROVIDES MULTIPLE PATHS.	.01	7	10	.7	Q.C. PROGRAM
			2. POOR BOND BETWEEN WIRE AND COLD STRAPS.			3	7	10	210	
			3. RIVET JUNCTION FAILURE.			3	7	10	210	
		2. ELECTRICAL SHORT CIRCUIT	IMPROPER ASSEMBLY.	VIBRATION MAY CAUSE A CHANGE IN OUTPUT.	WOULD BE DETECTED BY ACCEPTANCE TESTS.	3	7	10	210	

TABLE 14-5: 5 FAILURE MODE EFFECTS AND CRITICALITY ANALYSIS (FMECA)

ITEM		ASSUMED FAILURE MODE	ASSUMED CAUSE OF FAILURE	EFFECT ON MISSION PERFORMANCE	COMPEN-SATING PROVISIONS	FAILURE MODE OCCURRENCE			RISK PRIOR-ITY NO.	PROPOSED COURSE OF ACTION
DES-CRIP-TION	DETAIL					PROBA-BILITY OF	SEVER-ITY OF	DETEC-TION OF		
4. INSULATION		1. CAKING OR SIN-TERING CAUSING BLOCKING OF FOIL COLD STRAP.	TIME, EXCESSIVE OPERATING TEMPER-ATURE OR FOREIGN MATERIALS.		COMPATIBILITY TESTING TO DATE INDICATES NO PROBLEM AT OP-ERATING TEMP-ERATURE.	.5	5	10	25	Q.C. PROGRAM WITH PROPER INSULATION PROCESSING
		2. OUTGASSING OF WATER VAPOR.	PROPERTY OF INSU-LATION OR INSUFFIC-IENT PROCESSING.			.1	5	1	.5	
		3. INCREASED THERMAL CON-DUCTIVITY AFTER A PER-IOD OF OPERA-TION.	1. CHARACTERISTIC OF INSULATION.	REDUCED OUTPUT FROM INCREASED THERMAL LOSS.		1	2	10	20	
			2. CAUSED BY FOREIGN MATERIAL			2	1	10	20	
		4. MISELIGNMENT AND DISORIEN-TATION OF ASSEMBLIES	INSTALLATION OF INSULATION DISTURBS ASSEMBLIES			2	5	10	100	BLOWN INSUL-ATION STUDY.
5. COLD FRAME		POOR HEAT TRANSFER.	INADEQUACY OF TIN PLATING.	INCREASED ΔT BE-TWEEN COLD FRAME AND HOUSING RE-DUCING POWER OUT.		2	2	1	4	Q.C. PROGRAM

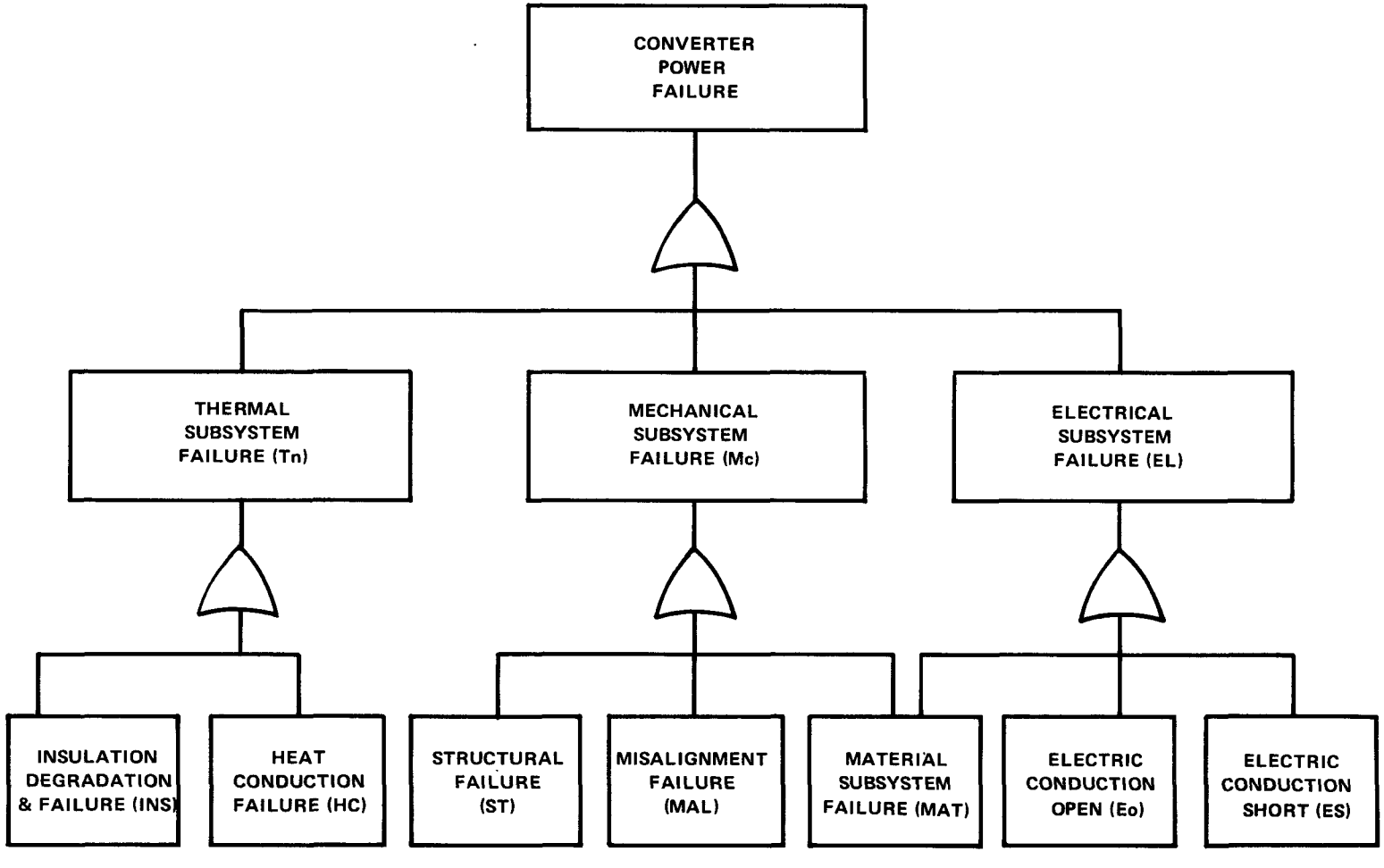

FIGURE 14-1: FAILURE MODE LOGIC DIAGRAM

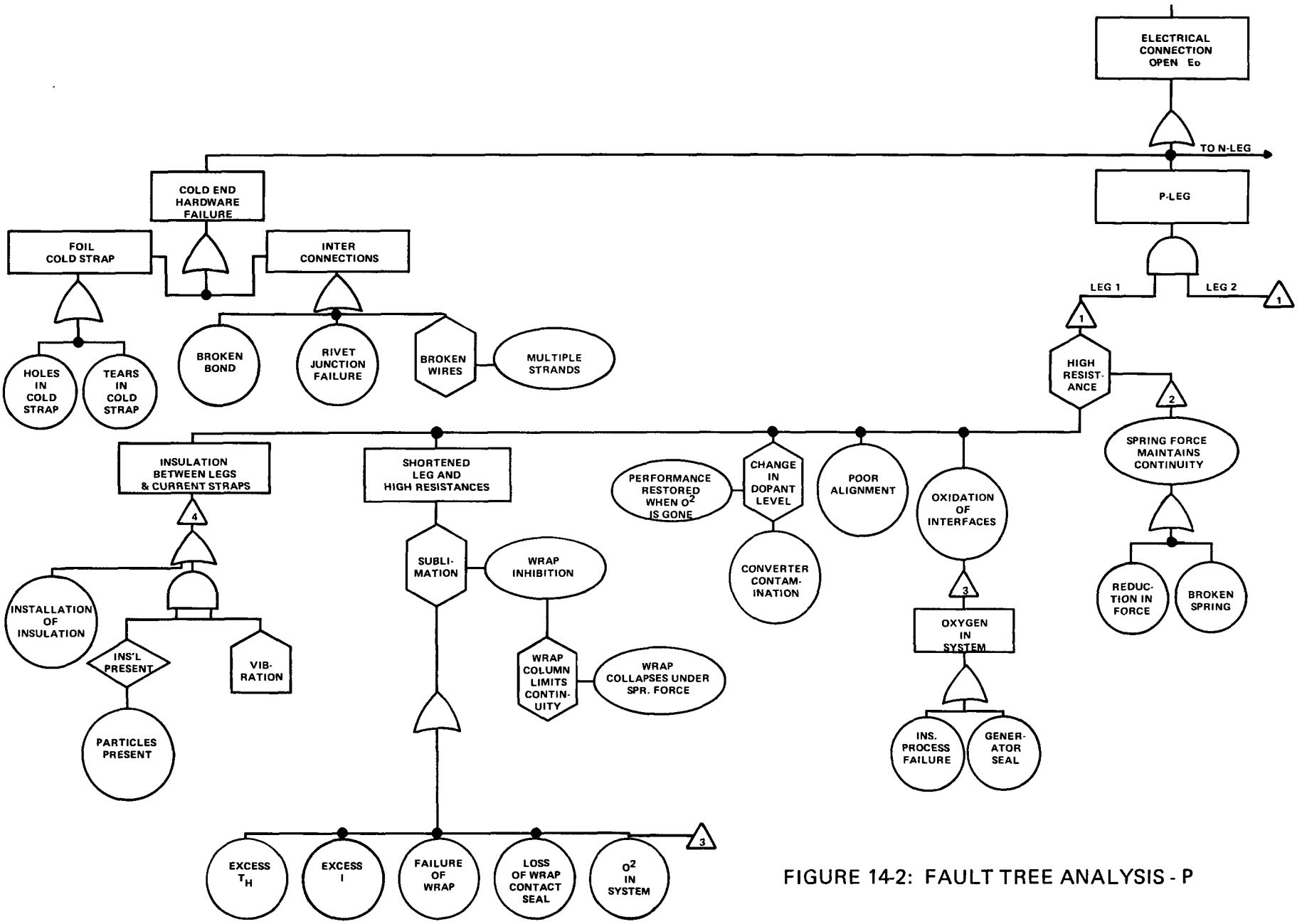

FIGURE 14-2: FAULT TREE ANALYSIS - P

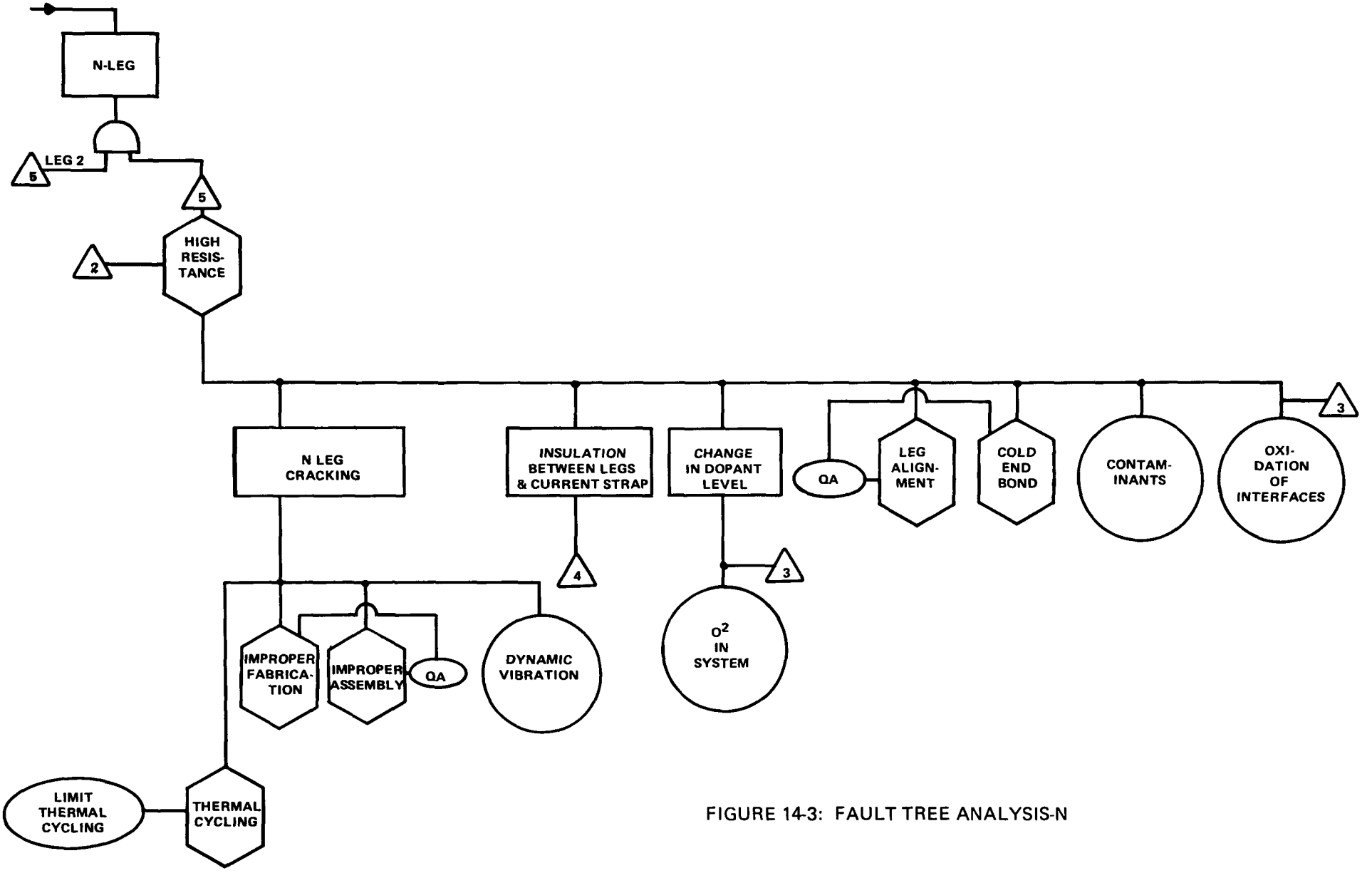

FIGURE 14-3: FAULT TREE ANALYSIS-N